Check for updates

Redescription of three basal anomodonts: a phylogenetic reassessment of the holotype of *Eodicynodon oelofseni* (NMQR 2913)

Alienor Duhamel[1,2]*, Julien Benoit[1], Brenen Wynd[3],
April Marie Wright[3] and Bruce Rubidge[1]

[1]Evolutionary Studies Institute, University of the Witwatersrand, Johannesburg, South Africa, [2]School of
Geosciences, University of the Witwatersrand, Johannesburg, South Africa, [3]Department of Biological
Sciences, Southeastern Louisiana University, Hammond, LA, United States

The Dicynodontia (Therapsida: Anomodontia) is one of the most successful
Permo-Triassic terrestrial tetrapod clades and the oldest specimens are recorded
from the middle Permian *Eodicynodon* Assemblage Zone of South Africa. Their
fossil record is abundant and species-rich across Pangea. By contrast, the
fossil record of the basal-most anomodonts, which includes non-dicynodont
anomodonts and early forms of dicynodonts, is patchy and their morphology
and phylogeny are deduced from relatively few specimens. Discovered in 1982
and described in 1990, the holotype of *Eodicynodon oelofseni* (NMQR 2913)
is one of the better-preserved early anomodont specimens. However, it has
been suggested that *E. oelofseni* does not belong to the genus *Eodicynodon*.
Here, using CT-scanning and 3D modeling, the skull of *Eodicynodon oelofseni*,
Patranomodon nyaphulii and *Eodicynodon oosthuizeni* are redescribed. In
the framework of this study, the application of 3D scanning technology to
describe anatomical structures which were previously inaccessible in these
fossils has enabled detailed redescription of the cranial morphology of the basal
anomodonts *Patranomodon*, *Eodicynodon oelofseni* and *E. oosthuizeni* and
led to a greater understanding of their cranial morphology and phylogenetic
relationships. Based on an anatomical comparison and phylogenetic analyses
(Bayesian and cladistics) the phylogenetic relationships of basal anomodonts are
reassessed and it is suggested that NMQR 2913 does not belong to the genus
Eodicynodon but likely represents a separate genus basal to other dicynodonts.
A new genus is erected for NMQR 2913. This presents one of the first applications
of Bayesian Inference of phylogeny on Therapsida.

KEYWORDS

Therapsida, Dicynodontia, *Eodicynodon*, phylogeny, Bayesian Inference, *Nyaphulia*

1 Introduction

Synapsida, one of the major groups of terrestrial amniotes, comprises both living
mammals and a diverse group of stem-taxa (Luo et al., 2002; Kemp, 2005; Benton,
2015; Angielczyk and Kammerer, 2018; Rougier et al., 2021). During the Permian Period,
the clade Anomodontia was the most species-rich clade of non-mammalian synapsids

(Fröbisch, 2009; Angielczyk and Kammerer, 2018) and was dominant in terms of specimen abundance, geographic range, species richness, and ecological diversity (Kemp, 2005; Fröbisch and Reisz, 2008; Fröbisch, 2009; Nicolas and Rubidge, 2010; Smith et al., 2012). They survived the devastating end-Permian extinction (Ruta et al., 2013) and persisted until the end of the Triassic (Dzik et al., 2008; Sulej et al., 2010). Anomodonts also were one of the first clades of herbivorous tetrapods to undergo a major evolutionary radiation (Reisz and Sues, 2000; Reisz, 2006) and their extensive fossil record has facilitated studies on their paleobiology and functional anatomy in great detail (Ray et al., 2004; Fröbisch and Reisz, 2009; Botha-Brink and Angielczyk, 2010; Chinsamy-Turan, 2011; Ruta et al., 2013; Kammerer et al., 2014; Benoit et al., 2018; Marilao et al., 2020).

The current phylogenetic and taxonomic framework suggests that Dicynodontia is a monophyletic group that does not include basal anomodont taxa such as the "Chainosauria" (*Patranomodon*, *Galeops*, *Galechirus*, *Anomocephalus*, *Galepus*), the "Venyukovioidea" (*Otsheria*, *Suminia*, *Ulemica*) and other basal taxa, such as *Biseridens* and *Tiarajudens* (Fröbisch and Reisz, 2008; Liu et al., 2010; Angielczyk et al., 2021). In contrast to derived dicynodonts, basal anomodonts are rare in the fossil record, and are known from only Brazil, China, Russia and South Africa. All South African specimens have been found at the base of the Karoo Beaufort Group, in the lower Abrahamskraal Formation, where the fossil record is patchy (Rubidge, 1995; Rubidge and Day, 2020). Previous authors suggested that the early anomodont radiation could have been accomplished in two waves happening in Laurasia and Gondwana (Liu et al., 2010).

Amongst dicynodonts, *Eodicynodon* is considered the basal-most genus (Fröbisch and Reisz, 2008; Kammerer et al., 2011; Angielczyk et al., 2021) and comprises two species: *Eodicynodon oosthuizeni*, represented by numerous specimens, and *Eodicynodon oelofseni* represented by a single specimen, NMQR 2913 which is housed in the National Museum of Bloemfontein (Rubidge, 1990a; Rubidge, 1990b). Recent phylogenetic works suggest that *E. oelofseni*, when coded separately from *E. oosthuizeni* in phylogenetic analyses, does not form a clade with the type species of the genus, and may thus belong to a separate genus (Kammerer et al., 2011; Angielczyk et al., 2021).

The present work, for the first time, examines and describes the internal cranial anatomy of the basal anomodonts *Patranomodon* and *Eodicynodon* based on CT scanned material. This technique to study internal cranial anatomy has proven effective on other anomodonts (Castanhinha et al., 2013). In addition to complete descriptions of four basal anomodont specimens, the study leads to a taxonomic reappraisal of *Eodicynodon oelofseni* and the genus *Nyaphulia* is introduced as the earliest-diverging dicynodont.

2 Materials and methods

Specimen NMQR 3000, *Patranomodon nyaphulii*, was found by Mr. John Nyaphuli in 1986 on the farm Combrinkskraal in the Prince Albert district, Western Cape, South Africa (Rubidge and Hopson, 1996). Geologically it is from the Combrinkskraal Member of the Abrahamskraal Formation, *Eodicynodon* Assemblage Zone, Karoo Beaufort Group, South Africa (Day and Rubidge,

2014; Benoit et al., 2018). The specimen comprises a relatively complete skull with lower jaw and various postcranial remains: vertebrae, complete manus, pelvic bones and femur (Rubidge and Hopson, 1996). It was described as the holotype of *P. nyaphulii*, a monospecific genus (Rubidge and Hopson, 1990). Only the skull was CT scanned for this study.

Specimen BP/1/6230 of *E. oosthuizeni*, was found by Mr. Charlton Dube, on the farm Bloukrans in the Prince Albert district, Western Cape, South Africa (Jinnah and Rubidge, 2007) in the *Eodicynodon* Assemblage Zone of the Abrahamskraal Formation (Jinnah and Rubidge, 2007; Rubidge and Day, 2020; Smith et al., 2020). The specimen, which is dorsoventrally compressed, is identified as *E. oosthuizeni* because of the presence of "postcanine teeth lateral to the lower jaw" and a "laterally flared pterygoid processes" (Jinnah and Rubidge, 2007). Specimen BP/1/6230 comprises a complete skull with lower jaw and some postcranial material attached and articulated to the skull.

Specimen NMQR 2978 of *E. oosthuizeni*, was found on the farm Rietkuil (previously named Zwartgrond), in the Rietbron district, Eastern Cape, South Africa (Karoo collection database and Rubidge, 1990b), in the *Eodicynodon* Assemblage Zone, Karoo Beaufort Group (Benoit et al., 2018). The specimen, comprisisng a complete skull with two large tusks, was described as *E. oosthuizeni* (Rubidge, 1990b).

Specimen NMQR 2913, *Eodicynodon oelofseni* was found on the farm Botterkraal, in the Prince Albert District, Western Cape, South Africa (Rubidge, 1990a) in the *Eodicynodon* Assemblage Zone, Abrahamskraal Formation, Karoo Beaufort Group, South Africa. It was found by John Nyaphuli in October 1982 in a calcareous nodule (Rubidge, 1990a). The nodule was broken into four pieces which had weathered separately, resulting in some parts of the skull being missing. The specimen was mechanically and acid prepared by Mr. John Nyaphuli and was described as the holotype of *Eodicynodon oelofseni* (Rubidge, 1990a). Since then, the delicate specimen has been accidentally broken several times and some sections of the skull, described in the original publication, are now lost.

2.1 Scanning parameters and 3D reconstruction

All scans were performed at the Evolutionary Studies Institute using X-ray µCT with a Nikon Metrology XTH 225/320 LC. CT scans were initially performed for a separate study, so we lack exact exposure times for direct replication, but note that to our knowledge, no filters were used during scanning. Specimens NMQR 3000, BP/1/6230, NMQR 2913 and NMQR 2978 were each scanned in single sessions using the following parameters:

- NMQR 3000, holotype of *Patranomondon nyaphulii*
  A beam energy of 70 kV was used, with a flux of 80 µA at a voxel size of 35.6 µm
- BP/1/6230, referred specimen of *Eodicynodon oosthuizeni*
  A beam energy of 100 kV was used, with a flux of 140 µA at a voxel size of 64.6 µm
- NMQR 2978, referred specimen of *Eodicynodon oosthuizeni*
  A beam energy of 125 kV was used, with a flux of 135 µA at a voxel size of 73.9 µm

- NMQR 2913, holotype of *Eodicynodon oelofseni*
  A beam energy of 100 kV was used, with a flux of 140 μA at a voxel size of 42.3 μm

Three-dimensional reconstructions and visualisation of CT data of all specimens were generated using AVIZO 9.0 lite (FEI VSG, Hillsboro, OR, United States of America) and VG Studio Max (Volume Graphics GmbH). Three-dimensional renderings were obtained using manual segmentation with AVIZO 9.0 lite (FEI VSG, Hillsboro, OR, United States of America).

2.2 Matrix construction

The phylogenetic matrix used in this study is based on the discrete character matrix of Angielczyk et al. (2021) updated with some characters from Surkov and Benton (2004), personal observations and the descriptions provided in the literature (Barry, 1974; Brinkman, 1981; Rubidge, 1990a; Rubidge, 1990b; Rubidge and Hopson, 1996; Modesto et al., 1999; Ivakhnenko, 2003; Modesto et al., 2003; Sullivan and Reisz, 2005; Castanhinha et al., 2013). Mesquite v3.04 (Maddison and Maddison, 2015) was used for the analysis.

This study focuses on the cranial and endocranial anatomy of *Patranomodon* and *Eodicynodon* that are some of the most basal anomodonts. Accordingly, the matrix of Angielczyk et al. (2021) was edited to retain only cranial characters, and endocranial characters from Surkov and Benton (2004) were added. The most derived dicynodont taxa were removed from the analysis with the exception of those where braincase characters had been previously scored and referred to in the literature (Surkov and Benton, 2004), and the character list was modified accordingly.

To assess the taxonomic affiliation and phylogenetic position of NMQR 2913, the holotype of *Eodicyodon oelofseni*, all specimens described were scored separately, including the holotype of *E. oosthuizeni*. The phylogenetic matrix contains a total of 34 taxa and 151 discrete unordered morphological characters.

2.3 Phylogenetic analysis parameters

2.3.1 Parsimony

To run the cladistic analysis, TNT (Tree analysis using New Technology; Goloboff et al., 2003) version 1.5 was applied (Goloboff and Catalano, 2016). A heuristic search (New Technology Analysis) was performed to find the most parsimonious trees. The Random Sectorial Search was defined with a minimum and maximum size of the sector of 5 and 17 respectively. The Consensus-Based Sectorial Search was set for 100 rounds and the minimum size of the sector was 5. The Ratchet algorithm was limited to a total of 5,000 iterations. A hundred rounds were selected for the Tree Fusing algorithm, and the trees were obtained by the random addition of a thousand sequences. Other parameters for the algorithms used were kept as default.

2.3.2 Bayesian Inference

In addition to the TNT analysis, a Bayesian analysis was run with MrBayes v3.2.7a (Huelsenbeck and Ronquist, 2001). The software uses Markov chain Monte Carlo (MCMC, a random walk sampling method that explores the parameter and tree space to optimise their value; see Metropolis et al., 1953; Hastings, 1970; Green, 1995; Geyer, 1991; Larget and Simon, 1999; Huelsenbeck and Ronquist, 2001) to find the best parameters of an evolutionary model (Mk(v) model for a morphological dataset, see Lewis, 2001) given the morphological matrix. The gamma model was used for the substitution rate among characters (the lognormal model, specific to MrBayes and often used in vertebrate analysis, gave similar results) and an exponential distribution for the branch length. This is the first application of Bayesian Inference aimed at investigating the earliest diverging therapsids and their relationships.

Additionally, we performed a more complex set of model estimation approaches in RevBayes (Höhna et al., 2016). Sequence model is shown to strongly affect topology in molecular analyses (Brown and Lemmon, 2007). Comparatively little attention has been paid to this in morphological analyses, with most researchers using the standard Mk model (Lewis, 2001). However, more models of evolution are possible for morphological traits. We tested the Site-Heterogeneous Discrete Morphology model [SHDM] (Nylander et al., 2004; Wright et al., 2016). This model allows for asymmetrical rates of transition (such as different probabilities of gain and loss in a trait) across characters in a discrete matrix.

In testing these models in comparison with the Mk model, we employed reversible-jump Markov Chain Monte Carlo to perform model averaging (Wasserman, 2000). This technique uses MCMC to fit not just the parameters of the model of evolution, but to choose the model itself. We ran this model using two replicate runs and 1,000,000 generations. RevBayes runs multiple MCMC moves per iteration, meaning that an overall lower number of MCMC generations is needed, than other phylogenetic estimation approaches (e.g., MrBayes; Höhna et al., 2016). We assess convergence in Tracer, and judge parameter convergence based on reaching or exceeding an effective sample size of 200 (Rambaut et al., 2018).

Institutional abbreviations—BP/ESI, Evolutionary Studies Institute, Johannesburg, South Africa; NMQR, National Museum, Bloemfontein.

Cranial abbreviations—acst, anterior crus of the stapes; ang, angular; app, anterior process of the parietal; apbo, anterior process of the basioccipital; apro, anterior process of the prootic; apt, anterior process of the pterygoid; apobsh, anterior process of the orbitosphenoid; art, articular; ascc, attachment of the anterior semicircular canal; aso, anterior estension of the supraoccipital; bo, basioccipital; bot, basioccipital tubera; bsh, basisphenoid; bshw, basisphenoid wing; bptp, basipterygoid process; c, caniniform tooth; cc, crus communis; co, occipital condyle; cor, coronoid; d, dentary; da, dentary apex; dpq, dorsal plate of the quadrate; dpro, dorsal process of the prootic; dpsur, dorsal process of the surangular; ds, dorsum sellae; dsh, dentary shelf; dspt, dorsal septum of the pterygoid; dsq, dorsal process of the squamosal; dt, dentary table; ect, ectopterygoid; eo, exoccipital; f, frontal; fo, fenestra ovalis; i, incisiform tooth; icgq, intercondylar groove of the quadrate; iptv, interpterygoid vacuity; ivv, intervomerine vacuity; j, jugal; l, lacrimal; lcq, lateral condyle of the quadrate; lf, lacrimal foramen; lnq, lateral notch of the quadrate; lpro, lateral bulge of the prootic; lt, lower jaw teeth; m, maxilla; mf, mandibular fenestra;

mcq, medial condyle of the quadrate; mpqj, medial process of the quadratojugal; mxd, maxilla depression; n, nasal; npm, nasal process of the premaxilla; obsh, orbitosphenoid; op, opisthotic; opfeo, opisthotic facet of the exoccipital; p, parietal; pafeo, pro-atalas facet of the exoccipital; pal, palatine; palb, palatal boss of the palatine; palp, palatal pad of the palatine; pao, paroccipital process; part, pre-articular; pbs, parabasisphenoid; pc, postcanine; pcst, posterior crus of the stapes; pcult, processus cultriformis; pcultc, processus cultriformis crest; pculta, processus cultriformis sulcus; pf, postfrontal; pla, pila antotica; pm, premaxilla; po, postorbital; pob, postorbital bar; pp, postparietal; ppf, posterior process of the frontal; ppm, palatal process of the premaxilla; prc, precanine; prsh, presphenoid; prf, prefrontal; pro, prootic; prp, preparietal; psh, parasphenoid; pt, pterygoid; ptf, postemporal fenestra; q, quadrate; qj, quadratojugal; qpt, quadrate process of the pterygoid; rl, reflected lamina; rt, replacement tooth; smtobsh, semi tubular region of the orbitosphenoid; smx, septomaxilla; soap, supraoccipital anteriorly projected crest; so, supraoccipital; spl, splenial; st, stapes; sth, stapedial head; stfp, stapedial footplate; stu, sella turcica; sq, squamosal; srspo, skull roof section of the postorbital; sur, surangular; t, tabular; tpt, transverse process of the pterygoid; tq, trochlea of the quadrate; v, vomer; vas, vomer anterior septum; vitptp, vomer inter-pterygoid plate; vkobsh, ventral keel of the orbitosphenoid; vkp, ventral keel of the palate; vps, vomer posterior septum; vksur, ventral keel of the surangular; vs, vomerine septum; vsq, ventral process of the squamosal; zsq, zygomatic process of the squamosal.

Neuromuscular system abbreviations—cf, carotid foramen; crso, canal for the ramus supraorbitalis; csss, canal for the superior sagittal sinus; E, opening for the endolymphatic duct in the floccular cavity; ff, facial foramen; flo, floccular fossa; jf, jugular foramen; lf, lacrimal foramen; mxs, maxillary sinus; oc, olfactory cavity; lpf, lateral palatal foramen; smxf, septomaxilla foramen; stf, stapedial foramen; vest, vestibule; V, opening for the cranial nerve V, VII, foramen for the cranial nerve VII, XII, foramen for the cranial nerve XII or hypoglossal nerve.

3 Results

3.1 Description

3.1.1 *Patranomodon nyaphulii*

SYSTEMATIC PALEONTOLOGY
THERAPSIDA Broom, 1905
ANOMODONTIA Owen, 1859

Definition—The most common ancestor of *Biseridens*, *Anomocephalus*, *Patranomodon*, *Galeops*, *Eodicynodon* and *Dicynodon* and all of its descendants.

Diagnosis—after Sidor (2001), antorbital region shortened to less than 50% of total skull length; presence of a lateral mandibular fenestra; zygomatic arch elevated above the margin of upper tooth row which fully exposes the quadrate and the quadratojugal in lateral view; squamosal with long ventral ramus supporting the quadrate; preparietal is present; teeth of upper tooth row decrease in size posteriorly with upper canine barely or not at all differentiated.

Genus *Patranomodon* Rubidge and Hopson, 1990

Type species—*P. nyaphulii*.
Diagnosis—As for the species.

Patranomodon nyaphulii Rubidge and Hopson, 1990

Material—NMQR 3000, the holotype from the National Museum in Bloemfontein, South Africa. A second specimen, BP/1/8740, was found in 2021, also on the farm Combrinkskraal, and is currently undergoing preparation and study at the Evolutionary Studies Institute.

Type locality—Combrinkskraal farm, Combrinkskraal member of the Abrahamskraal Formation. *Eodicynodon* Assemblage Zone, Beaufort Group, Karoo Supergroup, South Africa.

List of figures—Figures 1–6.

Diagnosis—after Rubidge and Hopson (1996), short palatal exposure of the premaxilla; premaxilla not closely approaching palatine medial to the maxilla; tabular extending ventrally towards the level of the postemporal foramen, covering the contact with the squamosal; the interpterygoid vacuity is an elongate slit between the ventral ridges of the pterygoids; the articulation surface between the quadrate and the articular is screw-shaped, precluding fore-aft sliding movement of articular on quadrate.

Description—Specimen NMQR 3000 is a well preserved skull with lower jaw, with very little compression or distortion (Rubidge and Hopson, 1990; Rubidge and Hopson, 1996). This description of the skull is based on the CT-scan and 3D reconstruction (Figure 1). Cranial elements were fully described by Rubidge and Hopson (1990) and Rubidge and Hopson (1996). This paper brings additional information and focuses on the connections and elements revealed *via* CT scanning. The lower jaw was not scanned for this study and is described by Rubidge and Hopson (1996). The bone surface of the skull is smooth, without external ornamentation or pachyostosis (Figure 1). In lateral view, the skull of *Patranomodon* is broadly rectangular with a domed dorsal margin (Figures 1A,B, 5A,B). The orbit faces anterolaterally (Figure 1C,G) and is about 1.5 times larger than the temporal fenestra. The occiput is well preserved and its surface is perpendicular to the skull roof (Figure 1A,B,H).

The premaxilla of NMQR 3000 is a relatively small paired bone forming the anteriormost part of the skull (Figures 1, 2). The anterior-most tip of the premaxilla is broken and the internarial bar is missing. Dorsally, the nasal process of the premaxilla forms a narrow strip of bone located on the sagittal line above the external naris (Figure 1C,G). The two processes do not touch medially such that the nasals are visible from the ventral side (Figure 1G).

In ventral view, the palatal process of the premaxilla forms the anterior portion of the palate (Figure 1D, I). It contacts the maxilla laterally and the vomers posteromedially (Figure 1D). The suture with the vomer is interdigitated. As noted by Rubidge and Hopson (1996), *Patranomodon* does not have a secondary palate, unlike the condition in dicynodonts such as *Eodicynodon*. As a result, the internal choana opens immediately posterior to the incisors, at the level of the first and the second maxillary teeth (Figure 1D). In ventral view, the palatal process of the left premaxilla is pierced laterally by a small incisive foramen (Figure 2D).

The maxilla is the largest cranial bone in *Patranomodon* (Figures 1, 2) and covers about 60% of the lateral surface of the snout (Figures 1A, B, 2A, B). It forms the posterior margin of the
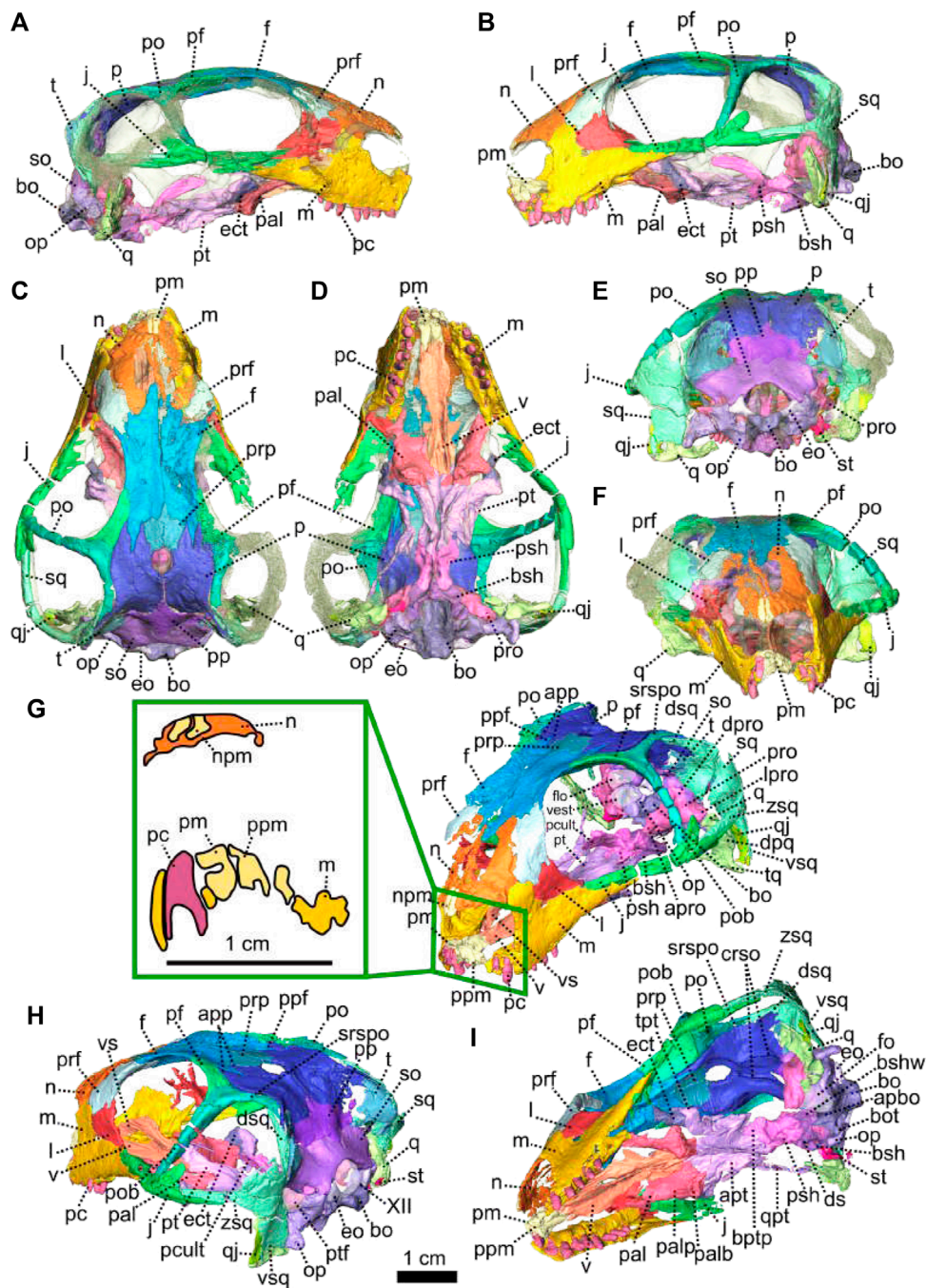
FIGURE 1
Patranomodon nyaphulii, NMQR 3000, from Combrinkskraal farm, Prince Albert district, Western Cape, South Africa; *Eodicynodon* AZ, Guadalupian, Beaufort Group, Karoo Supergroup. 3D rendering in **(A)**, right lateral view; **(B)**, left lateral view; **(C)**, dorsal view; **(D)**, ventral view; **(E)**, posterior view and **(F)**, anterior view; **(G)**, anterolateral view; **(H)**, posterolateral view and **(I)**, ventrolateral view. **(G)**, Transverse section at the level of the nasal process of the premaxilla, showing the premaxilla protruding into the nasals. Abbreviations: acst, anterior crus of the stapes; ang, angular; app, anterior process of the parietal; apobsh, anterior process of the orbitosphenoid; apt, anterior process of the pterygoid; art, articular; bo, basioccipital; bot, basioccipital tubera; bsh, basisphenoid; bshw, basisphenoid wing; bptp, basipterygoid process; c, caniniform tooth; dpq, dorsal plate of the quadrate; d, dentary; ds, dorsum sellae; dsq, dorsal process of the squamosal; ect, ectopterygoid; eo, exoccipital; f, frontal; fo, fenestra ovalis; icgq, intercondylar groove of the quadrate; ivv, intervomerine vacuity; j, jugal; l, lacrimal; lpro, lateral bulge of the prootic; m, maxilla; mcq, medial condyle of the quadrate; n, nasal; npm, nasal process of the premaxilla; op, opisthotic; p, parietal; pal, palatine; palb, palatal boss of the palatine; palp, palatal pad of the palatine; pc, postcanine; pcult, processus cultriformis; pf, postfrontal; po, postorbital; pob, postorbital bar; ppf, posterior process of the frontal; ppm, palatal process of the premaxilla; prsh, presphenoid; prf, prefrontal; pro, prootic; prp, preparietal; psh, parasphenoid; pt, pterygoid; ptf, postemporal fenestra; q, quadrate; qj, quadratojugal; qpt, quadrate process of the pterygoid; smtobsh, semi tubular region of the orbitosphenoid; so, supraoccipital; spl, splenial; st, stapes; sth, stapedial head; stf, stapedial foramen; stfp, stapedial footplate; sq, squamosal; srspo, skull roof section of the postorbital; sur, surangular; t, tabular; tpt, transverse process of the pterygoid; v, vomer; vkobsh, ventral keel of the orbitosphenoid; vkp, ventral keel of the palate; vps, vomer posterior septum; vs., vomerine septum; zsq, zygomatic process of the squamosal. Scale bar = 1 cm.
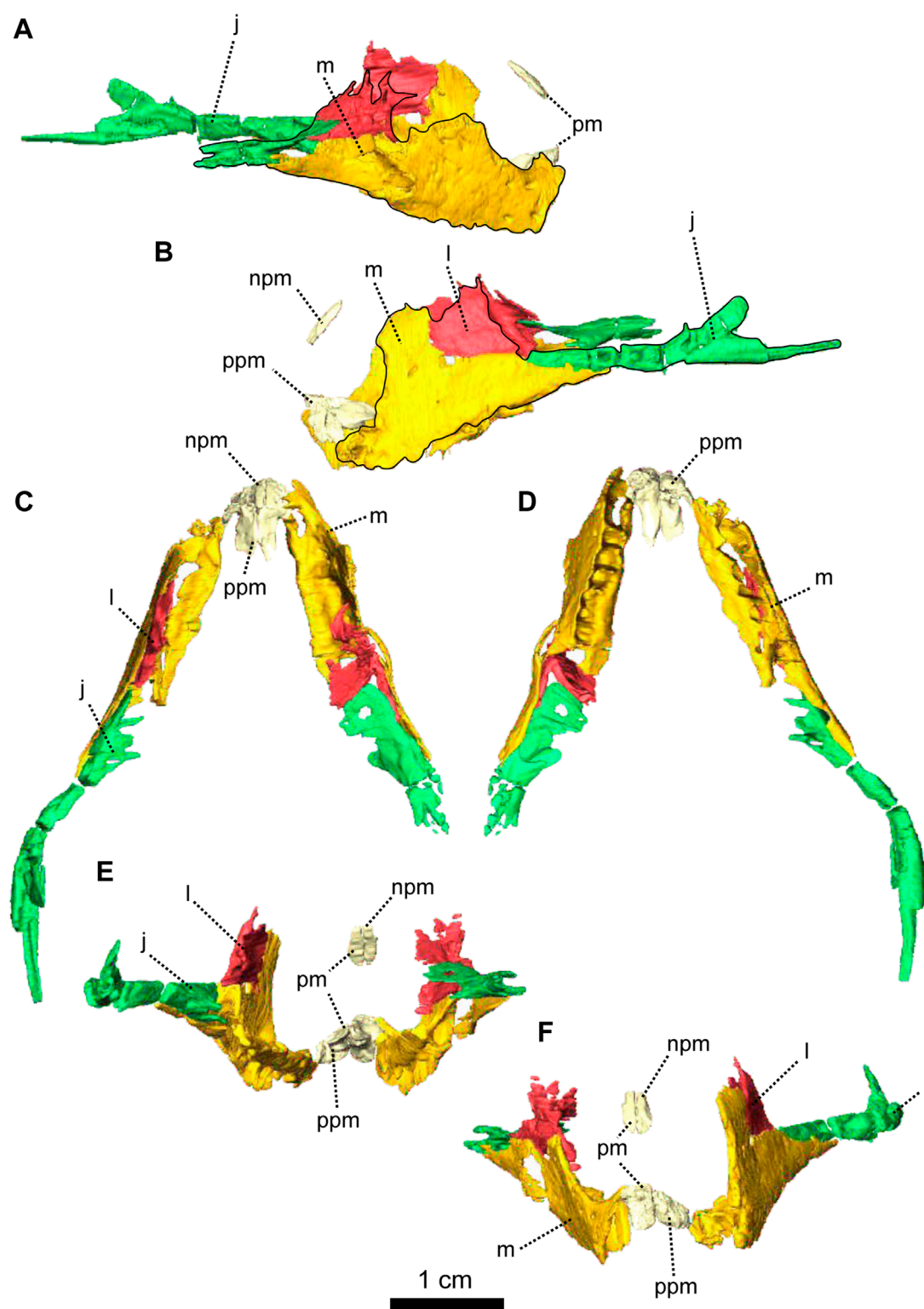
FIGURE 2
Paired maxillae and associated masticatory elements of *Patranomodon nyaphulii*, NMQR 3000, from Combrinkskraal farm, Prince Albert district, Western Cape, South Africa; *Eodicynodon* AZ, Guadalupian, Beaufort Group, Karoo Supergroup. 3D rendering in **(A)**, right lateral view; **(B)**, left lateral view; **(C)**, dorsal view; **(D)**, ventral view; **(E)**, posterior view and **(F)**, anterior view. Abbreviations: j, jugal; l, lacrimal; m, maxilla; n, nasal; npm, nasal process of the premaxilla; pm, premaxilla; ppm, palatal process of the premaxilla.

FIGURE 3
Parietal and associated dorsal elements of *Patranomodon nyaphulii*, NMQR 3000, from Combrinkskraal farm, Prince Albert district, Western Cape, South Africa; *Eodicynodon* AZ, Guadalupian, Beaufort Group, Karoo Supergroup. 3D rendering in **(A)**, right lateral view; **(B)**, left lateral view; **(C)**, dorsal view; **(D)**, ventral view; **(E)**, posterior view; **(F)**, anterior view. Abbreviations: app, anterior process of the parietal; apbo, anterior process of the basioccipital; apro, anterior process of the prootic; crso, canal for the ramus supraorbitalis; f, frontal; p, parietal; ppf, posterior process of the frontal; pf, postfrontal; po, postorbital; pob, postorbital bar; prf, prefrontal; srspo, skull roof section of the postorbital. Scale bar = 1 cm.

FIGURE 4
Occipital bones of *Patranomodon nyaphulii*, NMQR 3000, from Combrinkskraal farm, Prince Albert district, Western Cape, South Africa; *Eodicynodon* AZ, Guadalupian, Beaufort Group, Karoo Supergroup. 3D rendering in **(A)**, right lateral view; **(B)**, left lateral view; **(C)**, dorsal view; **(D)**, ventral view; **(E)**, posterior view and **(F)**, anterior view. Abbreviations: V, opening for the cranial nerve V, VII, foramen for the cranial nerve VII, XII, foramen for the cranial nerve XII or hypoglossal nerve; acst, anterior crus of the stapes; apbo, anterior process of the basioccipital; apro, anterior process of the prootic; ascc, attachment of the anterior semicircular canal; aso, anterior estension of the supraoccipital; bo, basioccipital; bot, basioccipital tubera; cc, crus communis; dpq, dorsal plate of the quadrate; dpro, dorsal process of the prootic; dsq, dorsal process of the squamosal; jf, jugular foramen; eo, exoccipital; fo, fenestra ovalis; icgq, intercondylar groove of the quadrate; jf, jugular foramen; lcq, lateral condyle of the quadrate; lnq, lateral notch of the quadrate; lpro, lateral bulge of the prootic; mcq, medial condyle of the quadrate; mpqj, medial process of the quadratojugal; op, opisthotic; opfeo, opisthotic facet of the exoccipital; pafeo, pro-atalas facet of the exoccipital; pla, pila antotica; pp, postparietal; pro, prootic; ptf, postemporal fenestra; q, quadrate; qj, quadratojugal; qpt, quadrate process of the pterygoid; so, supraoccipital; st, stapes; sth, stapedial head; stfp, stapedial footplate; sq, squamosal; t, tabular; tq, trochlea of the quadrate; vsq, ventral process of the squamosal; zsq, zygomatic process of the squamosal. Scale bar = 1 cm.

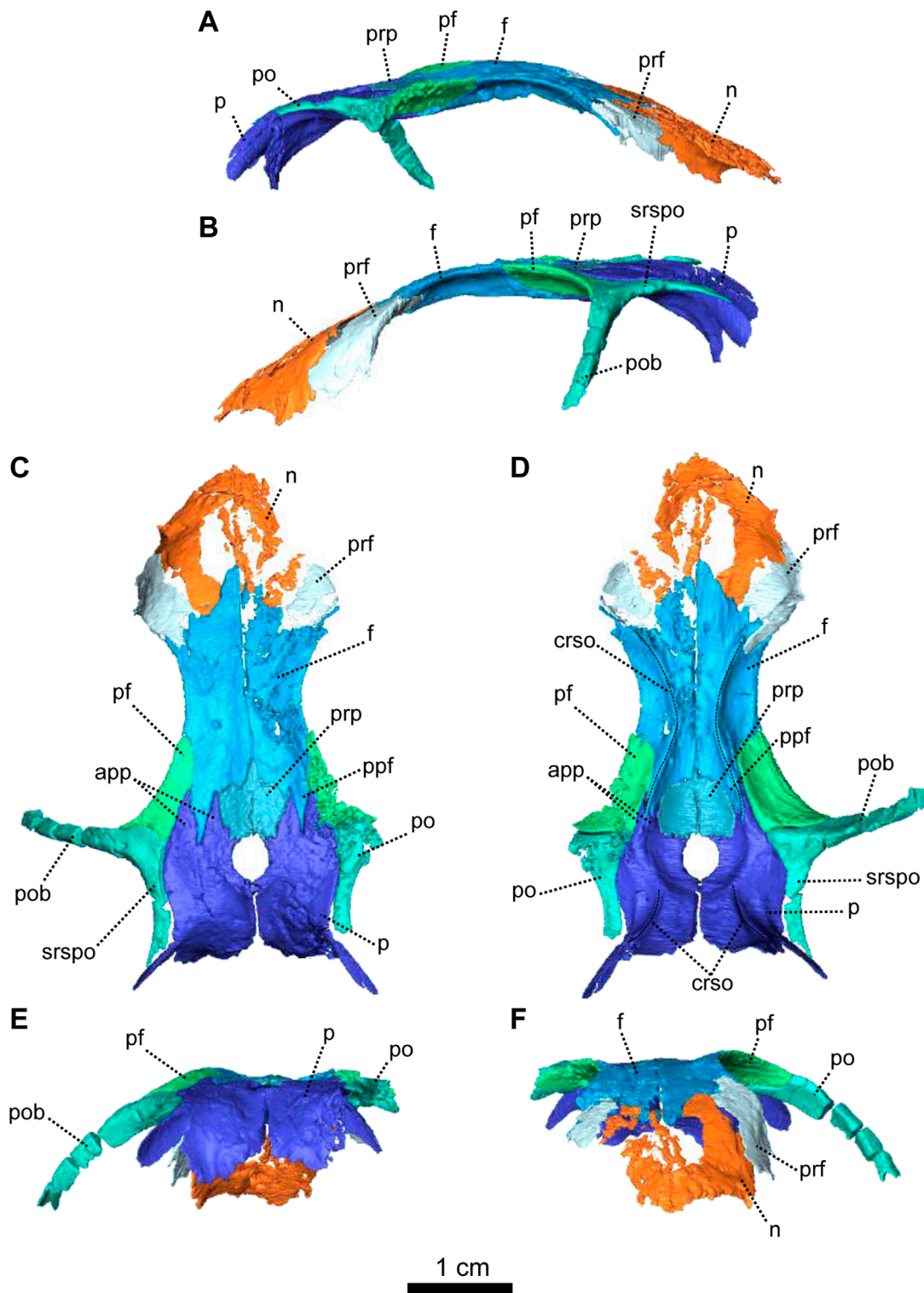**FIGURE 5**
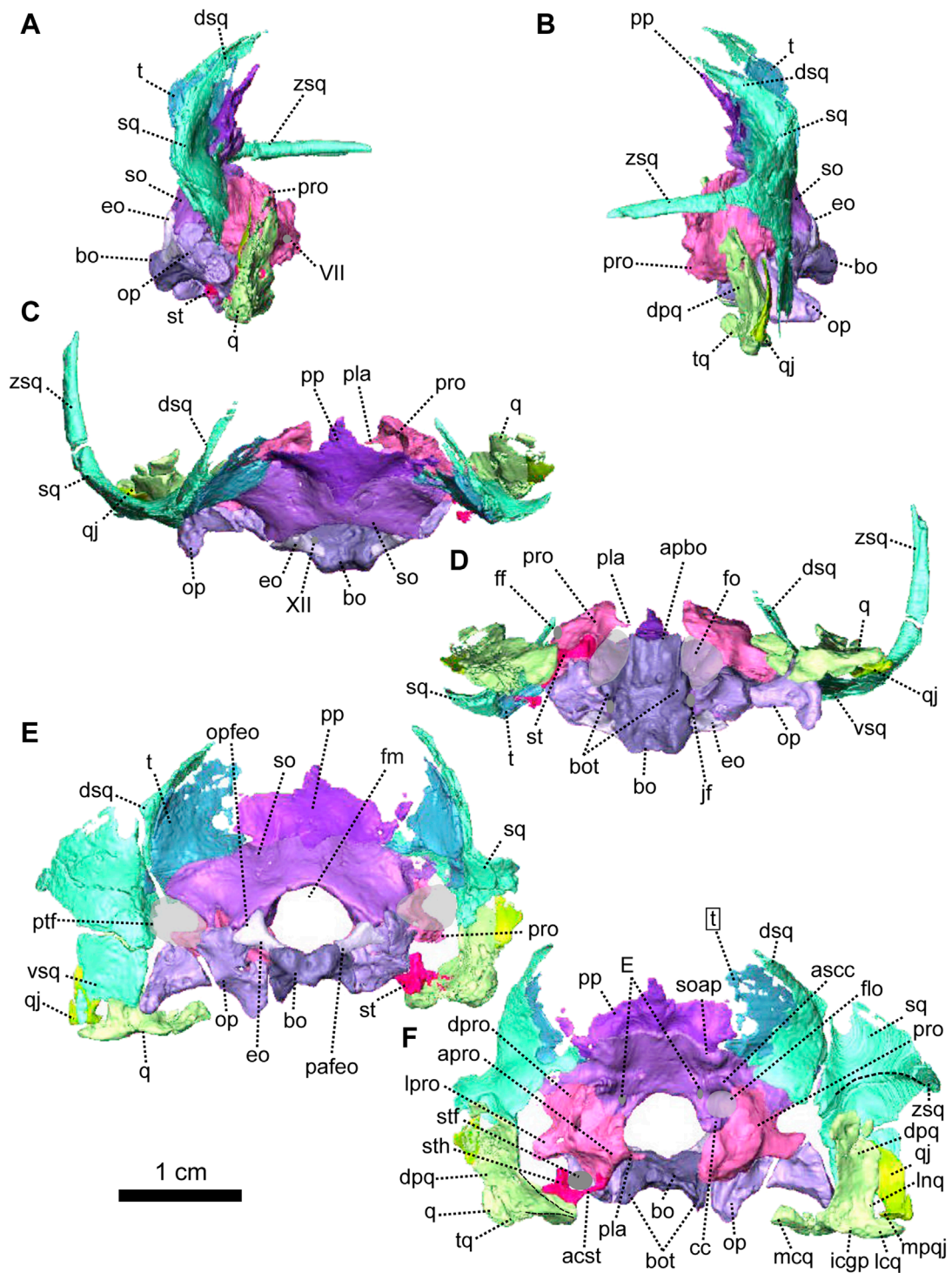Anatomical details of *Patranomodon nyaphulii*, NMQR 3000, from Combrinkskraal farm, Prince Albert district, Western Cape, South Africa; *Eodicynodon* AZ, Guadalupian, Beaufort Group, Karoo Supergroup. 3D rendering of the posterior part of the skull in **(A)**, left ventral view; **(B)**, left medial view and **(C)**, right anterodorsal view. Scale bar = 1 cm. Abbreviations: V, opening for the cranial nerve V, VII, foramen for the cranial nerve VII, XII, foramen for the cranial nerve XII or hypoglossal nerve; acst, anterior crus of the stapes; apbo, anterior process of the basioccipital; apro, anterior process of the prootic; ascc, attachment of the anterior semicircular canal; bo, basioccipital; bot, basioccipital tubera; cc, crus communis; dpq, dorsal plate of the quadrate; dpro, dorsal process of the prootic; dsq, dorsal process of the squamosal; eo, exoccipital; fo, fenestra ovalis; icgq, intercondylar groove of the quadrate; jf, jugular foramen; lcq, lateral condyle of the quadrate; lnq, lateral notch of the quadrate; lpro, lateral bulge of the prootic; mcq, medial condyle of the quadrate; mpqj, medial process of the quadratojugal; op, opisthotic; pla, pila antotica; pp, postparietal; pro, prootic; q, quadrate; qj, quadratojugal; soap, supraoccipital anteriorly projected crest; so, supraoccipital; st, stapes; sth, stapedial head; stfp, stapedial footplate; sq, squamosal; t, tabular; vest, vestibule; vsq, ventral process of the squamosal; zsq, zygomatic process of the squamosal.
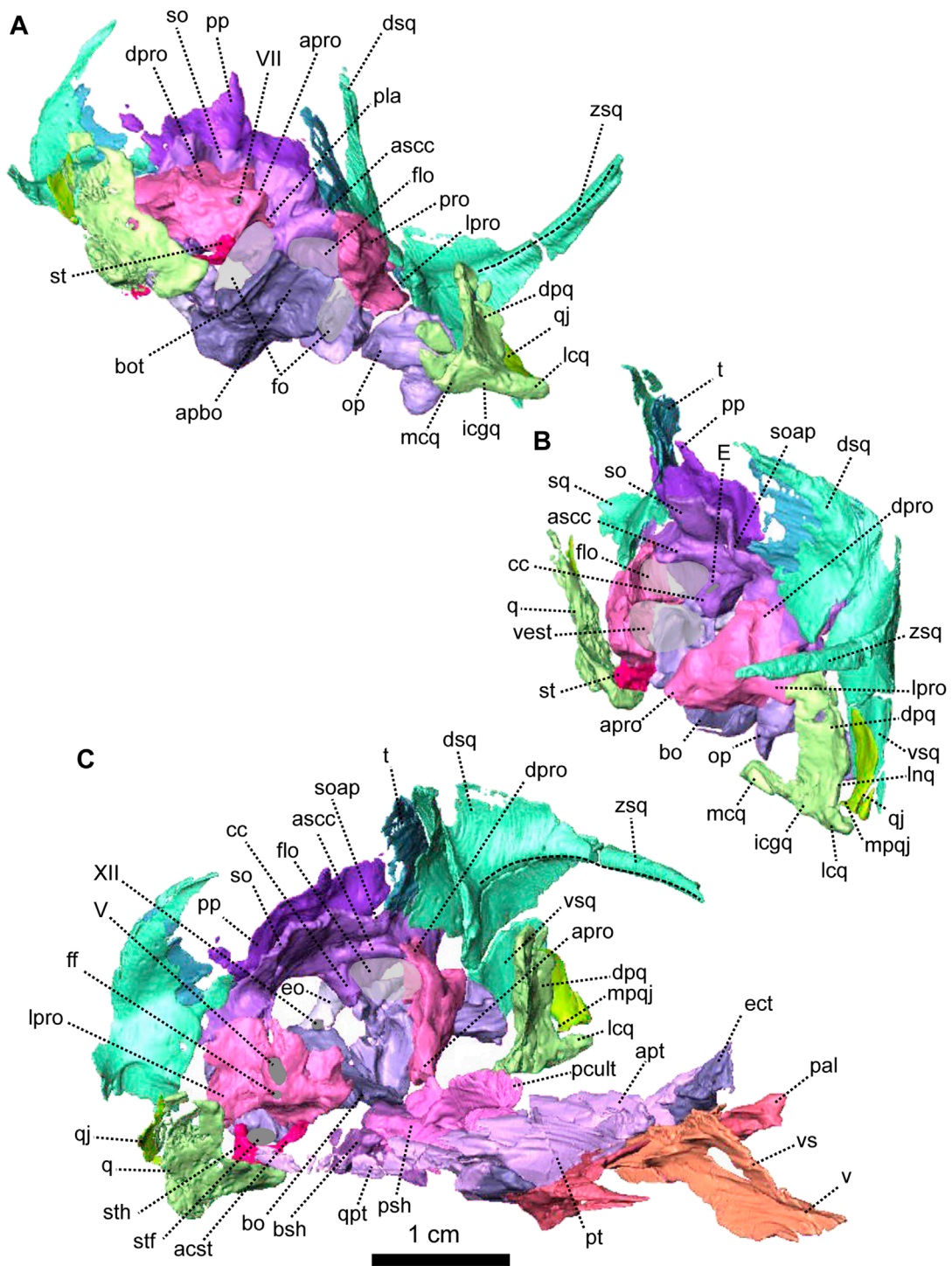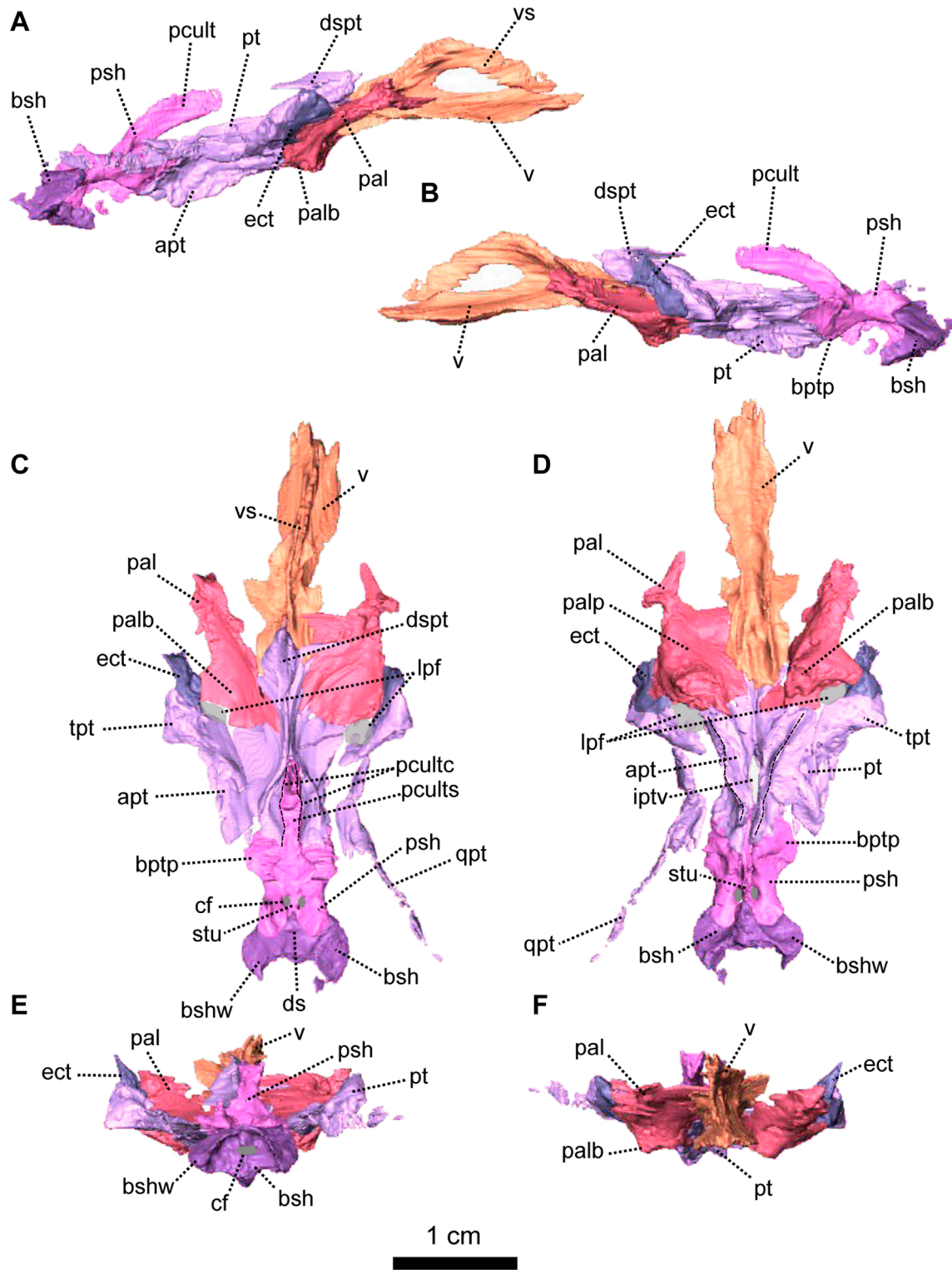
FIGURE 6
Palatal bones of *Patranomodon nyaphulii*, NMQR 3000, from Combrinkskraal farm, Prince Albert district, Western Cape, South Africa; *Eodicynodon* AZ, Guadalupian, Beaufort Group, Karoo Supergroup. 3D rendering in **(A)**, right lateral view; **(B)**, left lateral view; **(C)**, dorsal view; **(D)**, ventral view; **(E)**, posterior view and **(F)**, anterior view. Abbreviations: apt, anterior process of the pterygoid; bot, basioccipital tubera; bsh, basisphenoid; bshw, basisphenoid wing; bptp, basipterygoid process; cf, carotid foramen; ds, dorsum sellae; dspt, dorsal septum of the pterygoid; ect, ectopterygoid; iptv, interpterygoid vacuity; lpf, lateral palatal foramen; pal, palatine; palb, palatal boss of the palatine; palp, palatal pad of the palatine; pcult, processus cultriformis; pcultc, processus cultriformis crest; pcults, processus cultriformis sulcus; psh, parasphenoid; pt, pterygoid; qpt, quadrate process of the pterygoid; stu, sella turcica; tpt, transverse process of the pterygoid; v, vomer; vs., vomerine septum. Scale bar = 1 cm.

external naris (Figure 1B, G). In lateral view, the maxilla sends a dorsal process towards the nasal bone (Figures 1B) and the suture between the nasal and maxilla is slightly curved dorsally (Figure 1B). Posterodorsally, the maxilla contacts the prefrontal, and the lacrimal posteriorly (Figure 1B, 2B). Posteriorly, the zygomatic process of the maxilla forms the anteroventral margin of the suborbital bar. It extends along the ventral border of the jugal and tapers posteriorly below the middle of the orbit (Figure 1B, G). In ventral view, the maxilla comprises two processes, a short medial one toward the palatine and a longer zygomatic extension (Figures 1D, I, 2D). The maxilla does not form a secondary palate (Figure 2C, E). This suggests that the anterior portion of the palate of *Patranomodon* was likely soft. Another possibility is that *Patranomodon* did not have a palatal separation between the nasal cavity and the mouth. In medial view, the maxillary sinus is visible on the right side (Figure 1H). It is broadly triangular and located at the base of the zygomatic process of the maxilla. It is partially hidden by some broken pieces of the maxilla. Nine postcanines are preserved in the right maxilla and six in the left (Figures 1A, B, D, 2A, B, D). An additional potential empty socket is present at the back of the left maxilla. The disparity in the number of teeth between the right and left side of the maxilla could be due to preservation bias.

The left nasal bone of *Patranomodon* is almost complete, but the surface of the right nasal is weathered and fragmentary (Figures 1, 3). The nasal borders the dorsal margin of the external naris anterolaterally (Figure 1B). Posteromedially, the nasals share a W-shaped suture with the frontals (Figures 1C, G, 3). Anterolaterally, the nasal is overlapped by the maxilla, and the prefrontal on the posterolateral side (Figures 1F, 3F). Ventrally the internal surface of the nasal is slightly concave and smooth (Figure 3F).

The lacrimal is well preserved on the left side of the skull, but is incomplete on the right (Figures 1, 2). It makes up the anteroventral margin of the orbit (Figures 1B, H, 2B). In lateral view, the lacrimal has an oblique dorsal contact with the prefrontal (Figure 1B) and is bordered by the maxilla anteriorly and ventrally (Figure 2A, B). On the dorsal side of the zygomatic arch, the lacrimal extends posteriorly towards the anterior tip of the jugal bone, with which it shares a suture (Figures 1H, 2A–C). In posterior view, the intraorbital process of the lacrimal forms a vertical rectangular strip of bone (Figure 2E). The lacrimal foramen is not preserved.

The jugal is the largest bony element of the suborbital bar (Figure 1). In NMQR 3000, the left jugal is complete but the right one is missing (Figures 1, 2). It has a short contact with the lacrimal anteriorly at the level of the palatine (Figures 1B, D, 2B, D). Posteriorly, it extends below the squamosal to form the temporal portion of the zygomatic bar (Figure 1B, H) and contacts the postorbital at the base of the postorbital bar (Figure 1B). From this contact, the postorbital process of the jugal extends posterodorsally (Figures 1, 2). This process is flat and rounded dorsally in lateral view (Figure 2B). In lateral view, the jugal bears a small horizontal ridge at the level of the postorbital bar (Figures 1A, 2A). In dorsal view, the jugal appears bowed as it curves anteriorly beneath the orbit (Figure 2C) and tapers posteriorly (Figure 2C–E).

The left postorbital is complete but the right one has been damaged by weathering (Figures 1, 3, 5). The postorbital is a thin, curved bone which makes up the entire postorbital bar and a section of the skull roof (Figures 1G, H, 3). The postorbital bar separates the orbit from the temporal fenestra (Figure 1B, G, H)

and forms the anterior and anterodorsal margin of the temporal fenestra (Figures 1, 3). It reaches the zygomatic arch ventrally and meets the jugal (Figure 1B, H) with an oblique suture in lateral view (Figure 1B). The postorbital bar curves dorsally to become the horizontal skull roof section of the postorbital (Figures 3B, 5B). This section contributes to the intertemporal space, where it extends to the level of the anterior margin of the pineal foramen (Figures 1H, 3C). Anterodorsally, the postorbital overlaps and intrudes into the postfrontal (Figure 1B, C). Medially, the postorbital contacts the parietal (Figures 1C, D, 3C, D) and dorsally, the postorbital tapers and contributes to the occiput wall between the squamosal and the parietal (Figure 1C).

The left squamosal of NMQR 3000 is almost complete, but the right one is badly damaged by weathering (Figures 1, 4, 5). The squamosal comprises three processes: a ventral process, a dorsal process and a zygomatic process (Figures 1, 4, 5). The ventral process occupies a large surface on the occiput (Figure 4E) and overlaps the dorsal process of the quadrate ventrally (Figures 1, 5). The dorsal process of the squamosal forms the posterodorsal margin of the temporal fenestra (Figure 1H) and extends dorsomedially towards the postorbital along the parietal (Figure 1E, H). In posterior view, the dorsal process of the squamosal is concealed by the overlapping tabular and supraoccipital (Figures 4E, F, 5B, C). It reaches the supraoccipital in anterior view (Figure 1G). The zygomatic process forms the ventral margin of the postemporal fenestra (Figure 1B, H) and tapers anteriorly to the level of the postorbital bar (Figures 1B, H, 4B). The squamosal has a long horizontal contact with the jugal anteroventrally, such that the squamosal rests on top of the posterior process of the jugal, beneath the temporal fenestra (Figure 1B, H). On its posteromedial surface, the zygomatic process of the squamosal bears a horizontal ridge (Figures 4F, 5A, C). A similar condition is found on the more derived anomodont *Niassodon* (Castanhinha et al., 2013).

As noted by Rubidge and Hopson (1996), the squamosal is not folded backward (condition seen in dicynodonts, see NMQR2978 below and *Niassodon* in Castanhinha et al. (2013)) but is rather convexly rounded dorsally. A similar condition is found in Biarmosuchia and Dinocephalia (Rubidge and Hopson, 1996; Sidor, 2003; Kruger et al., 2018; Duhamel et al., 2021) and is believed to be plesiomorphic for therapsids (Rubidge and Hopson, 1996).

Both prefrontals are preserved on NMQR 3000, but the left one is slightly larger and better preserved (Figures 1, 3). The prefrontal in NMQR 3000 borders the anterodorsal margin of the orbit (Figure 1H). In both dorsal and ventral views, the contact between the frontal and prefrontal is V-shaped posteromedially, such that the prefrontal extends posteriorly into a notch that is just medial to the anterolateral-most margins of the frontals (Figures 1B, C, D, 3B, C, D). In lateral view, the prefrontal contacts the dorsal margin of the lacrimal ventrally (Figure 1B, G). The contact is oblique anteriorly, and becomes S-shaped posteriorly; as previously recognized by Rubidge and Hopson (1996). Above the lacrimal, the prefrontal has a short anteroventral contact with the dorsal extension of the maxilla (Figure 1B, G) and has a longer oblique contact with the nasal anterodorsally (Figure 3B, D).

The frontal forms most of the dorsal margin of the orbit, between the prefrontal anteriorly and the postfrontal posteriorly (Figure 1, 3). As in most therapsids, the paired frontals constitute a large portion of the supraorbital skull roof and contact each other along

the midline. The midline suture is straight and non-interdigitated (Figure 13C, D). In dorsal view, the frontal has a short contact with the prefrontal anterolaterally (Figure 3C) and meets with the nasal anteriorly (Figure 3C). Unlike most dicynodonts, in which the suture is transverse, the frontals intrude into the nasals forming a V-shaped suture, such that the anteromedial-most extension of the frontals are anterior to the posterolateral-most extensions of the nasals (see BP/1/6230, NMQR 2978 and Damiani et al., 2007; Castanhinha et al., 2013; Kammerer, 2016b; Angielczyk and Kammerer, 2017; Angielczyk et al., 2019). The frontal shares a curved suture with the postfrontal posterolaterally (Figure 3C). In both dorsal and ventral view, the frontal has a posterior process that incises the parietal (Figures 1, 3–C, D) as in other non-mammalian therapsids (van Heerden, 1972; Rubidge and Kitching, 2003; Fröbisch and Reisz, 2008; Castanhinha et al., 2013; Kammerer, 2016a; Kammerer, 2016b; Pusch et al., 2019; Pusch et al., 2020). In ventral view, the frontal bears a medially curved ridge (Figures 1I, 3D) which has its origin on the prefrontal and extends posteriorly onto the parietal. This ridge represents the external margin of the olfactory tract posteriorly and the olfactory cavity anteriorly (*ramus supraorbitalis*). No foramen could be identified on the frontal of NMQR 3000.

The postfrontal on NMQR 3000 is an elongated, roughly triangular, flat bone bordering the dorsal margin of the orbit (Figures 1, 3). It is bordered by the frontal anteromedially, the parietal posteromedially and the postorbital posteriorly (Figure 3C). The contact between the frontal and postfrontal is curved (Figure 3C). In ventral view, the postfrontal overlaps the frontal medially (Figure 3D). The contact between the postfrontal and parietal is oblique, both in dorsal and ventral views (3-C and D). Posteriorly, the postfrontal has a curved sutural contact with the postorbital (Figure 3C). In dorsal view, at the contact with the postorbital, the postfrontal projects two small triangular processes posterolaterally and posteromedially respectively. In ventral view, the suture between the postfrontal and postorbital is transverse (Figure 3D). The ventral side of the postfrontal is excavated by a shallow fossa.

In dorsal view, the preparietal is a small, trapezoidal bone, bordering the anterior margin of the pineal foramen (Figures 1, 3) and has a short triangular process extending anteriorly between the two frontals (Figure 3C). This triangular process is less pronounced and thinner in ventral view (Figures 1I, 3D). In dorsal view, the preparietal contacts the parietal laterally and posterolaterallly (Figure 3C). The contact is straight laterally and becomes interdigitated posteriorly (Figure 3C, D). Importantly, the remnant of a midline suture is visible on the posterior part of the preparietal (Figure 3C). In ventral view, the preparietal has a rounded anterolateral margin (Figures 1I, 3D).

The parietal is a large smooth paired bone forming most of the posterior part of the skull roof (Figures 1, 3) and extends posteroventrally on the occipital face (Figure 1). Both parietals suture along the midline (Figure 3) and border the lateral and posterior margins of the pineal foramen (Figures 1H, 3E). In dorsal and posterior views, the parietal shows two equal-sized triangular anterior processes: one lateral and the other medial (Figure 3C, D). The anterolateral process extends between the postfrontal and the frontal bones and the more medial process is situated between the frontal and the preparietal. The anterior suture of the parietal with

the preparietal is tranversely straight in ventral view and further laterally the suture with the frontal forms a W around the olfactory ridge (Figures 1I, 3D).

On the occiput, the parietal is overlapped by both the tabular and the postparietal (Figures 1E, 3E) such that the parietal extends laterally beneath the tabular and incises the dorsal process of the squamosal (Figures 1B, C, E, 3C, E). In ventral view, the parietal has a well-formed depression around the pineal foramen (Figure 3D).

The occiput of NMQR 3000 is damaged on the right side and well preserved on the left (Figure 1). As a consequence, the following description is based mainly on the left side (Figures 1, 4, 5). The external surface is smooth and does not show any ornamentation (Figures 1, 4). The foramen magnum is large, rounded and bordered by the supraoccipital dorsally, the exoccipitals laterally, and the basioccipital ventrally (Figure 4E). The postemporal fenestra is half the size of the foramen magnum and is formed by the tabular dorsally, the squamosal laterally, the opisthotic ventrally, and the supraoccipital medially (Figures 1E, H, 4E, F).

The postparietal is a narrow unpaired bone located on the dorsal-most half of the occiput (Figures 1, 4, 5). Its external surface is flat and the internal surface slightly wrinkled (Figures 4E, F, 5B, C). In posterior view, the dorsal side of the postparietal overlaps the parietal (Figure 1E, H). In the same view, the postparietal is a transversely elongated bone with pointed dorsal and ventral processes (Figure 4E) and the dorsal process overlaps the parietal (Figure 1C, E, H). In occipital and anteromedial views it is evident that the postparietal overlaps the supraoccipital ventrally (Figure 4C, 5B). In posterior view, the postparietal contacts the tabular laterally (Figures 1E, 4E) but the contact is not well preserved. On its internal surface, the postparietal exhibits a broad and blunt vertical midline ridge (Figures 4F, 5).

The tabular, which forms the dorsolateral part of the occipital surface on NMQR 3000, is a thin bone (Figures 1E, H, 4E). The tabular overlaps the posterolateral portion of the parietal along the posteromedial border of the temporal fenestra (Figure 1C, E) and laterally overlies the medial side of the squamosal (Figure 1H, 5C). As a result, the anterior exposure of the tabular in anterior view is greatly reduced (Figures 4E, F, 5B, C). In posterior view, the tabular shares a transverse suture with the supraoccipital ventrally and forms the dorsolateral margin of the postemporal fenestra (Figure 4E).

As in other therapsids, the inner ear system of *Patranomodon* is housed by the supraoccipital, prootic, opisthotic, exoccipital, and basioccipital (Olson, 1944; Cox and Broom, 1962; Fourie, 1974; Sigogneau, 1974; Luo et al., 1995; Luo, 2001; Cifelli et al., 2004; Surkov and Benton, 2004; Araújo et al., 2017; Pusch et al., 2019). With the exception of the basioccipital, all these bones accommodate part of the semicircular canals (Pusch et al., 2019) and the auditory capsule is formed by the prootic, the opisthotic and the supraoccipital (Cluver, 1971). The supraoccipital and the prootic enclose the floccular fossa dorsally, while the prootic and the opisthotic enclose the vestibular fossa ventrally (Figure 5B, C).

The supraoccipital is the largest of the occipital bones in anomodonts (Rubidge and Hopson, 1996; Fröbisch and Reisz, 2008; Castanhinha et al., 2013). This bone is well preserved in NMQR 3000 (Figures 1, 4, 5) and makes up the rounded dorsal margin of the foramen magnum (Figure 4E, F). In posterior view, the supraoccipital bears two small symmetrical depressions that extend dorsally onto the surface of the postparietal (Figure 4E).

Dorsally, the supraoccipital is overlapped by the postparietal (Figure 4C, E, F). Dorsolaterally, it has a curved contact with the tabular (Figure 4E, F). Ventromedially, in posterior view, the supraoccipital has an oblique contact with the exoccipital and meets the opisthotic (Figure 4E). Laterally, the supraoccipital has a diagonal edge that borders the postemporal fenestra (Figure 4E). In anterior view, the supraoccipital overlaps part of the ventromedial section of the squamosal (dorsal ramus of the squamosal, Figure 5B, C). In the same view, the supraoccipital bears an anteriorly projected dorsal crest, and the anterior semicircular crests laterally (see Macungo et al. (2022); Figures 4F, 5B, C). The semicircular crest of the supraoccipital accommodates the anterior semicircular canals, at the level of the contact with the prootic (Araújo et al., 2017; Pusch et al., 2019; Macungo et al., 2022). This crest delineates the dorsal margin of the floccular fossa (Figure 5B). Ventral to the floccular fossa, the supraoccipital bears a crest that forms the attachment for the crus communis (Figures 4F, 5C).

The prootic, sometimes referred to by the mammalian term periotic (fusion of the opisthotic, the prootic, the epiotic and sometimes the supraoccipital, see Angielczyk et al., 2021) is positioned on the anterior side of the occipital wall in anomodonts (Rubidge and Hopson, 1996; Surkov and Benton, 2004; Castanhinha et al., 2013) and forms part of the sidewall of the braincase (Castanhinha et al., 2013; Laaß, 2015a; Laaß, 2015b). It comprises three parts: the prootic dorsal process, prootic lateral bulge, and prootic anterior process (Figures 4, 5). The latter extends ventromedially into the pila antotica (Figures 4D, F, 5A). The pila antotica, only preserved on the right prootic, is incomplete. It forms a slender triangular process.

The dorsal process of the prootic is triangular in anterior view (Figure 4F) and contacts the supraoccipital posteriorly at the level of the postemporal fenestra (Figure 5C). It forms the attachment of the anterior semicircular canal dorsally along with the supraoccipital (Figures 4F, 5B, C). In medial view, the dorsal process of the prootic is curved with a dorsal and a posterior process (Figure 5B), which form the anterior margin of the floccular fossa.

The lateral process of the prootic, which is rectangular in anterior view, extends laterally toward the quadrate (Figures 4, 5B, C, F) and forms a smooth angle with the dorsal process. In ventral view, the surface of the lateral process of the prootic is concave (Figure 4D). It contacts the opisthotic posteriorly (Figures 4D, 5A).

The anterior process of the prootic is roughly triangular in lateral and lateroventral views (Figures 4A, B, 5A) and forms the curved anterior margin of the vestibular chamber (Figure 5B). In anterolateral view, the anterior process of the prootic contacts the parasphenoid anteriorly (Figure 5C) and turns into the dorsal process at the level of the foramen for the cranial nerve V (Figure 5C). The foramen is large and leads into the vestibular chamber where it contacts the opisthotic posteriorly. Below the foramen for cranial nerve V, is the small foramen for the facial nerve (Figure 5C). The foramen for the nerve VII is positioned at the anterioventral side of the anterior process of the prootic; and is visible in lateral and lateroventral views (Figures 4A, 5A). Also in ventral and in lateroventral views, the prootic has a short curved posterior contact with the stapes (Figures 4A, 5B). The anterior process of the prootic forms the anterolateral margin of the fenestra ovalis, where it bears a slight depression towards the pila antotica (Figures 4D, 5A).

The opisthotic constitutes a large part of the posterior portion of the periotic region. It is sometimes fused with the prootic (to form the periotic) and/or the exoccipitals. It forms the posterior border of the vestibular fossa (Figure 5B). Posteriorly, it forms the ventral margin of the postemporal fenestra (Figures 1, 4, 5A). In posterior view, the opisthotic has two robust triangular ventral processes, one lateral and one medial, the latter being the paroccipital process (Figure 4E). Between these two processes, the ventral margin of the opisthotic is notched by the opening of the fenestra ovalis (Figure 4E). The ventrolateral process is the longest and contacts the quadrate ventrolaterally (Figure 4E, F), and dorsolaterally has an oblique suture with the squamosal (Figure 4E). The ventromedial process shares a vertical contact with the basioccipital tubera on the medial side. In ventral view, the jugular foramen is positioned between the opisthotic and the basioccipital (Figure 4D).

In contrast with the condition in more derived therapsids (Pusch et al., 2019) and dicynodonts (Castanhinha et al., 2013; Macungo et al., 2022), the opisthotic of NMQR 3000 is not fused to the prootic. In lateral view, the suture between the opisthotic and the prootic is slightly oblique and located anterior to the opisthotic (Figure 4A). Both the prootic and the opisthotic enclose the vestibular fossa (Figure 5B). In ventral view, the left opisthotic forms a thick semicircular ridge contributing to the posterior margin of the fenestra ovalis (Figure 4D). In lateral view, the ventrolateral process of the opisthotic is excavated by a deep ventral fossa (Figure 4A). In posterior view, the opisthotic meets the squamosal laterally (Figure 4E) and is overlapped by the exoccipital dorsomedially.

The exoccipital is a small trapezoidal bone forming the ventrolateral margin of the foramen magnum (Figures 1, 4). The exoccipital of NMQR 3000 is not fused to any surrounding bones, nor to the basioccipital condyle, unlike in more derived anomodonts (Castanhinha et al., 2013). In posterior view, the exoccipital tapers medially, such that it is broader laterally than medially. Its dorsal-most margin is accommodated within a triangular notch in the supraoccipital (Figure 4E). The ventromedial suture with the basioccipital is similar (Figure 4E) and forms the proatlas facet.

The basioccipital encloses the braincase ventrally (Figures 4, 5). It is formed by the occipital condyle, two dorsal lobes, the basioccipital tubera and a saddle-shaped anterior process (Figures 1, 4, 5). The basioccipital contributes to the medial and the posteromedial margin of the fenestra ovalis (Figures 4D, 5A). In posterior view, the basioccipital forms the ventromedial margin of the foramen magnum and its two dorsolateral lobes suture with the exoccipitals (Figure 4E). The occipital condyle has a rounded occipital pit. In the same view, the basioccipital tubera are triangular (Figure 4E). They contact the opisthotic laterally and the contact is flat, vertical and at the level of the jugular foramen. In dorsal view, the basioccipital is roughly rectangular, with its longest axis oriented anteroposteriorly. On its dorsal surface, the foramen for the hypoglossal nerve (cranial nerve XII) is located on the suture between the basioccipital and exoccipital (Figures 1, 4C, 5C). The anterior process of the basioccipital bears the longitudinal intertuberal ridge (Figure 4C) and reaches the basioccipital anteriorly (Figure 1D). In ventral and lateroventral view, the surface of the basioccipital is excavated by a shallow anteroposteriorly oriented fossa that forms a concave surface (Figures 4D, 5A). The fossa is bordered by two longitudinal ridges

that separate the main body of the basioccipital bone from the fenestra ovalis. In the same views, the two basioccipital tubera, that are oriented towards the opisthotic, contribute to the posteromedial margin of the fenestra ovalis (Figures 4D, 5A).

In NMQR 3000, the stapes is a small bone positioned between the dorsomedial side of the quadrate and the lateral margin of the fenestra ovalis (Figures 4D, 5A). The right stapes is missing and the left one is partially broken (Figures 4, 5). The stapes of NMQR 3000 is missing its posterior crus and the stapedial footplate. When fully preserved, it would have most likely been shaped with two crura (the bicrurate condition), a stapedial head and footplate. This differs from the condition observed in Dicynodontia, where the stapes is often hourglass-shaped (Sullivan and Reisz, 2005; Castanhinha et al., 2013). The anterior crus is thin and short (Figures 4F, 5C). Medially, it contacts the ventral margin of the anterior process of the prootic. The contact is short and curved in lateral and lateroventral views (Figures 4A, 5A). Lateroventrally, the anterior crus contacts the stapedial head (Figure 5C). In lateral and lateroventral views, the stapedial head is roughly triangular (Figures 4A, 5C) and has a posterodorsal process similar to that of the cynodont *Thrinaxodon* (Pusch et al., 2019). In anterior view, the stapedial head contacts the medial condyle of the quadrate's trochlea laterally (Figure 4F). The contact is oblique in ventral view (Figure 4D) and roughly horizontal in medial view (Figure 5B). The stapedial head and the anterior crus form the lateral and anterior margins of the stapedial foramen (Figures 4F, 5C).

The quadrate comprises a ventral trochlea and a dorsal vertical plate (Figures 1, 4, 5). The dorsal plate is a thin transverse extension (Figures 4B, 5B) and is overlapped posteriorly by both the quadratojugal and the squamosal (Figures 1, 4, 5B). The dorsal plate bears a lateral notch, that would have accommodated the medial process of the quadratojugal (Figure 5B, C). The trochlea of the quadrate is the articulation surface for the articular bone of the lower jaw (Figure 4B, F). It is formed by the rounded and well-defined lateral condyle of the quadrate, a smaller medial condyle, and a concave intercondylar groove (Figures 4F, 5A, B). In anterior view, the medial condyle of the right quadrate bears two small oblique ridges that originate respectively on the dorsal plate and lateral condyle (Figure 4F), before joining on the medial condyle of the trochlea.

In lateral view, the quadratojugal is a vertical strip of bone located between the squamosal posteriorly and the quadrate anteriorly (Figures 1G, H, 4E, F, 5B, C). Both quadratojugals are preserved in NMQR 3000. The left quadratojugal thickens ventrally to form a small flat surface (Figure 4B, D, E) that bears a small ventromedial hook (Figures 4E, F, 5B, C). This is the medial process of the quadratojugal that is accommodated by the lateral notch of the quadrate (Pusch et al., 2019).

The palate of NMQR 3000 is overall well preserved but most of the sphenethmoidal bones are missing (Figures 1, 5A, C, 6) and only the parasphenoid is preserved on the specimen (Figures 1G, I, 5C, 6). One notable anatomical feature is that the parasphenoid and the basisphenoid are two distinct bones, contra Rubidge and Hopson (1996) who considered that they were fused. In therapsids, they are usually fused to form the parabasisphenoid (Sidor and Rubidge, 2006; Pusch et al., 2019) but for them to be unfused is not uncommon among anomodonts (Castanhinha et al., 2013; Macungo et al., 2022).

The vomer comprises a ventral plate and a long and tall dorsal septum (Figures 1, 5, 6). The ventral plate reaches the premaxillary palatal process anteriorly at the level of the third maxillary tooth (Figure 1D) and the dorsal septum divides the nasal cavity medially (Figures 1H, 6). In lateral view, a large hole is present in the vomerine dorsal septum (Figures 6A, B) and is likely due to postmortem damage. However, Ivakhnenko (2008) reported the presence of a large foramen in some therapsids in the same area of the internasal septum. In ventral view, the ventral plate of the vomer is excavated by a deep midline groove bordered by two sharp lateral ridges (Figure 6D). Posterolaterally the vomer contacts the palatine and posteriorly forms the anterior margin of the interpterygoid vacuity at the level of the posterior end of the maxilla (Figures 1D, 6D). It was previously suggested that the vomer of *Patranomodon* may be a paired structure (Rubidge and Hopson, 1996), but no suture could be identified on the CT images.

In ventral view, the palatine is positioned posteromedially to the maxilla and extends posteriorly up to the anterior ramus of the pterygoid (Figures 1I, 7D). It comprises mainly the palatine pad (Castanhinha et al., 2013), which includes a well-defined and thick edentulous palatine boss (Figure 6A, B, D, F). In ventral view, the palatine pad extends anteriorly to reach the maxilla behind the last maxillary tooth (Figure 1D, I). In the same view, the palatine contacts the ectopterygoid posterolaterally, at the level of the palatine bosses. The palatine pad contacts the pterygoid posteromedially (Figure 1D, I) and forms the medial and the anterior margins of the lateral palatal foramen (Figure 6D). On its dorsal surface, the palatine bears a steep depression posteriorly, which corresponds to a negative image of the corresponding palatine boss (Figure 6C).

The pterygoid of NMQR 3000 is paired and presents the typical tripartite therapsid morphology with anterior, transverse and quadrate rami (Figures 1, 5C, 6). The interpterygoid vacuity of NMQR 3000 is narrow and diamond-shaped 6-D). *Patranomodon* does not show the pronounced ventrally oriented transverse ramus which is characteristic of *Eodicynodon* specimens. On the right, the transverse ramus is detached from the main body but the left side is intact (Figure 6C, D). In ventral view, the transverse ramus is roughly triangular (Figure 6D), forms the posterior margin of the lateral palatal foramen, and contacts the ectopterygoid anteriorly (Figures 5C, 6), with an oblique suture in lateral view (Figure 6A). The transverse ramus forms an angle of 90° with the sagittal plane of the skull (Figure 6D).

The anterior ramus comprises a ventral ridge, dorsal septum and median plate (Figures 1I, 5C, 6A–D). The median plate contacts the palatine anteriorly at the level of the palatine bosses. This contact is oblique in ventral view (Figure 6D) and transverse in dorsal view (Figure 6C). The median plates contact anteriorly, enclosing the interpterygoid vacuity anteriorly.

The ventral ridge of the anterior ramus is oblique in ventral view (Figure 6D). Both rami contact posteriorly and enclose the interpterygoid vacuity posteriorly. In lateral view, the ventral ridge becomes taller posteriorly (Figure 6A) and contacts the palatine anteriorly. This contact is oblique in ventral view (Figure 6D).

Dorsally, the anterior ramus of the pterygoid is laterally flattened, and projects into a vertical septum medially (Figure 6A–C). This septum extends between the two palatine bones to reach the vomer's septum anteriorly at the level of the ectopterygoid (Figures 5C, 18A, B). The contact is oblique in lateral

and anterolateral views. In ventral view, the anterior ramus of the pterygoid meets the parasphenoid posteromedially at the level of the basipterygoid process. The contact is oblique in lateral view (Figures 1I, 6A, B) and forms the floor of the hindbrain (Castanhinha et al., 2013; Pusch et al., 2019). No medial plate, usually found in derived anomodonts at the contact with the parabasisphenoid (Castanhinha et al., 2013; Laaß and Schillinger, 2015; Laaß et al., 2017), could be identified in the specimen.

The quadrate ramus of the pterygoid is preserved only on the right side and is detached from the main body of the pterygoid (Figures 1I, 5C, 6C, D). This ramus is slender posteriorly and thickens at the level of the parasphenoid. It makes an angle of 45° with the sagittal plane of the skull.

Both ectopterygoids are present and are small elements forming the anterolateral aspect of the transverse process of the pterygoid (Figures 5C, 6). An ectopterygoid is present in most anomodont taxa (Castanhinha et al., 2013), but has been lost in derived dicynodonts such as *Lystrosaurus* (Cluver, 1971), although it is retained in some juveniles (Benoit pers. obv.). In lateral view, the ectopterygoid is roughly triangular and extends dorsally (Figure 6B) and the contact between the ectopterygoid and the pterygoid is oblique. In ventral view, the ectopterygoid contacts the palatine medially (Figure 6D). It forms the lateral margin of the lateral palatal foramen (Figure 6C, D).

The sphenethmoidal complex of NMQR 3000 is poorly preserved, and of the internal bones that support the hindbrain and the forebrain, only the parasphenoid and the basisphenoid remain (Figures 5C, 6).

The parasphenoid is unpaired and includes the processus cultriformis (often called parasphenoid rostrum (Castanhinha et al., 2013; Macungo et al., 2022)) anteriorly, two hourglass-shaped processes laterally, and the sella turcica medially (Figures 5C, 6). The two carotid foramina are present and visible in both dorsal and ventral views (Figure 6C, D). They form two separate canals. The *canalis vidii* (the palatal branch of the cranial nerve VII) is not visible on NMQR 3000.

The processus cultriformis is a rod-like structure, originating on the sella turcica and curving anterodorsally to the level of the anterior margin of the interpterygoid vacuity (Figures 5C, 6). The base of the processus is large and the processus becomes thinner anteriorly (Figure 6C). In both dorsal and lateral views, the base of the processus cultriformis is triangular (Figure 6B, C). The dorsal surface of the process bears two lateral crests and a median sulcus (Figure 6C). The base of the processus cultriformis supports the anteroventral section of the hindbrain behind the hypophysis (Castanhinha et al., 2013).

Two hourglass-shaped processes form the lateral margin of the carotid foramina (Figure 6C, D) and contact the prootic posterodorsally (Figures 1A, B, 5C). The anterior-most part of the hourglass-shaped process is formed by the basipterygoid processes, referred as the basisphenoidal tubers in Macungo et al. (2022) (Figure 6). In lateral view, the basipterygoid process is roughly triangular (Figure 6B) and bears a small ventral keel, referred to as the parasphenoid keel in Araújo et al. (2017). It has a reversed V-shaped contact anteriorly with the anterior ramus of the pterygoid. At this point, the basipterygoid process tapers to a mediolaterally thin point where it contacts the pterygoid. In lateral view, the hourglass-shaped process has a V-shape contact with the

basiphenoid posteriorly (Figure 6A, B). In dorsal and ventral views, the contact between the parasphenoid and the basisphenoid is round (Figure 6C, D).

The sella turcica forms the central part of the parasphenoid (Figure 6C). It makes up the medial and posterior margin of the carotid foramina and extends ventrally in a thin septum (Figure 6A, B, D).

The basisphenoid is unpaired, lies at the base of the hindbrain and encloses posteroventrally the brain cavity in therapsids (Castanhinha et al., 2013). In NMQR 3000, the basisphenoid is bordered by the parasphenoid anteriorly and the basioccipital posteriorly (Figures 1I, 5C, 6). In dorsal view, the dorsum sellae is a thin medial triangular process (Figure 6C) that tapers between the hourglass-shaped processes of the parasphenoid and is surrounded by two laterally projecting symmetrical wings (Figures 1I, 6C, D). In ventral view, the wings form the anterior margin of the fenestra ovalis and have a depression between them (Figure 1D, I). In the same view, the basisphenoid bears a triangular process medially that differs from the sella turcica. In lateral view, this process makes an angle of 30° with the horizontal plane ventrally (Figure 6A, B). It contacts the ventral septum of the parasphenoid anterodorsally. In the same view, the basisphenoid wings make an angle of 30° dorsally and contact the parasphenoid with a reverted V-shaped suture (Figures 6A, B). In posterior view, the basisphenoid is partially hollow for the articulation with the basioccipital, and the opening of the internal carotid canal is in the centre (Figure 6E).

As in most basal anomodonts, the dentition of *Patranomodon* is homodont (Rubidge and Hopson, 1996; Rybczynski and Reisz, 2001; Kemp, 2005; Cisneros et al., 2015). Similar-shaped teeth are present in both the maxilla and premaxilla, and there is not an enlarged caniniform tooth or tusk (Figure 1G, H and see Supplementary Material). The specimen has nine maxillary teeth on the right side, all of similar sizes, except the posterior-most tooth, which is smaller. On the left side, six teeth of similar shape and size are preserved (Figure 1G, H). The difference in number on the left and right sides is possibly due to preservation. On the right, it is evident that the anterior-most tooth is rooted at the suture between the maxilla and the premaxilla (Figure 1D, I).

3.1.2 *Eodicynodon oosthuizeni*

<div align="center">

SYSTEMATIC PALEONTOLOGY

THERAPSIDA Broom, 1905

ANOMODONTIA Owen, 1859

DICYNODONTIA Owen, 1859

</div>

Definition—All taxa more closely related to *Dicynodon lacerticeps* than *Galeops whaitsi* (Kammerer and Angielczyk, 2009).

Diagnosis—after Sidor (2001) and Kammerer and Angielczyk (2009), alveolar margin of the premaxilla recurved; ventral surface of the premaxilla has a median ridge with a flattened and expanded anterior area; vomerine process of the premaxilla lost so that vomer abuts the body of the premaxilla; internal narial shelf well-developed and formed primarily by the premaxilla and the maxilla; interpterygoid vacuity relatively long but does not reach the level of the palatal exposure of the palatines; lateral palatal foramen present at the level of the anterior expanded palatal exposure of the palatines; transverse flange of the pterygoid reduced and oriented longitudinally; squamosal with lateral fossa for muscle

FIGURE 7
Eodicynodon oosthuizeni, BP/1/6230, from Bloukrans farm, Prince Albert district, Western Cape, South Africa; *Eodicynodon* AZ, Guadalupian, Beaufort Group, Karoo Supergroup. 3D rendering in **(A)**, right lateral view; **(B)**, left lateral view; **(C)**, dorsal view; **(D)**, ventral view; **(E)**, posterior view; **(F)**, anterior view; **(G)**, posterolateral view and **(H)**, dorsolateral view. Abbreviations: ang, angular; app, anterior process of the parietal; art, articular; bo, basioccipital; bot, basioccipital tubera; bsh, basisphenoid; c, caniniform tooth; d, dentary; dsq, dorsal process of the squamosal; ect, ectopterygoid; eo, exoccipital; f, frontal; j, jugal; l, lacrimal; lf, lacrimal foramen; m, maxilla; mf, mandibular fenestra; n, nasal; obsh, orbitosphenoid; op, opisthotic; p, parietal; pal, palatine; part, pre-articular; pc, postcanine; pf, postfrontal; pm, premaxilla; po, postorbital; pob, postorbital bar; pp, postparietal; ppf, posterior process of the frontal; ppm, palatal process of the premaxilla; prf, prefrontal; prp, preparietal; psh, parasphenoid; pt, pterygoid; ptf, postemporal fenestra; q, quadrate; qj, quadratojugal; qpt, quadrate process of the pterygoid; so, supraoccipital; sq, squamosal; srspo, skull roof section of the postorbital; st, stapes; sur, surangular; t, tabular; tpt, transverse process of the pterygoid; v, vomer; vkp, ventral keel of the palate; vsq, ventral process of the squamosal; zsq, zygomatic process of the squamosal. Scale bar = 1 cm.

origination; squamosal anterior process dorsoventrally compressed; squamosal with a distinct dorsolateral notch in posterior view; quadratojugal is plate-like distally; vomer forms the anterior margin of the interpterygoid vacuity; foramen magnum much taller than wide; splenial visible in lateral view near the jaw symphysis; medial section of the angular extends long and nearly reaches the symphysis; vertical lamina of the surangular absent; prearticular without a lateral exposure; premaxillary teeth absent; caniniforms long and tusk-like; postcanines reduced or absent; caniniform process present.

Eodicynodon Barry, 1974

Diagnosis—after Rubidge (1990a), intertemporal and interorbital regions broad with large parietal exposure; skull relatively deep and zygoma not emarginated as much as other dicynodonts; medially unfused premaxilla; anterior medial tip of premaxilla on the ventral side flattened to form a broad fan-shaped ridge which tapers posteriorly to a thin ridge which protrudes ventrally; no teeth on the anterior part of the premaxilla or dentary; postcanine teeth present, maxilla borders the lateral side of internal nares and separate the premaxillae and the palatines; vomers and premaxillae paired; stongly developed and ventrally directed lateral process of the pterygoid; palatine bulbous and rugose; median interpterygoidal crest enlarged to form a large ventral boss; squamosal separated from the maxilla by the jugal on the zygomatic arch; fully developed sliding contact between the quadrate and the articular condyle; postemporal foramen situated medially to suture between the squamosal and exoccipital; stapes often pierced by stapedial foramen; dentary with dentary shelf which has a triangular fossa on the posterodorsal side for insertion of the lateral external adductor muscle; and rounded dentary tables situated on anterodorsal side of each ramus of the lower jaw.

Eodicynodon oosthuizeni Barry, 1974

Holotype—ROZ 1, from the private collection of Mr. Roy Oosthuizeni, now curated at Iziko South African Museum in Cape Town, South Africa.

Referred Material—NMQR 2902 to 2912, NMQR 2978, NMQR 2988 to 2996, NMQR 2998 to 3003, 3005, 3007, 3014, 3026, 3094 and 3095, 3139, NMQR 3153 to 3155 to 3159, NMQR 3330, 3333, 3339, 3392, SAM-PK-011879, SAM-PK-K07914, SAM-PK-K10019, BP/1/5577, 5573, 5574, 6230, 6975, ROZ B95, ROZ 5, 7, 9 and 11.

Type locality—farm Zwartskraal, Prince Albert district, Western Cape, South Africa; *Eodicynodon* Assemblage Zone, Beaufort Group, Karoo Supergroup.

Diagnosis—after Rubidge (1990a), caniniform tusk-like teeth present; maxillary teeth commonly present and situated on lateral side of maxilla either posterior or medial to the tusk; palatal rim interrupted by a deep cleft in front of maxillary tusk; low coronoid eminence on posterodorsal surface of the dentary.

List of figures—Figures 7–19.

Description—The skull of two specimens of *E. oosthuizeni* are described in unprecedented detail thanks to CT-scanning and manual segmentation. These specimens of *E. oosthuizeni* were previously reported by Rubidge (1990b) and Jinnah and Rubidge (2007) and are from the *Eodicynodon* Assemblage Zone of the South African Karoo Beaufort Group.

Specimen BP/1/6230 is a small complete skull with lower jaw and associated postcranial elements (Figure 7). The skull is slightly distorted (Figure 7F) as the occipital bones have been flattened and shifted towards the horizontal plane by diagenesis (Figure 7E). The specimen was identified as a pathological double-tusked specimen of *E. oosthuizeni* (Jinnah and Rubidge, 2007). This interpretation has been supported by a more recent study (Olroyd et al., 2021).

Specimen NMQR 2978, comprising a complete skull without a lower jaw (Figure 8), was mentioned for the first time by Rubidge (1990b), along with other *E. oosthuizeni* specimens in a paper describing the general morphology of *E. oosthuizeni*. Preservation of the specimen is good, but the posterior left section of the skull (at the level of the postemporal fenestra) has been crushed. Part of the dorsal skull roof is damaged by an obscuring crack that made 3D reconstruction of this section difficult. As a result, a preparietal was not identified in the specimen, but is likely present. The temporal fenestra is about 1.5 times the size of the orbit. The following description is a composite of the best-preserved parts of the two specimens.

The premaxilla is an edentulous bone that forms the anteriormost part of the snout and encloses the anteroventral and anterior margin of the external naris. Ventrally, it forms a secondary palate that separates the nasal cavity from the oral cavity. The premaxilla, which is a paired bone as pointed out by Rubidge (1990b), is better preserved in NMQR 2978 than in BP/1/6230 (Figures 7, 8). In ventral view, the inter-premaxillary suture is straight and extends along the midline (Figure 9D) but does not reach the posterior margin of the premaxilla (Figures 8D, 9D) ending at the level of the anterior margin of the tusk. In anterior view, the contact between the two premaxillae is Y-shaped (Figures 8F, 9F). The premaxilla comprises the nasal and palatal processes (Figures 9, 10). The nasal process is not preserved in BP/1/6230.

The nasal process forms the anterior border of the external naris (Figures 8G, 9A, B). In anterior view, it extends dorsally into a thick internarial process that separates the two nares (Figure 9F). In anterior view, the premaxilla has an inverted U-shaped contact with the nasal dorsally (Figure 8F).

The palatal process forms the anteroventral margin of the naris (Figures 8G, H, 9A, B), is slightly concave and roughly triangular in ventral view (Figure 9D). It has an oblique contact with the maxilla posterolaterally, in both ventral and lateral views (Figure 9A, B, D).

The maxilla forms the posterior margin of the external naris (Figures 7, 8) and is triangular in ventral view (Figure 9D). In lateral view, the maxilla is roughly rectangular (Figures 10B, 9B) and has a well-formed oblique depression anterior to the tusk (Figure 9B). It contacts the nasal dorsally with an oblique suture (Figures 7A, 8A). In lateral view, the maxilla has a long horizontal posterodorsal contact with the lacrimal at the level of the tusk (Figure 8A, B) and meets the jugal posteriorly (Figure 9A). The contact is oblique in both lateral and posterior views (Figures 8H, 9B, E, 10B, E). In ventral view, the maxilla sutures with the premaxilla anteromedially (Figures 10D, 9D) and the contact is oblique in both dorsal and ventral views (Figure 9C, D).

On the ventral side, the maxilla bears a large posteromedial ovoid depression to accommodate the palatine (Figures 8D, 9D) and has a short contact with the ectopterygoid posteriorly (Figures 8D, 18G). This contact is longer and vertical in lateral view (Figure 8A, H). The maxilla bears tusks and postcanines in

FIGURE 8
Eodicynodon oosthuizeni, NMQR 2978, farm Rietkuil (previously named Zwartgrond), Rietbron district, Eastern Cape, South Africa; *Eodicynodon* AZ, Guadalupian, Beaufort Group, Karoo Supergroup. 3D rendering in **(A)**, right lateral view; **(B)**, left lateral view; **(C)**, dorsal view; **(D)**, ventral view; **(E)**, posterior view; **(F)**, anterior view; **(G)**, anterolateral view and **(H)**, posteroventral view. Abbreviations: Abbreviations: apt, anterior process of the pterygoid; bo, basioccipital; bot, basioccipital tubera; bsh, basisphenoid; c, caniniform tooth; dsq, dorsal process of the squamosal; ect, ectopterygoid; eo, exoccipital; f, frontal; j, jugal; l, lacrimal; m, maxilla; mxd, maxilla depression; n, nasal; npm, nasal process of the premaxilla; op, opisthotic; p, parietal; pal, palatine; pc, postcanine; pcult, processus cultriformis; pf, postfrontal; pm, premaxilla; po, postorbital; pob, postorbital bar; pp, postparietal; ppm, palatal process of the premaxilla; prf, prefrontal; pro, prootic; prp, preparietal; psh, parasphenoid; pt, pterygoid; q, quadrate; qj, quadratojugal; qpt, quadrate process of the pterygoid; so, supraoccipital; sq, squamosal; srspo, skull roof section of the postorbital; sur, surangular; t, tabular; tpt, transverse process of the pterygoid; v, vomer; vkp, ventral keel of the palate; vsq, ventral process of the squamosal; zsq, zygomatic process of the squamosal. Scale bar = 1 cm.

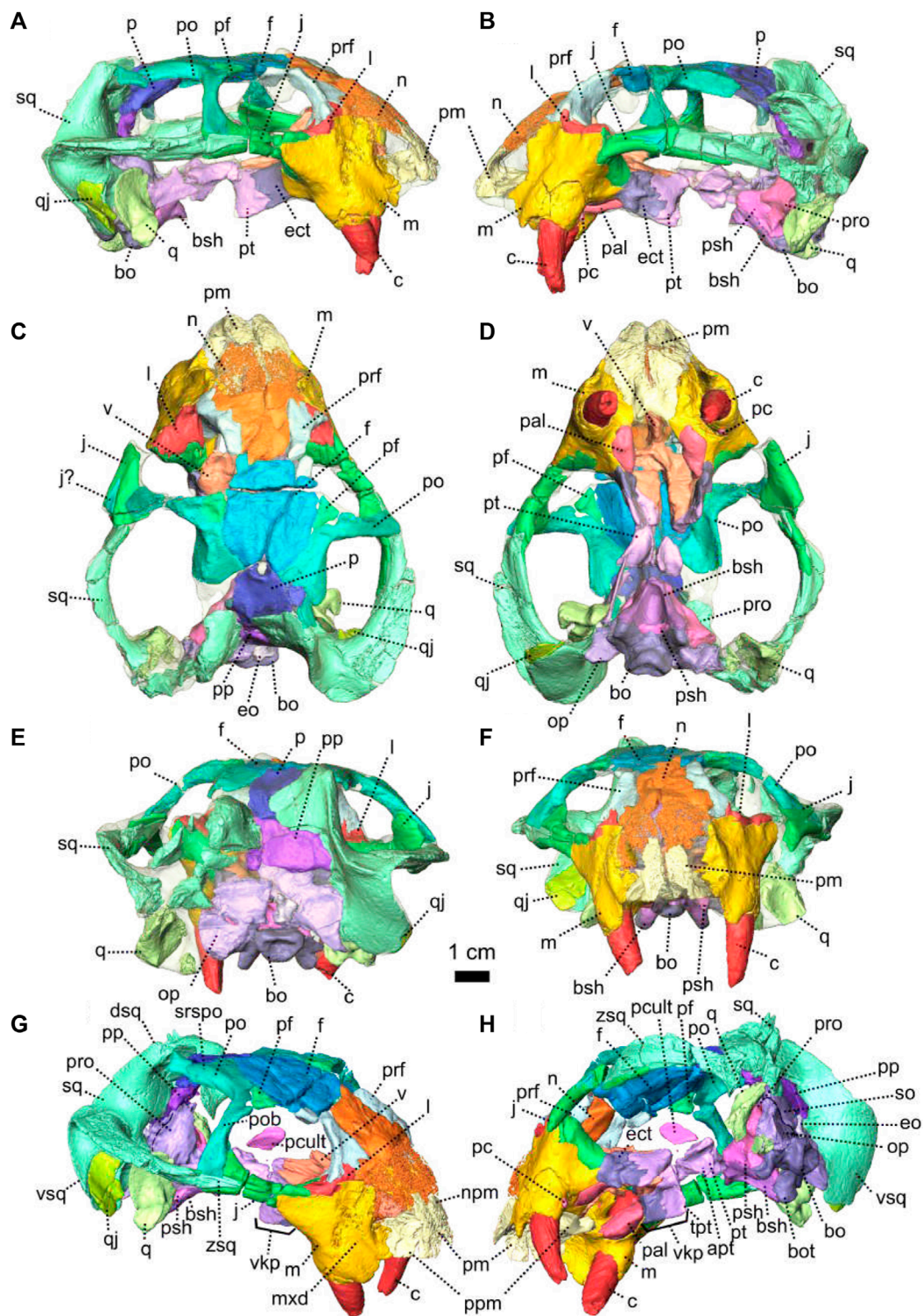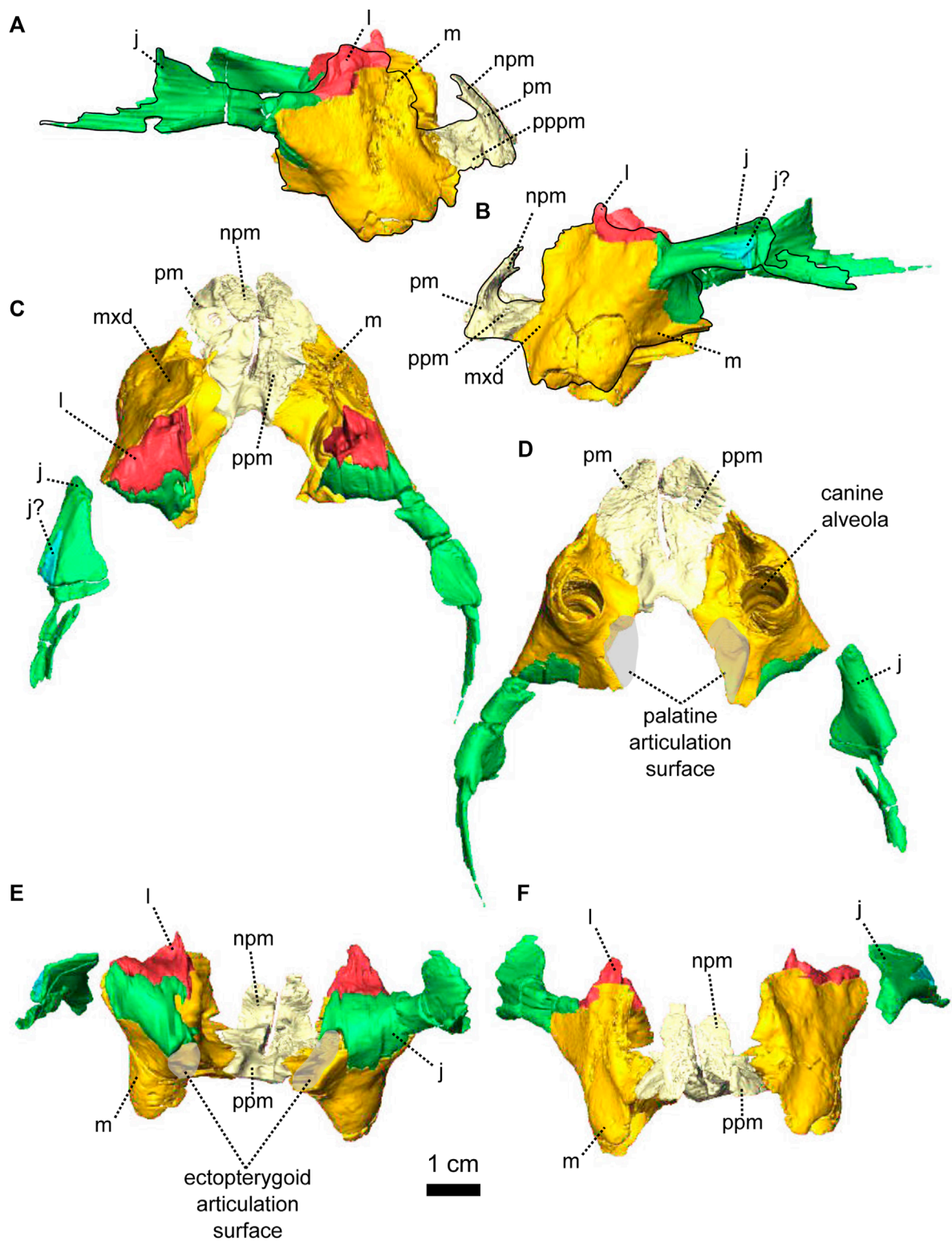**FIGURE 9**
Paired maxillae and associated masticatory elements of *Eodicynodon oosthuizeni*, NMQR 2978, farm Rietkuil (previously named Zwartgrond), Rietbron district, Eastern Cape, South Africa; *Eodicynodon* AZ, Guadalupian, Beaufort Group, Karoo Supergroup. 3D rendering in **(A)**, right lateral view; **(B)**, left lateral view; **(C)**, dorsal view; **(D)**, ventral view; **(E)**, posterior view and **(F)**, anterior view. Abbreviations: j, jugal; l, lacrimal; m, maxilla; mxd, maxilla depression; n, nasal; npm, nasal process of the premaxilla; pm, premaxilla; ppm, palatal process of the premaxilla. Scale bar = 1 cm.

FIGURE 10
Paired maxillae and associated masticatory elements of *Eodicynodon oosthuizeni*, BP/1/6230, from Bloukrans farm, Prince Albert district, Western Cape, South Africa; *Eodicynodon* AZ, Guadalupian, Beaufort Group, Karoo Supergroup. 3D rendering in **(A)**, right lateral view; **(B)**, left lateral view; **(C)**, dorsal view; **(D)**, ventral view; **(E)**, posterior view; **(F)**, anterior view. Abbreviations: j, jugal; l, lacrimal; m, maxilla; mxd, maxilla depression; n, nasal; npm, nasal process of the premaxilla; pm, premaxilla; ppm, palatal process of the premaxilla. Scale bar = 1 cm.

both BP/1/6230 and NMQR 2978, but specimen BP/1/6230 has an additional pathological tusk on the left (Figures 7, 8).

The nasal is a paired bone that forms most of the anterodorsal part of the snout (Figures 7, 8, 13, 14) and makes up the dorsal margin of the naris (Figures 7A, B, 8A, B). In lateral view, the nasal has a small anteroventral triangular extension, posterior to the naris (Figure 9B). This extension is overlapped by the maxilla ventrally in both lateral and anterior views (Figures 8B, F, 7A, F). In dorsal view, the nasal contacts the prefrontal posterolaterally with a slightly oblique contact (Figure 13C). Posteriorly, the nasal contacts the frontal (Figure 14) and in both dorsal and anterior views, the contact forms an inverted V (Figure 14C, F).

The lacrimal is a relatively small horizontal bone in *E. oosthuizeni* and does not extend dorsally as far as in *Patranomodon* (Figures 2, 9). It forms the anteroventral margin of the orbit (Figures 7G, 9) and in lateral view, has a long horizontal ventral contact with the maxilla (Figure 9B). In posterolateral view, the nasal has a horizontal contact with the prefrontal dorsally, at the level of the lacrimal foramen (Figures 7G). In dorsal view, the lacrimal is roughly triangular and has an oblique contact with the jugal posteriorly (Figure 9C) and transverse in posterior view (Figure 9E). The lacrimal foramen is present as a large circular opening (Figure 7A).

The jugal forms the ventral margin of the orbit, the anterior-most section of the zygomatic arch (Figures 7, 8) and makes up the anteroventral margin of the temporal fenestra (Figures 7B, 8B). In lateral view, the jugal contacts the maxilla anteriorly with an oblique contact (Figure 10B). Half-way along the length of the jugal, it contacts the postorbital bar dorsally with a horizontal suture (Figure 8A, B, G). In lateral view, the jugal has a horizontal depression posteriorly to accommodate the zygomatic ramus of the squamosal (Figures 7B, 8B, 10B). In dorsal view, the jugal contacts the lacrimal anteriorly (Figure 9C) and in ventral view, the jugal contacts the maxilla at the level of the palatine bosses (Figures 9D, 10D).

The postorbital makes up part of the skull roof above the anterior end of the temporal opening and comprises the entire postorbital bar (Figures 7, 8, 13, 14). In dorsal view, it contacts the postfrontal anteromedially with a curved suture, reaches the parietal medially with a slightly oblique contact (Figure 14C) and has a short contact with the dorsal process of the squamosal posteriorly (Figures 7C, 8C). The postorbital bar separates the orbit from the temporal fenestra (Figures 7H, 8G). In lateral view, the postorbital bar thickens as it contacts the jugal ventrally with a horizontal suture (Figure 8A, B) and a marked vertical groove is present on the postorbital bar (Figure 14B). In ventral view, the skull roof section of the postorbital shows a prominent depression, with the lateral margin being thicker than the medial margin, which meets the parietal medially (Figures 13D, 14D).

The squamosal of BP/1/6230 and NMQR 2978, folds around the back of the skull, enclosing the temporal fenestra posteriorly (Figures 7, 8, 11) as in other dicynodonts (Hammer and Cosgriff, 1981; Angielczyk, 2007; Kammerer et al., 2011; Castanhinha et al., 2013; Hancox et al., 2013; Boos et al., 2016; Olroyd et al., 2018). Similar to the situation in other dicynodonts, the squamosal of *E. oosthuizeni* comprises three thin processes: the flat zygomatic, dorsal, and ventral processes (Figures 7G, 8G, H, 11, 12). The zygomatic process of the squamosal extends anteriorly and makes up the posteroventral margin of the temporal fenestra

(Figures 7B, G, H, 8B, G). In dorsal view, the zygomatic process has a flat anteromedial contact with the jugal (Figure 8C). In posterior view, the dorsal process of the squamosal folds anterodorsally (Figure 8E) and is overlapped medially by the parietal-postparietal complex (Figure 7C, E). In dorsal view, the dorsal process of the squamosal has a short anterior contact with the postorbital (Figure 7C). In posterior view, the spatulate ventral process extends ventrally (Figures 12E, 11E) and contacts the supraoccipital and the opisthotic medially (Figures 12E, 11E). In lateral view, the squamosal masks both the dorsal plate of the quadrate and the quadratojugal (Figures 11, 12), and the ventral process of the squamosal slopes at an angle of 45° to the vertical plane (Figure 11A).

The orbital region of both BP/1/6230 and NMQR 2978 is well preserved (Figures 7, 8). With the exception of the sclerotic rings all the bones surrounding the orbit and eye are present. The postorbital bar, which closes the orbit posteriorly, is broken on BP/1/6230 and does not reach the zygomatic bar (Figure 7C) but for *E. oosthuizeni*, the orbit is surrounded by the jugal and lacrimal anteriorly, the prefrontal, frontal and postfrontal dorsally, and the postorbital posteriorly.

The prefrontal forms the anterior border of the orbit (Figures 7G, B, 8, 5A, 13) and is roughly triangular in lateral view (Figure 13B). The prefrontal contacts the lacrimal above the lacrimal foramen (Figure 7G, H). The contact is oblique in lateral and anterolateral view (Figure 8A, B, G). In dorsal view, the prefrontal contacts the nasal medially with an oblique contact (Figure 13C) and extends posteriorly to contact the frontal.

With the parietal, the frontal is the largest bone of the *Eodicynodon* skull (Figures 7, 8, 13, 14) and makes up the dorsal margin of the orbit (Figures 7A, B, C, H). Although the frontal is a paired bone in dicynodonts, the midline suture between the two frontals could not be determined in BP/1/6230, and the frontal of NMQR 2978 is damaged by a crack (Figures 13, 14). In dorsal view, the frontal contacts the nasal anteriorly with a V-shaped suture (Figures 14C, 13C) and has a short contact with the prefrontal anterolaterally (Figure 14A, B, C). In dorsal, lateral and ventral views, the frontal overlaps the postfrontal posterolaterally with an oblique contact in dorsal view (Figures 14A, C, D, 16C) and meets the preparietal posteriorly with a curved contact (Figure 14C). In ventral view, the contact between the frontal and the preparietal could not be determined (Figure 14D). In dorsal view, the posterior process of the frontal wedges between the postfrontal laterally and the parietal medially, with its apex bordering on the pineal foramen. This process is not visible in ventral view (Figure 14D) and implies that the posterior process of the frontal overlaps the dorsal side of the parietal (Figure 16C). In ventral view, the transverse suture between the frontal and the parietal is straight (Figure 14D) and the frontal bears a lateral ridge that extends from the nasal anteriorly, to the parietal-frontal suture posteriorly (Figure 14D). This ridge (often not preserved in dicynodonts) houses a neurovascular canal (*ramus supraorbitalis*) and borders the forebrain laterally up to the olfactory bulbs (Laaß et al., 2017; de Simão-Oliveira et al., 2019; Pusch et al., 2019).

The postfrontal forms the posterodorsal margin of the orbit between the frontal anteriorly and the postorbital posteriorly (Figures 7, 8, 13, 14). In dorsal view, it is triangular and contacts the frontal anteromedially with an oblique suture (Figure 14C).

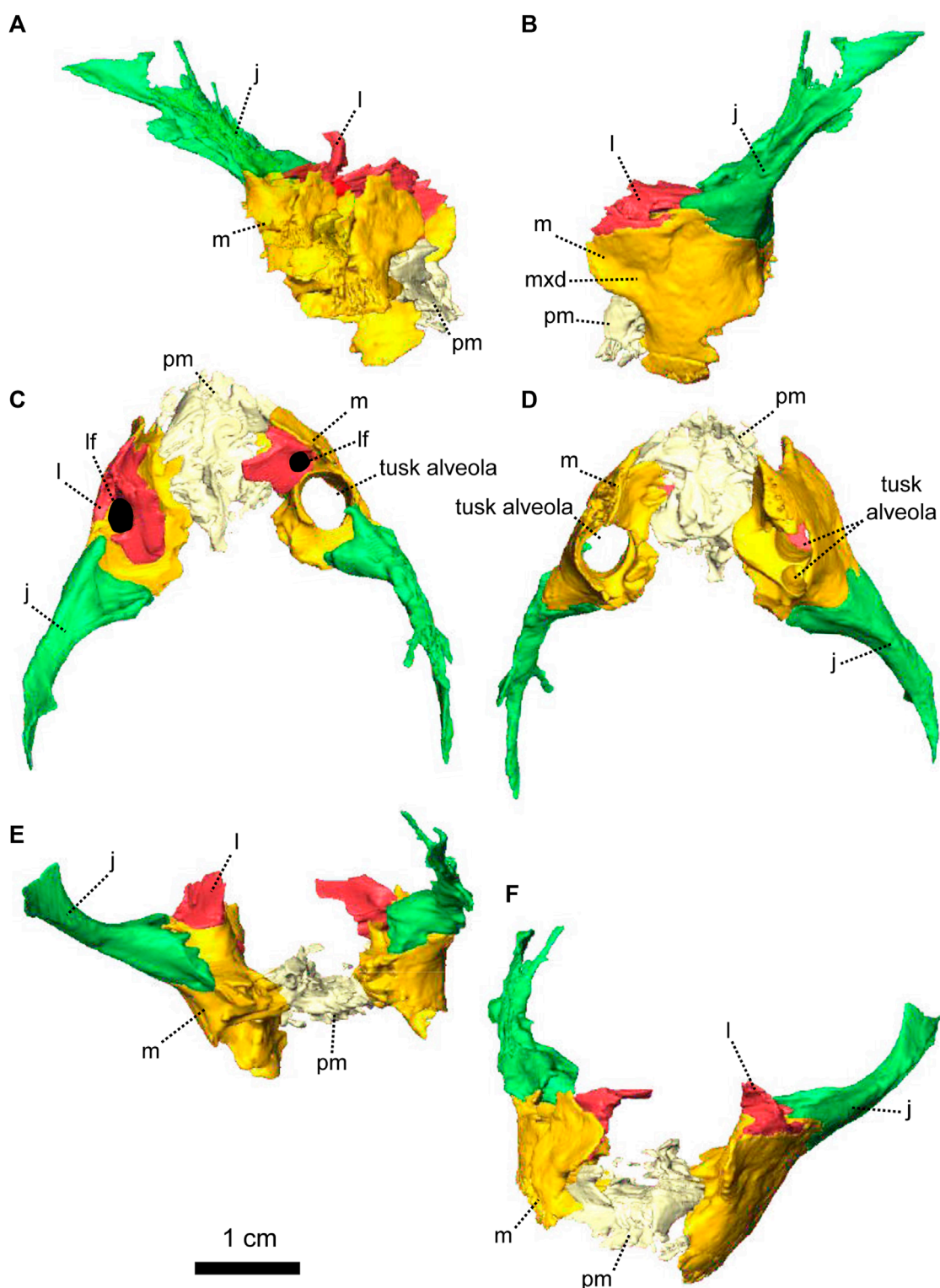**FIGURE 11**
Occipital bones of *Eodicynodon oosthuizeni*, NMQR 2978, farm Rietkuil (previously named Zwartgrond), Rietbron district, Eastern Cape, South Africa; *Eodicynodon* AZ, Guadalupian, Beaufort Group, Karoo Supergroup. 3D rendering in **(A)**, right lateral view; **(B)**, left lateral view; **(C)**, dorsal view; **(D)**, ventral view; **(E)**, posterior view and **(F)**, anterior view. Abbreviations: bo, basioccipital; bot, basioccipital tubera; dpq, dorsal plate of the quadrate; dsq, dorsal process of the squamosal; eo, exoccipital; fm, foramen magnum; fo, fenestra ovalis; icgq, intercondylar groove of the quadrate; lcq, lateral condyle of the quadrate; mcq, medial condyle of the quadrate; op, opisthotic; opfeo, opisthotic facet of the exoccipital; pp, postparietal; pro, prootic; ptf, postemporal fenestra; q, quadrate; qj, quadratojugal; so, supraoccipital; sq, squamosal; vsq, ventral process of the squamosal; zsq, zygomatic process of the squamosal. Scale bar = 1 cm.

FIGURE 12
Occipital bones of *Eodicynodon oosthuizeni*, BP/1/6230, from Bloukrans farm, Prince Albert district, Western Cape, South Africa; *Eodicynodon* AZ, Guadalupian, Beaufort Group, Karoo Supergroup. 3D rendering in **(A)**, right lateral view; **(B)**, left lateral view; **(C)**, dorsal view; **(D)**, ventral view; **(E)**, posterior view and **(F)**, anterior view. Abbreviations: acst, anterior crus of the stapes; bo, basioccipital; dpq, dorsal plate of the quadrate; dsq, dorsal process of the squamosal; eo, exoccipital; icgq, intercondylar groove of the quadrate; lcq, lateral condyle of the quadrate; lnq, lateral notch of the quadrate; mcq, medial condyle of the quadrate; opfeo, opisthotic facet of the exoccipital; pafeo, pro-atalas facet of the exoccipital; pcst, posterior crus of the stapes; pp, postparietal; pro, prootic; ptf, postemporal fenestra; q, quadrate; qj, quadratojugal; so, supraoccipital; st, stapes; sth, stapedial head; stf, stapedial foramen; stfp, stapedial footplate; sq, squamosal; vsq, ventral process of the squamosal; zsq, zygomatic process of the squamosal. Scale bar = 1 cm.

FIGURE 13
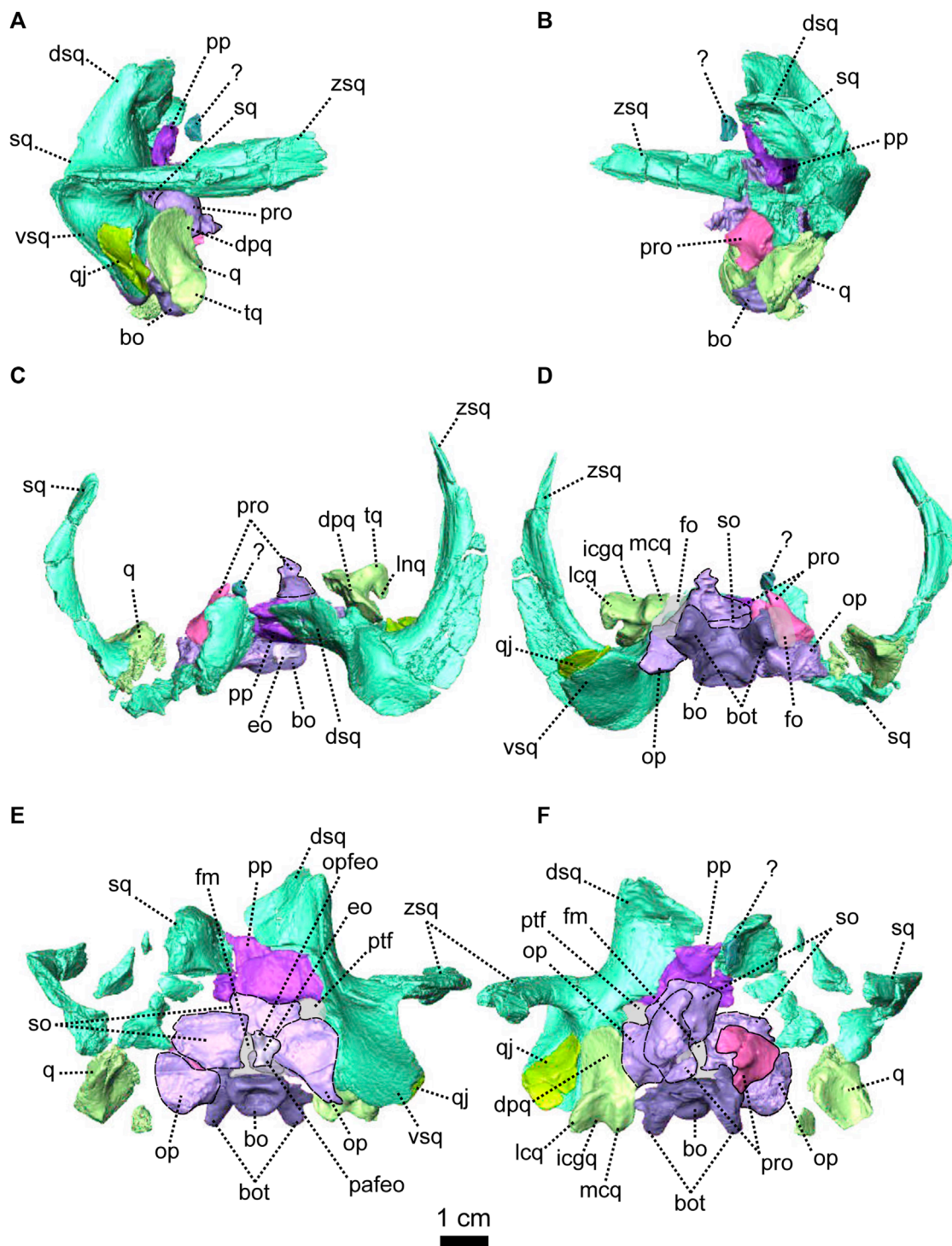Parietal and associated dorsal elements of *Eodicynodon oosthuizeni*, NMQR 2978, farm Rietkuil (previously named Zwartgrond), Rietbron district, Eastern Cape, South Africa; *Eodicynodon* AZ, Guadalupian, Beaufort Group, Karoo Supergroup. 3D rendering in **(A)**, right lateral view; **(B)**, left lateral view; **(C)**, dorsal view; **(D)**, ventral view; **(E)**, posterior view; **(F)**, anterior view and **(G)**, anteroventral view, anteroventral view. Abbreviations: crso, canal for the ramus supraorbitalis; f, frontal; n, nasal; p, parietal; pf, postfrontal; po, postorbital; pob, postorbital bar; prf, prefrontal; srspo, skull roof section of the postorbital. Scale bar = 1 cm.

FIGURE 14
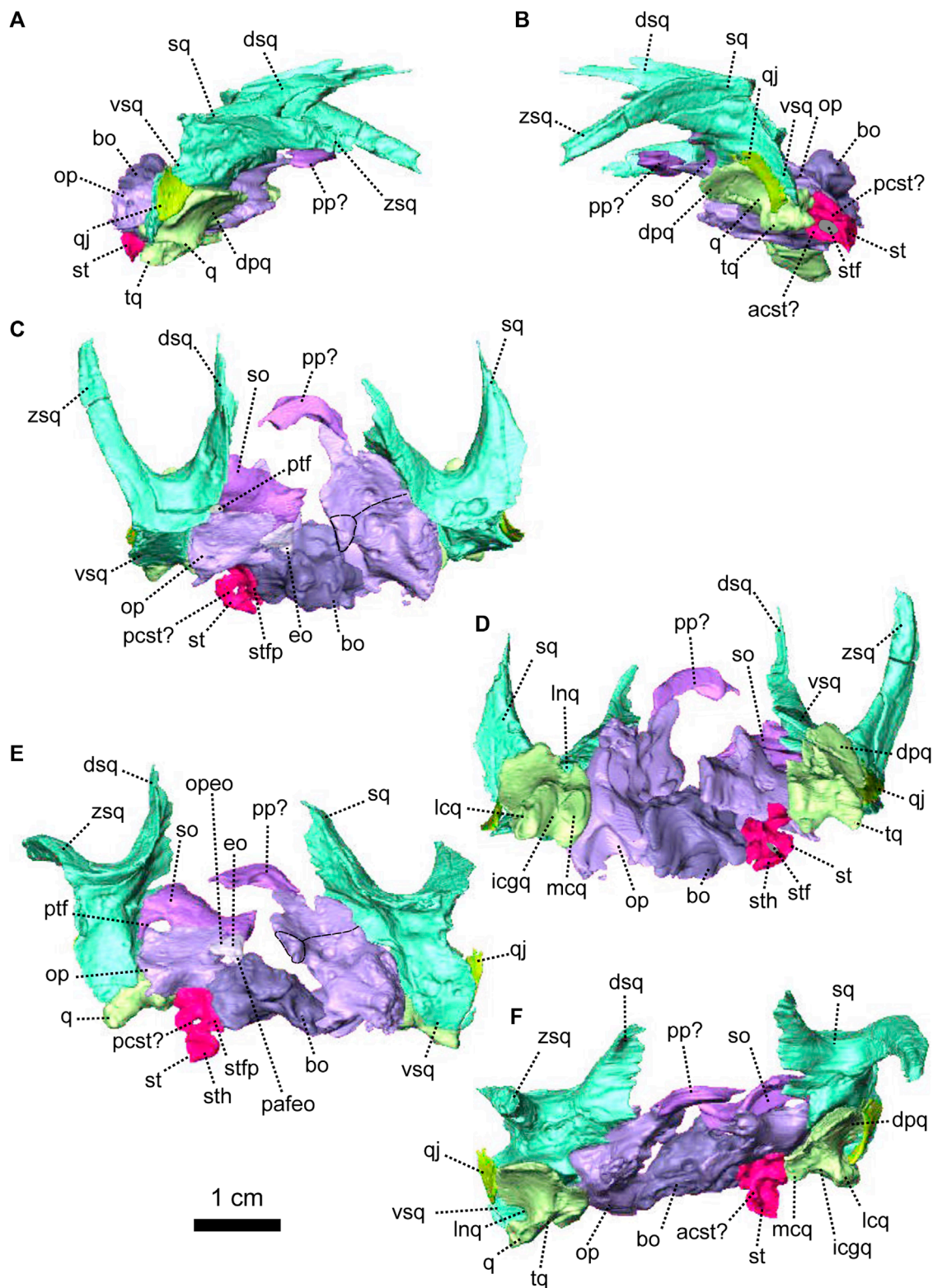Parietal and associated dorsal elements of *Eodicynodon oosthuizeni*, BP/1/6230, from Bloukrans farm, Prince Albert district, Western Cape, South Africa; *Eodicynodon* AZ, Guadalupian, Beaufort Group, Karoo Supergroup. 3D rendering in **(A)**, right lateral view; **(B)**, left lateral view; **(C)**, dorsal view; **(D)**, ventral view; **(E)**, posterior view and **(F)**, anterior view. Abbreviations: app, anterior process of the parietal; crso, canal for the ramus supraorbitalis; f, frontal; n, nasal; p, parietal; pf, postfrontal; ppf, posterior process of the frontal; po, postorbital; pob, postorbital bar; prf, prefrontal; prp, preparietal; srspo, skull roof section of the postorbital. Scale bar = 1 cm.

Symmetrically, in dorsal view, the postfrontal has a curved posteromedial contact with the postorbital and a short contact with the parietal posteriorly (Figure 14C). In lateral and ventral views, the postfrontal is overlapped by the frontal anteromedially (Figure 14A, C).

The preparietal, positioned along the midline between the anterior processes of the paired parietals, is a narrow rectangular bone in dorsal view (Figures 7, 14) and square in ventral view (Figure 14C, D). It forms the anterior margin of the pineal foramen (Figure 14C, D). In dorsal view, the preparietal has a longitudinal contact with the parietal and meets the frontal with a curved suture (Figure 14C). In ventral view, the anterior part of the preparietal is covered by the parietal and the preparietal does not reach the frontal (Figure 14D). This may be an artefact of segmentation, as this feature is absent on other well-preserved anomodonts (see Figure 3D; Castanhinha et al., 2013).

The parietal forms the lateral and posterior margins of the pineal foramen (Figures 13, 14) and comprises most of the intertemporal region (Figure 13C). As in the case of the frontal, the midline suture is not visible and the parietal appears to be unpaired (Figures 13, 14). In BP/1/6230, no sutures between the parietal and the postparietal could be recognised on the CT-scan, so the parietal is likely to be co-ossified with the postparietal (Figure 7E). In dorsal view, the anterior process of the parietal extends anteriorly between the preparietal medially and the frontal laterally (Figure 14C) but is notably absent in ventral view (Figure 14D). In dorsal view, the parietal has a short posterior contact with the postparietal and a longer oblique contact with the postorbital (Figure 14C). In posterior view, the parietal, which has a vertical medial nuchal crest (Figures 7E, 14E), overlaps the dorsal process of the squamosal laterally (Figure 7E) and meets the postparietal ventrally (Figure 8E). In ventral view, the parietal manifests a thick rectangular process (Figures 14D, 13D). It bears the curved canals for the *ramus supraorbitalis* laterally and the groove for the superior sagittal sinus medially (Figure 13D, G). In the same view, the parietal has two small bosses that are likely to be part of the epipterygoid (Figures 14D, 16C).

The occiput of NMQR 2978 is poorly preserved, apart from the basioccipital and the prootic (Figures 8, 11). The tabular and the left exoccipital are not preserved (Figure 11E). As in most dicynodonts, the supraoccipital, opisthotic and prootic are co-ossified, and no sutures could be identified on the CT slices (Figure 11).

The occiput of BP/1/6230 is vertically crushed and compressed (Figure 7) and the tabular, postparietal, prootic and right stapes are missing and several bones have been damaged such as the supraoccipital which has been shattered (Figure 12). The right supraoccipital and opisthotic are co-ossified, and it appears that the postparietal is co-ossified with the parietal. The jaw articulation (quadrate and quadratojugal) and the squamosal are well preserved, and the left postemporal fenestra is undeformed and well preserved (Figures 7E, 12E).

The postparietal, which is poorly preserved in NMQR 2978 (Figures 11, 15), is rectangular in posterior view (Figure 11E). The bone surface is smooth in posterior view, but shattered in anterior view (Figure 11E, F). The postparietal of NMQR 2978 is displaced so that it abnormally overlaps the supraoccipital and forms the dorsal margin of the postemporal fenestra ventrally (Figures 21E, F, 15). In posterior view, the postparietal contacts the dorsal ramus of the squamosal laterally (Figure 11E). The

contact is slightly oblique in both occipital and anterior views (Figure 11E, F).

The supraoccipital is poorly preserved in both *E. oosthuizeni* specimens and forms the dorsal margin of the postemporal fenestra (Figures 12E, 11E). In NMQR 2978, the supraoccipital is fused with the opisthotic and right prootic (Figure 11). In BP/1/6230, the right supraoccipital is fused with the opisthotic and the exoccipital (Figure 12). In posterior view, the supraoccipital forms the lateral margin of the triangular foramen magnum (Figure 12E) and contacts the exoccipital medioventrally (Figures 12E, 11E). It contacts the opisthotic ventrally with a horizontal suture laterally, that becomes oblique towards the exoccipital (Figure 12E). Similar to *Patranomodon*, the supraoccipital in *E. oosthuizeni* forms the posterior margin of the floccular cavity, where it contacts or fuses with the prootic (Figure 15A, B).

The walls of the floccular cavity, formed by the supraoccipital and the prootic, are relatively thicker in *E. oosthuizeni* than in *Patranomodon* and *E. oosthuizeni* it has a relatively smaller floccular cavity (Figures 4, 11, 12, 15).

Apart from the left prootic of NMQR 2978, the prootic of *E. oosthuizeni* is fused to the supraoccipital and the opisthotic (Figures 11, 12, 15). It forms the anterior walls of the floccular cavity and the vestibule (Figure 15B, D). The anterior, dorsal and lateral process of the prootic are smooth and less pronounced than in *Patranomodon* (Figures 4, 5, 11, 15). The pila antotica is not preserved and no foramina could be observed on the CT-images.

In ventral and anterior views, the prootic encloses the fenestra ovalis dorsally (Figures 11D, F, 15B). In lateral view, the prootic contacts the parasphenoid anteroventrally with an S-shaped suture (Figure 8B, G). In dorsolateral view the anterior process of the prootic contacts the parasphenoid, so that it encloses the base of the hindbrain area (Figure 15D). Also in dorsolateral view, the prootic contacts the opisthotic posteriorly, at the level of the vestibule. In anterior view, the prootic contacts the basioccipital ventrally (Figure 11F).

The opisthotic forms the ventral margin of the postemporal fenestra and is partially fused to the prootic, supraoccipital and exoccipital (Figures 11, 12, 15). Its ventral surface is curved, in between a lateroventral and a medioventral process (Figure 11D). In ventral view, the opisthotic forms the posterior border of the fenestra ovalis (Figures 11D, 15A).

In posterior view, the opisthotic supports the exoccipital medially and contacts the basioccipital ventromedially (Figures 12E, 11E) with a short and oblique suture in ventral and posterior views (Figures 12D, E, 11D, E). In the latter view, the opisthotic has a vertical lateral contact with the ventral process of the squamosal (Figures 12E, 11E). In dorsolateral view, the opisthotic forms the posterior wall of the vestibule, where it contacts the prootic (Figure 15A, D).

The exoccipital forms the lateral margin of the foramen magnum (Figures 12E, 11E). It is partially fused to the opisthotic (the right exoccipital cannot be differentiated from the opisthotic in BP/1/6230). In posterior view, the exoccipital is triangular, the proatlas facet is narrow while the opisthotic facet is broad (Figures 12E, 11E). The exoccipital has a short contact with the supraoccipital dorsally (Figure 12E). In the same view, it contacts the opisthotic laterally and the basioccipital ventrally. The contact
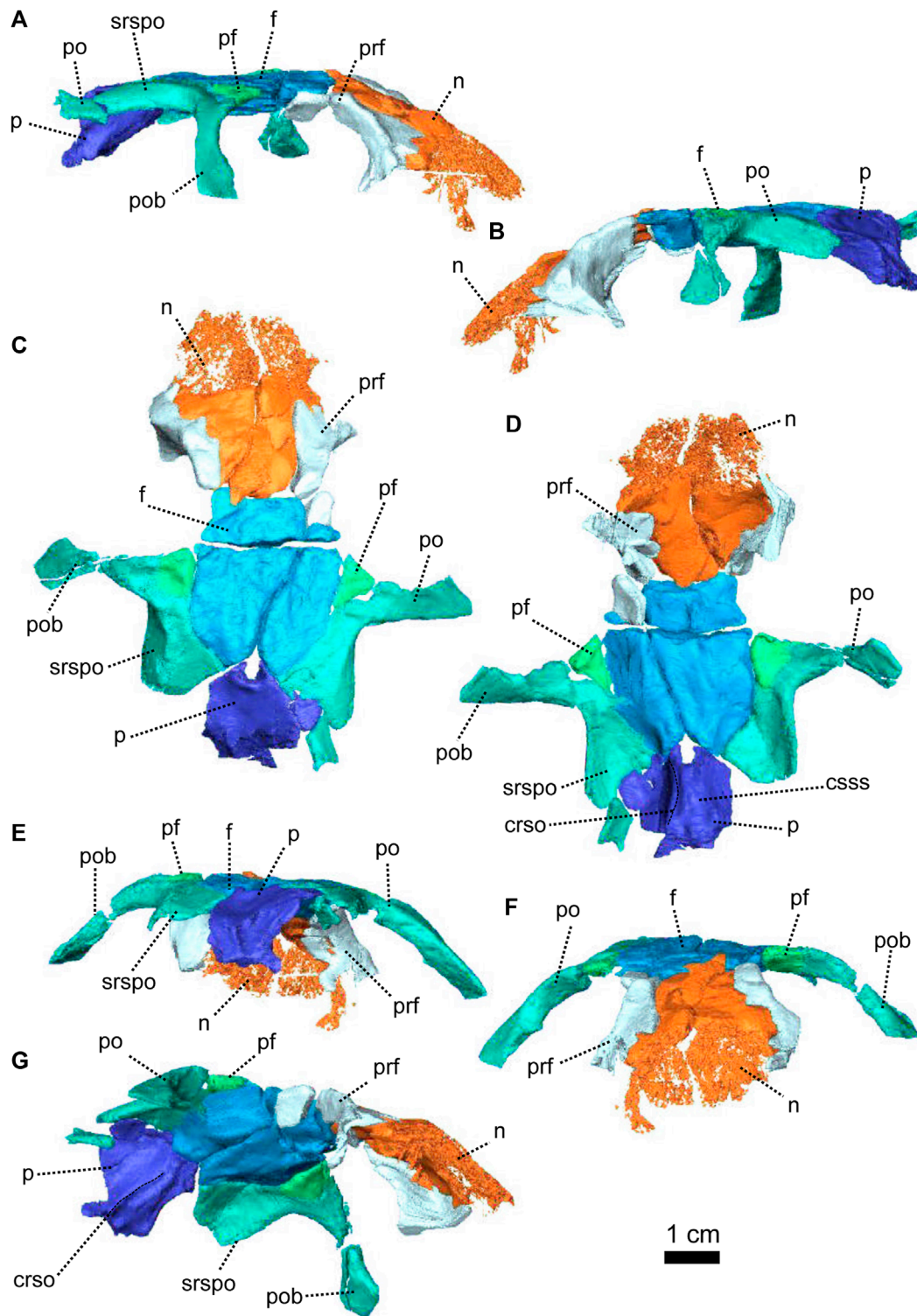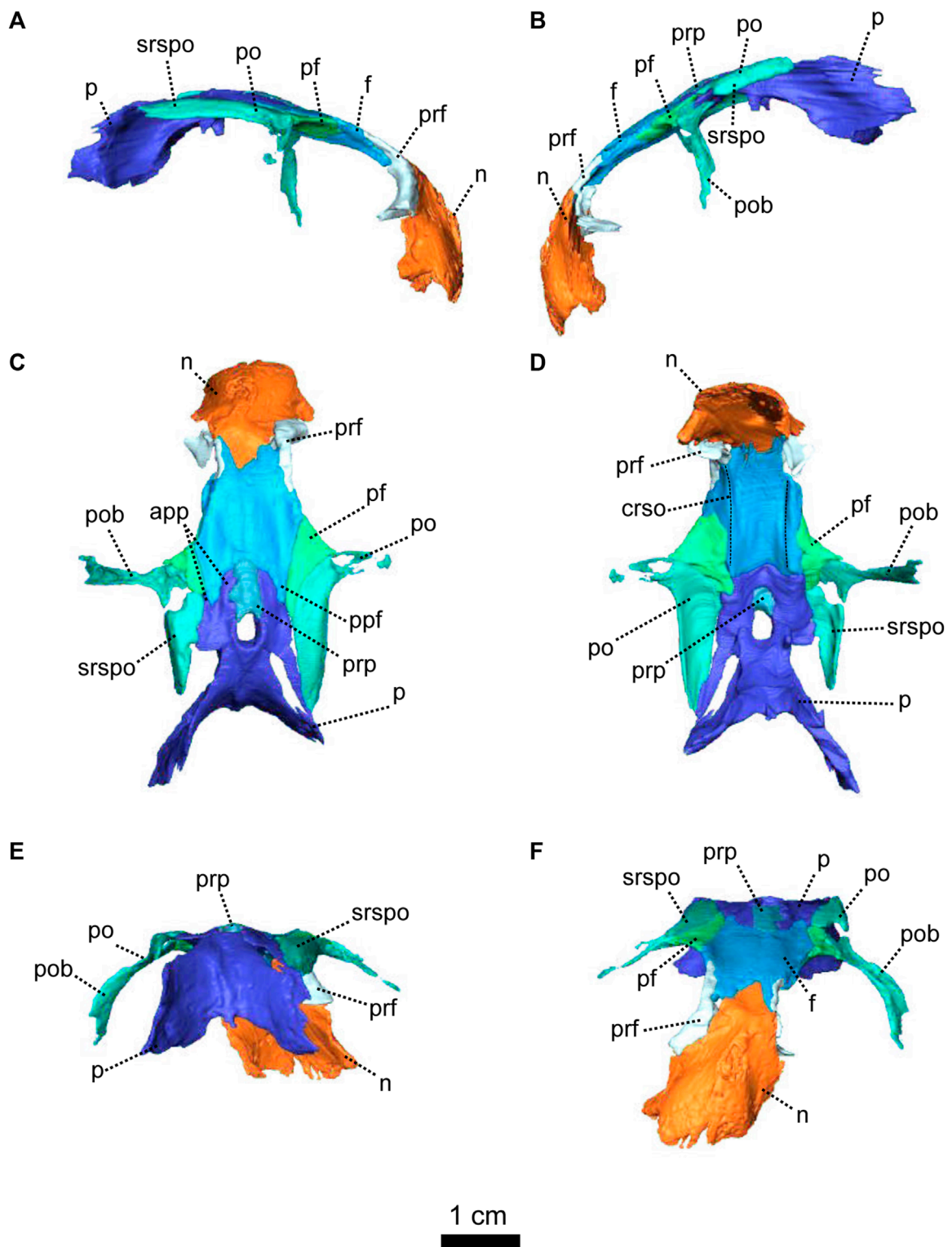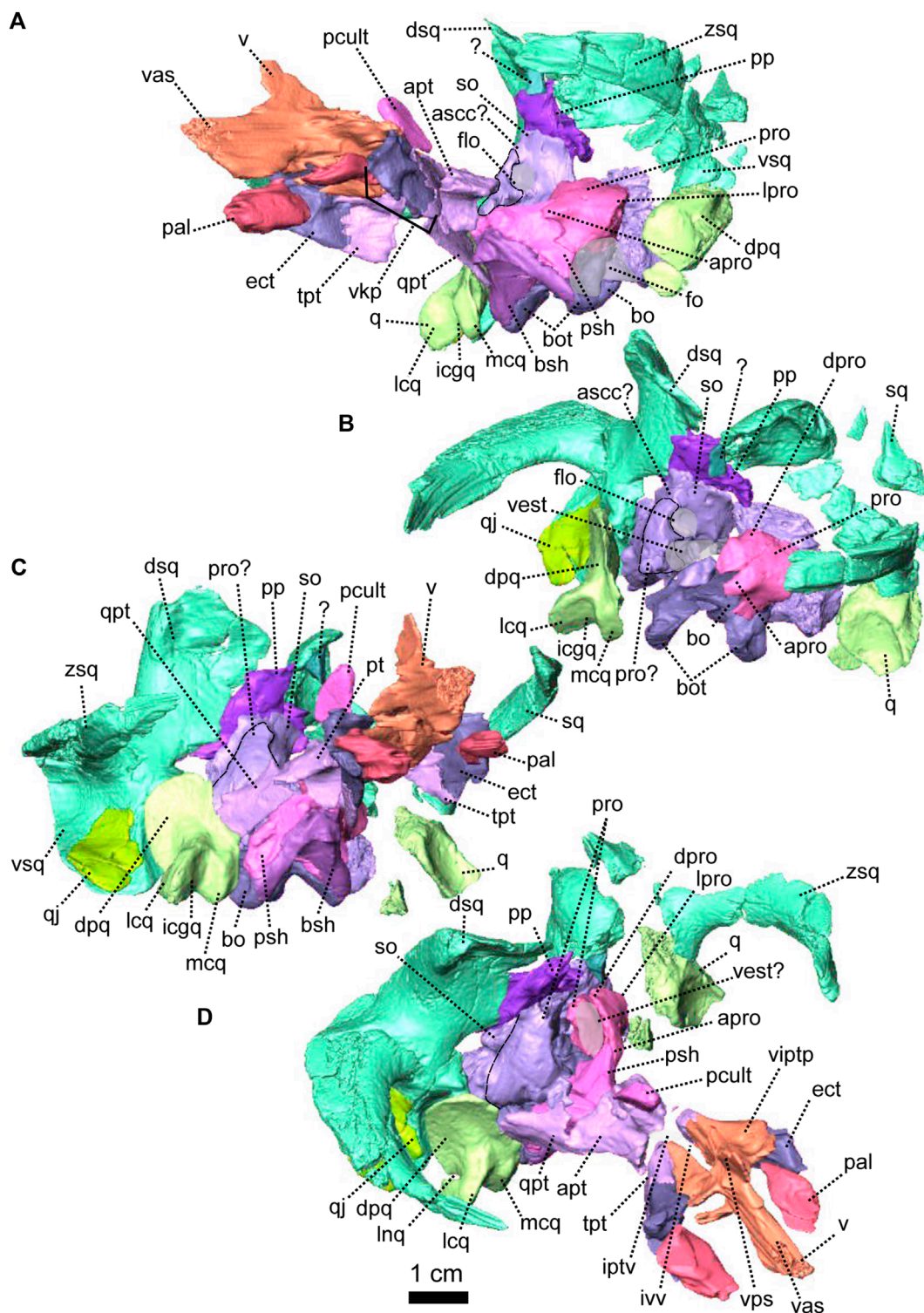
FIGURE 15
Occipital and palatal bones of *Eodicynodon oosthuizeni*, NMQR 2978, farm Rietkuil (previously named Zwartgrond), Rietbron district, Eastern Cape, South Africa; *Eodicynodon* AZ, Guadalupian, Beaufort Group, Karoo Supergroup. 3D rendering in **(A)**, left lateroventral view; **(B)**, left dorsolateral view; **(C)**, right lateroventral view and **(D)**, right laterodorsal view. Abbreviations: apro, anterior process of the prootic; apt, anterior process of the pterygoid; bo, basioccipital; bot, basioccipital tubera; bsh, basisphenoid; dpq, dorsal plate of the quadrate; dpro, dorsal process of the squamosal; ect, ectopterygoid; fo, fenestra ovalis; icgq, intercondylar groove of the quadrate; iptv, interpterygoid vacuity; ivv, intervomerine vacuity; lcq, lateral condyle of the quadrate; lnq, lateral notch of the quadrate; lpro, lateral bulge of the prootic; mcq, medial condyle of the quadrate; pal, palatine; pcult, processus cultriformis; pro, prootic; psh, parasphenoid; pt, pterygoid; q, quadrate; qj, quadratojugal; qpt, quadrate process of the pterygoid; so, supraoccipital; sq, squamosal; tpt, transverse process of the pterygoid; v, vomer; vas, vomer anterior septum; vest, vestibule; vitptp, vomer inter-pterygoid plate; vkp, ventral keel of the palate; vps, vomer posterior septum; vs., vomerine septum; vsq, ventral process of the squamosal; zsq, zygomatic process of the squamosal. Scale bar = 1 cm.

with the opisthotic is oblique while the contact with the basioccipital is short.

The basioccipital forms the ventral margin of the foramen magnum and the floor of the hindbrain region (Figures 11, 15). It comprises an anterior process and three lobes: the occipital condyle, and two basioccipital tubera (Figure 11). The dorsal surface of the basioccipital has been greatly eroded on both BP/1/6230 and NMQR 2978 specimens (Figures 11C, 12C). In ventral view, the basioccipital forms the medial border of the fenestra ovalis (Figure 11D). In posterior view, the basioccipital has a short contact with the proatlas facet of the exoccipital and contacts the opisthotic dorsolaterally with a short and oblique contact (Figure 12E). Below this contact, the basioccipital reaches the stapedial footplate. In ventral view, the occipital condyle is thick and extends posteriorly and has a large and rounded occipital pit which is visible in posterior view (Figure 11D, E). In ventral view, the basioccipital tubera extends anteroventrally from the lateral side of the basioccipital (Figure 11E) and the two tubera make an angle of 20° with the frontal plane (Figure 11E). In ventral view, the basioccipital tubera reach the parasphenoid anteriorly, with a transverse contact in ventral view, while this contact is oblique in lateral view (Figure 8B, D). In anterior view, the main corpus of the basioccipital has a short contact with the prootic laterally (Figure 8F), the contact being horizontal in lateral view (Figure 11B).

The stapes is a small bone linking the quadrate (external ear) to the soft inner ear in anomodonts. It is preserved in only four *Eodicynodon* specimens: ROZ 9, NMQR 3001, NMQR 2912 and R0Z B95 (Rubidge, 1990b). The stapes is not preserved in NMQR 2978 (Figures 8, 11) and only the left stapes is preserved in BP/1/6230 (Figures 7, 12, 16). It is deformed and displaced, but has a general bicrurate shape, in contrast to derived dicynodonts that have a rod-like shaped stapes (Castanhinha et al., 2013).

In lateral view, similarly to *Patranomodon*, the stapes comprises an anterior crus, posterior crus, stapedial head and stapedial footplate (Figure 16). The posterior crus is flattened to form a thin plate (Figures 12, 16). It forms the dorsal margin of the stapedial foramen (Figures 12B, 16A) and bears an opening towards the stapedial foramen in posterior view (Figure 12E). In lateral view, the anterior crus is thin and forms the ventral margin of the stapedial foramen (Figures 12B, 16A). In posterior view, the stapedial footplate is slightly distorted (Figure 12E). It contacts the opisthotic-prootic (=periotic) complex dorsally and the basioccipital medially. The stapedial head is positioned at the posterior end of the anterior crus, and contacts the posterior crus dorsally (Figure 16). In posterior view, the stapedial head is ovoid (Figure 12E).

The quadrate of *E. oosthuizeni* comprises the trochlea and dorsal plate (Figures 5, 11, 12, 16). In anterolateral view, the dorsal plate of the quadrate is roughly rectangular (Figure 5C) and has a flat posterior contact with the ventral process of the squamosal (Figures 5D, 11A, 12A). In anterior view, the dorsal plate of the quadrate contacts the quadratojugal laterally (Figure 11F) and in dorsolateral view a notch is present between the trochlea and the dorsal plate laterally (Figure 5D); also visible in ventral and dorsal view (Figure 4C, D). This notch accommodates the medial process of the quadratojugal. In anterodorsal view, the dorsal plate has a short dorsal contact with the opisthotic-prootic complex (Figure 15B).

The trochlea comprises two condyles (one medial and one lateral) and an intercondylar grove, visible in ventral and anterior view (Figures 8D, F, 12–D, F, 15, 16). Compared to the situation in *Patranomodon*, the lateral and medial condyles of *Eodicynodon* are massive and rounded, similar to the condyles found in *Niassodon* and *Lystrosaurus* (Cluver, 1971; Castanhinha et al., 2013). In ventral view, the lateral condyle of *Eodicynodon* is ovoid and the medial one is rectangular (Figure 11D). In anterior view, the lateral condyle extends ventrolaterally, while the medial condyle extends ventrally (Figure 11F).

The quadratojugal is a small and thin plate-like bone (Figures 11, 16) which is covered posteriorly by, and is in contact with, the ventral process of the squamosal, with what it shares a flat posterior contact (Figures 5C, 11A). In lateral view, the quadratojugal hooks onto the quadrate between the trochlea ventrally and the dorsal plate of the quadrate medially (Figures 11F, 12F).

The palate of NMQR 2978 is relatively well preserved (Figures 15, 17), but apart from the basisphenoid and part of the parasphenoid, most of the sphenethmoidal complex is absent.

The palate of BP/1/6230 is also in a good state of preservation, apart from the posterior section of the basioccipital and the anterior part of the palate (Figures 16, 18). The delicate presphenoid and orbitosphenoid are preserved (Figure 16C, D), but the ectopterygoids, hyoids and epypterygoids are missing (Figures 7, 18). Three unidentified bone fragments are possibly remnants of the quadrate process of the pterygoid and/or part of a displaced hyoid (Figure 18). The anterior section of the palate, including the premaxilla, is shattered, and the suture between the premaxilla and vomers is not identifiable (Figure 7D).

The vomer is a paired bone located at the anterior-most section of the palate (Figures 7D, 8D, 15, 16), and the midline suture is visible in anterior view in BP/1/6230 (Figure 18F). In lateral view, the vomer extends anterodorsally to form the septum which divides the air passage (Figure 16C). The anterior septae are fused dorsally in NMQR 2978 (Figures 15C, 17F). In both ventral and dorsal views, the vomer forms a paired inter-pterygoidal plate which is roughly triangular in dorsal view (Figures 15C, 17C, D). In ventral view, it contacts the ectopterygoid anterolaterally, and the transverse process of the pterygoid posterolaterally (Figure 17D). The suture with the pterygoid is oblique. In ventral and dorsal views, the intervomerine vacuity is positioned between the two vomers' inter-pterygoid plates (Figures 15C, 17C, D). It is roughly rectangular in ventral view and about 1.5 times wider than the interpterygoid vacuity (Figure 17D). The intervomerine vacuity is not present in *Patranomodon*. In lateral view, the two vomer inter-pterygoid plates join dorsally to form a posterior septum (Figures 15C, 17D, 18B). The vomer posterior septum is thin and divides dorsally to form a V-shaped process, similar to that of *Patranomodon* (Figure 18B). In lateral view, this process contacts the presphenoid anterodorsally. The anterior and posterior vomer septum observed in *E. oosthuizeni* were likely to have been connected and to form the vomerine process as evident in *Patranomodon* (Figures 6, 17, 18).

The palatine forms the large palatine pads characteristic of *Eodicynodon* (Figure 8D, H) and the ventral wall of the olfactory chamber (de Simão-Oliveira et al., 2019; Pusch et al., 2019). In contrast to the condition in *Patranomodon* the palatine pad of *E. oosthuizeni* is positioned close to the maxilla rather than close to the pterygoid (Figures 8D, 6D). In ventral view, the palatine is oval

FIGURE 16
Anatomical details of *Eodicynodon oosthuizeni*, BP/1/6230, from Bloukrans farm, Prince Albert district, Western Cape, South Africa; *Eodicynodon* AZ, Guadalupian, Beaufort Group, Karoo Supergroup. 3D rendering in **(A)**, left lateroventral view; **(B)**, left right lateroventral view; **(C)**, left lateroventral view and **(D)**, right lateroventral view. Abbreviations: acst, anterior crus of the stapes; apt, anterior process of the pterygoid; apobsh, anterior process of the orbitosphenoid; bo, basioccipital; bsh, basisphenoid; dpq, dorsal plate of the quadrate; dsq, dorsal process of the squamosal; ect, ectopterygoid; icgq, intercondylar groove of the quadrate; iptv, interpterygoid vacuity; ivv, intervomerine vacuity; j, jugal; lcq, lateral condyle of the quadrate; m, maxilla; mcq, medial condyle of the quadrate; n, nasal; obsh, orbitosphenoid; oc, olfactory cavity; pal, palatine; pcst, posterior crus of the stapes; pcult, processus cultriformis; pf, postfrontal; pm, premaxilla; po, postorbital; prsh, presphenoid; prf, prefrontal; psh, parasphenoid; pt, pterygoid; q, quadrate; qj, quadratojugal; qpt, quadrate process of the pterygoid; smtobsh, semi tubular region of the orbitosphenoid; so, supraoccipital; st, stapes; sth, stapedial head; stf, stapedial foramen; stfp, stapedial footplate; sq, squamosal; tpt, transverse process of the pterygoid; v, vomer; vitptp, vomer inter-pterygoid plate; vkobsh, ventral keel of the orbitosphenoid; vkp, ventral keel of the palate; vps, vomer posterior septum; vsq, ventral process of the squamosal; zsq, zygomatic process of the squamosal. Scale bar = 1 cm.

FIGURE 17
Palatal series of *Eodicynodon oosthuizeni*, NMQR 2978, farm Rietkuil (previously named Zwartground), Rietbron district, Eastern Cape, South Africa; *Eodicynodon* AZ, Guadalupian, Beaufort Group, Karoo Supergroup. 3D rendering in **(A)**, right lateral view; **(B)**, left lateral view; **(C)**, dorsal view; **(D)**, ventral view; **(E)**, posterior view and **(F)**, anterior view. Abbreviations: apt, anterior process of the pterygoid; bsh, basisphenoid; ect, ectopterygoid; iptv, interpterygoid vacuity; ivv, intervomerine vacuity; pal, palatine; pcult, processus cultriformis; pcultc, processus cultriformis crest; psh, parasphenoid; pt, pterygoid; qpt, quadrate process of the pterygoid; tpt, transverse process of the pterygoid; v, vomer; vas, vomer anterior septum; vitptp, vomer inter-pterygoid plate; vkp, ventral keel of the palate; vps, vomer posterior septum. Scale bar = 1 cm.

FIGURE 18
Palatal bones of *Eodicynodon oosthuizeni*, BP/1/6230, from Bloukrans farm, Prince Albert district, Western Cape, South Africa; *Eodicynodon* AZ, Guadalupian, Beaufort Group, Karoo Supergroup. 3D rendering in **(A)**, right lateral view; **(B)**, left lateral view; **(C)**, dorsal view; **(D)**, ventral view; **(E)**, posterior view; **(F)**, anterior view and **(G)**, ventral view with surrounding cranial bones. Abbreviations: apt, anterior process of the pterygoid; apobsh, anterior process of the orbitosphenoid; bo, basioccipital; bsh, basisphenoid; c, caniniform tooth; dpq, dorsal plate of the quadrate; ect, ectopterygoid; icgq, intercondylar groove of the quadrate; iptv, interpterygoid vacuity; ivv, intervomerine vacuity; j, jugal; lcq, lateral condyle of the quadrate; m, maxilla; mcq, medial condyle of the quadrate; n, nasal; obsh, orbitosphenoid; oc, olfactory cavity; op, opisthotic; pal, palatine; pcult, processus cultriformis; ppm, palatal process of the premaxilla; prsh, presphenoid; psh, parasphenoid; pt, pterygoid; q, quadrate; qj, quadratojugal; qpt, quadrate process of the pterygoid; sq, squamosal; st, stapes; smtobsh, semi tubular region of the orbitosphenoid; tpt, transverse process of the pterygoid; vitptp, vomer inter-pterygoid plate; vkobsh, ventral keel of the orbitosphenoid; vkp, ventral keel of the palate; vps, vomer posterior septum; zsq, zygomatic process of the squamosal. Scale bar = 1 cm.

(Figure 17D). It contacts the maxilla anterolaterally and anteriorly with a curved suture. Posterolaterally, the palatine contacts the ectopterygoid (Figures 8H, 17D) with an oblique suture in ventral view (Figure 17D) and vertical in medial view (Figure 8H).

Like in most non-mammalian synapsids, the pterygoid of *E. oosthuizeni* is a tripartite bone comprising the transverse flange (called palatal ramus in Cluver, 1971), anterior ramus (also called palatal ramus in Castanhinha et al., 2013) and quadrate ramus (Figures 15–18). In lateral view, the transverse flange forms, with the ectopterygoid, the ventral keel of the palate (Figures 15A, 16A, 17A, B, and 18A, B). A similar large palatal keel is found in *Prosictodon*, but is reduced in other dicynodonts (Sullivan and Reisz, 2005; Angielczyk and Rubidge, 2010; Castanhinha et al., 2013; Angielczyk et al., 2017). In posterior view, the palatal keel makes an angle of 80° with the horizontal plane. In the same view, the pterygoid contacts the ectopterygoid anteriorly (Figure 18E). In lateral view, the transverse flange of the pterygoid contacts the ectopterygoid anteriorly with an interdigitated suture (Figures 15B, 16A, 17A, B). In ventral view, the pterygoid has an oblique medial contact with the vomer (Figure 17D) and extends posteriorly to form the anterior process of the pterygoid (Figures 17D, 18D). The anterior process is triangular in both dorsal and ventral views (Figure 18C, D). In ventral view, the interpterygoid vacuity is diamond-shaped and positioned posterior to the intervomerine vacuity at the level of the contact between the transverse process and the anterior process of the pterygoid (Figures 17D, 18D). Posterior to the interpterygoid vacuity, in lateral view, the left and right anterior processes meet in the midline to form a vertical keel (Figures 16A, 17B, D, 18B, D). This keel is smaller than the transverse flange keel and contacts the parasphenoid posteriorly (Figure 16A) with an oblique suture when seen in lateral view (Figure 18B). The pterygoid expands dorsally into a conical boss which makes up the floor of the braincase. In dorsal view, this dorsal boss of the pterygoid meets with the presphenoid anteriorly (Figure 18C). The quadrate ramus is short and forms the posterolateral extension of the anterior process of the pterygoid (Figures 15–18). It curves posterolaterally toward the medial condyle of the quadrate (Figures 7D, 8D).

The ectopterygoid is positioned on the anterior side of the palatal keel (Figures 8, 15–17). In lateral view, the ectopterygoid is rectangular and contacts the pterygoid posteriorly (Figure 17A, B). In ventrolateral view, the ectopterygoid contacts the jugal anteriorly, has a short oblique contact with the maxilla anteriorly, and reaches the palatine anteroventrally (Figures 15B, 16D). In ventral view, the ectopterygoid meets the maxilla anterolaterally and the palatine anteromedially with an oblique suture on the anterior side (Figure 8D).

The sphenethmoidal complex includes internal bones that support the hindbrain anterior to the pila antotica and the forebrain up to the olfactory chamber (Benoit et al., 2017; Laaß et al., 2017; Pusch et al., 2019). It comprises the orbitosphenoid, presphenoid, epipterygoid (paired, possibly related to the mammalian alisphenoid see Crompton et al., 2018), parasphenoid, basisphenoid (called the parabasisphenoid when fused to the parasphenoid) and the paired hyoids. These bones are most often broken or not preserved in therapsids (as not fully ossified in come taxa, see Benoit et al. (2017)). With the exception of a few exceptional specimens (Barry, 1974), the hyoids have only been properly studied with the

recent development of CT-scanning technologies (Laaß, 2015b; Araújo et al., 2017; Benoit et al., 2017).

The orbitosphenoid (ethmoid in Castanhinha et al., 2013) supports the olfactory bulbs in the olfactory chamber (Barry, 1974; Laaß, 2015b; Araújo et al., 2017; Benoit et al., 2017; Macungo et al., 2022). In specimen BP/1/6230, the orbitosphenoid is slightly displaced anteriorly, and would initially have had a loose articulated contact with the frontal (Figure 16C). The paired orbitosphenoid of *E. oosthuizeni* comprises a semi-tubular region, ventral keel and anterior process (Figures 16, 18). The semi-tubular region is formed by two hemicylindrical orbitosphenoids which join ventrally and encapsulate the olfactory cavity of the forebrain. In dorsal view, the semi-tubular region is U-shaped (Figure 18C). In lateral view, the orbitosphenoid projects as a posteroventrally oriented keel which is roughly rectangular and has the same surface area as the semi-tubular region (Figures 16A, C, 18B).

The orbitosphenoid also extends anteriorly to form the anterior process of the orbitosphenoid. This process is hammerhead-shaped and is roughly triangular in dorsal view (Figure 18C). The ventral keel would have sutured anteriorly with the vomers and posteroventrally with the interorbital septum of the presphenoid (Barry, 1974; Benoit et al., 2017; Crompton et al., 2018), but the contact is lost in BP/1/6230.

The presphenoid forms a thin septum-like bone (Figures 16, 18) and is possibly fused to the processus cultriformis of the parasphenoid posteriorly (Figures 16C, 18). In lateral view, the posterior section is rectangular and extends anteriorly as a thin triangular ramus (Figure 18A, B) which has a medial depression on the dorsal side (Figure 18E). In ventral view, the presphenoid has a contact with the posterior side of the pterygoid dorsal boss (Figure 18A).

The parasphenoid and the basisphenoid, which are partially preserved in BP/1/6230 and NMQR 2978, are not fused in *Eodicynodon*. The parasphenoid forms the top of the parabasisphenoid complex and the basisphenoid forms the base (Figures 15A, C, 16, 17 and 18). The anterior portion of the processus cultriformis is an isolated septum which is rounded anterodorsally (Figures 8G, H, 15, 17A, B). In lateral view, the contact between the parasphenoid and the basisphenoid is oblique (Figures 15B, 17B) and in ventral view the main corpus of the parasphenoid has a transverse posterior contact with the basioccipital (Figure 8D). In dorsal view, the parasphenoid contacts the prootic posterolaterally at the level of the vestibule (Figures 8B, D and 15D). This forms the anterior wall of the base of the hindbrain (Figure 15D). In lateral view, the contact between the prootic and the parasphenoid is oblique (Figure 8A, B). Neither the carotid foramina nor the *canalis vidii* are preserved on NMQR 2978 and BP/1/6230. In lateral and ventral view, the basisphenoid shows two ventrolateral processes that reach the basioccipital posteroventrally (Figures 8D, 15A, C). In ventral view, the basisphenoid is triangular (Figure 17D). In lateral view, it makes an angle of 45° with the transverse plane (Figure 8B). In the same view, the basisphenoid contacts the base of the basioccipital tubera posteroventrally (Figure 8B, H).

No lower jaw is preserved with NMQR 2978 (Rubidge, 1990b) but BP/1/6230 preserves an articulated mandible (Figure 7). The posterior end of the lower jaw has been distorted as the result of the deformation of the occiput (Figures 7, 19). Both lower jaw rami are preserved showing a mandibular fenestra bordered by the dentary,
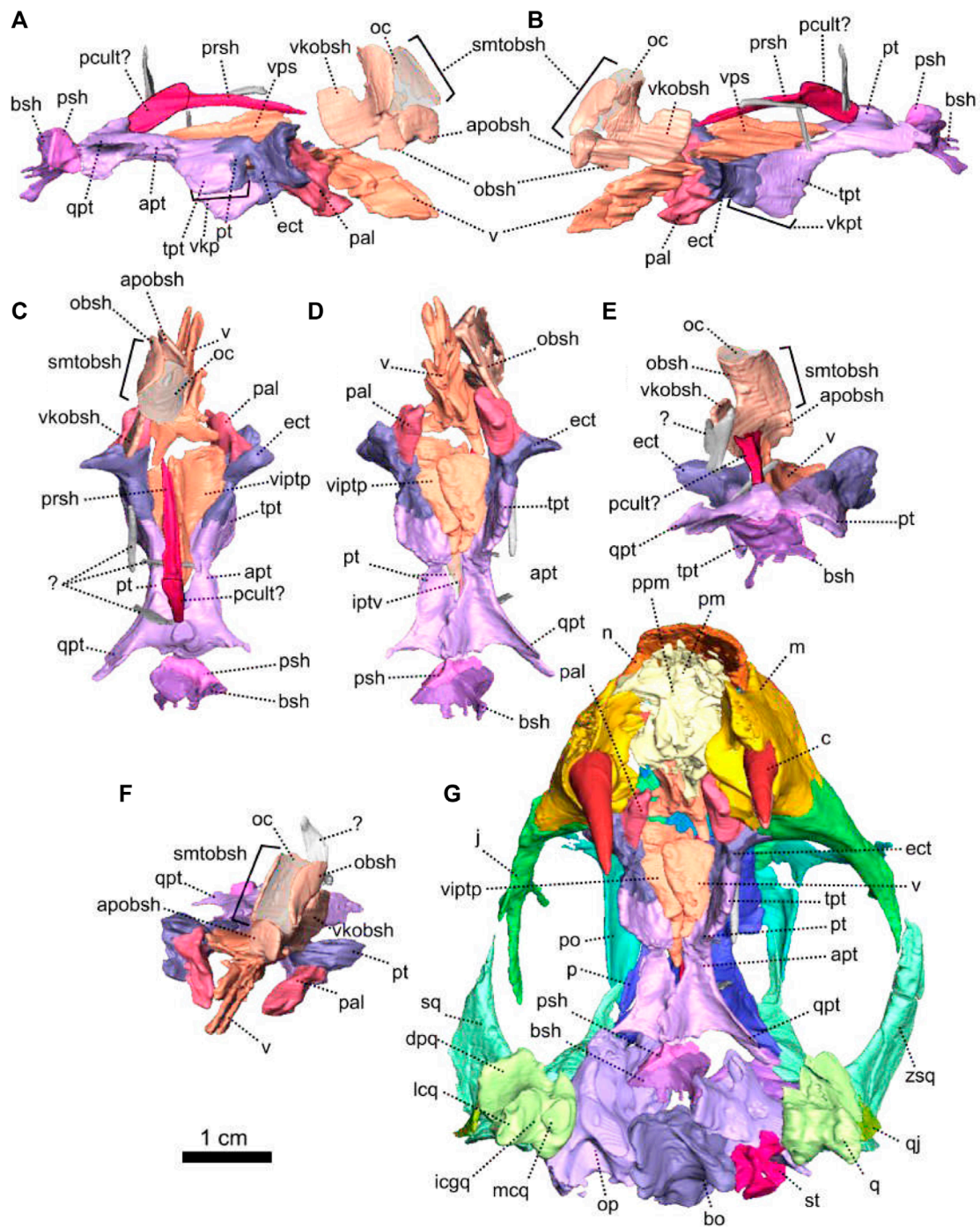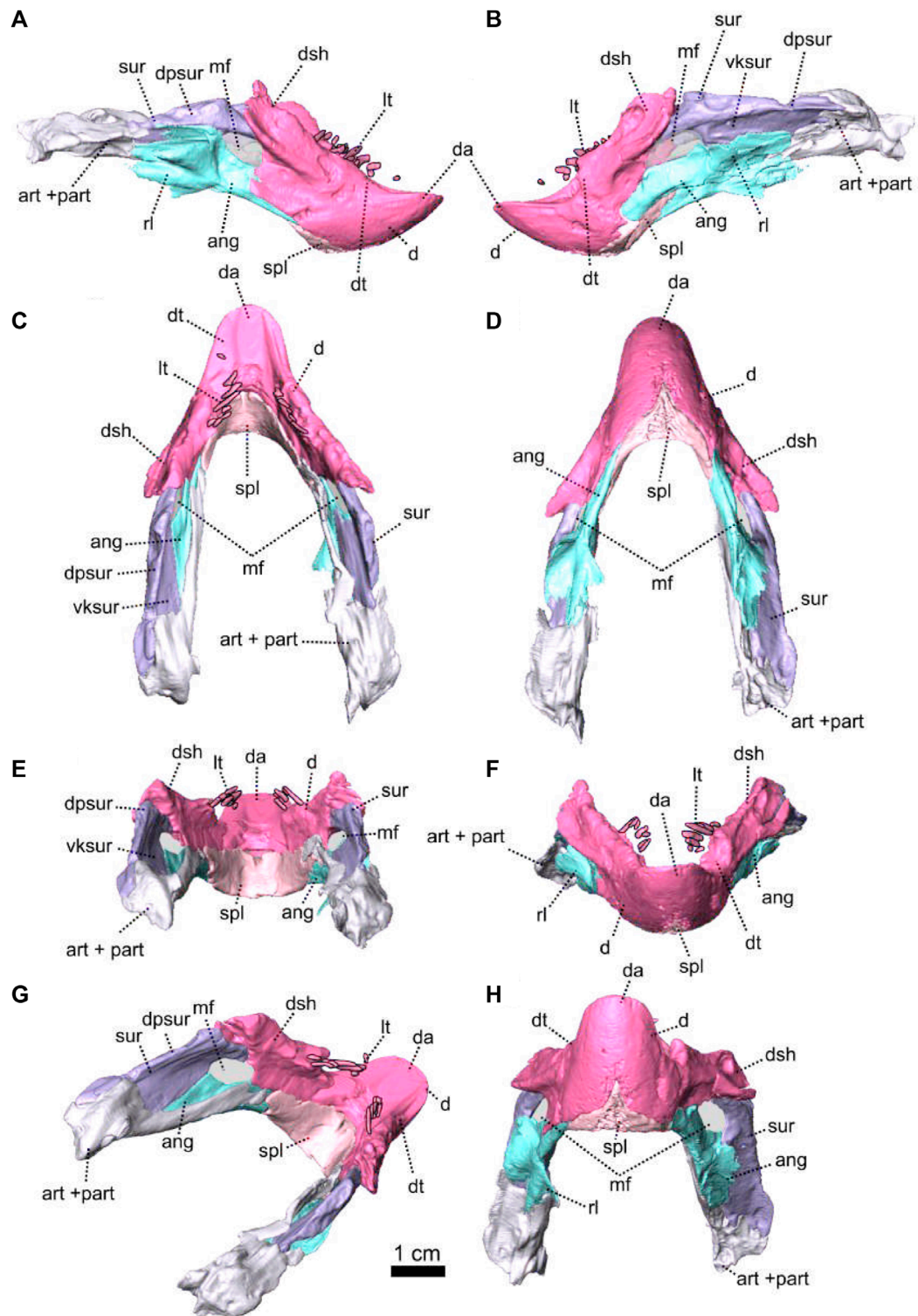
FIGURE 19
Lower jaw of *Eodicynodon oosthuizeni*, BP/1/6230, from Bloukrans farm, Prince Albert district, Western Cape, South Africa; *Eodicynodon* AZ, Guadalupian, Beaufort Group, Karoo Supergroup. 3D rendering in **(A)**, right lateral view; **(B)**, left lateral view; **(C)**, dorsal view; **(D)**, ventral view; **(E)**, posterior view; **(F)**, anterior view; **(G)**, right laterodorsal view and **(H)**, anteroventral view. Abbreviations: ang, angular; art, articular; d, dentary; da, dentary apex; dpsur, dorsal process of the surangular; dsh, dentary shelf; dt, dentary table; lt, lower jaw teeth; mf, mandibular fenestra; part, pre-articular; rl, reflected lamina; spl, splenial; sur, surangular; vksur, ventral keel of the surangular. Scale bar = 1 cm.

surangular and angular (Figure 19) as is present in all anomodonts (Modesto et al., 1999).

The dentary is well preserved as a single element (Figures 7, 19). In anterior view, the symphysis is fused dorsally (Figure 19F, H) and is triangular in ventral view (Figure 19F, H). No signs of the nutrient foramina, usually associated with the presence of a keratinous beak, are evident. In ventral view, the dentary contacts the splenial anteromedially, and the angular posteromedially (Figure 19D). The contact with the angular is long and oblique and the contact with the splenial is V-shaped (Figure 19D, H).

Overall, the dentary has a typical dicynodont morphology, with an edentulous and round anterior apex and two posterior processes, with the lateral dentary shelf and table on the dorsal side (Figure 19A). In lateral view, the posterior processes form the anterior margin of the mandibular fenestra (Figure 19A). In dorsal view, the dentary apex bears a gentle groove, bordered by the two dentulous dentary tables (Figure 19C, G). In lateral view, the anterior portion of the dentary table has a deep depression anterior to the mandibular teeth (Figure 19B). The dentary table extends posterodorsally to form the dentary shelf (Figure 19A, B) which extends onto the surangular above the mandibular fenestra where it exhibits a thick and rounded lateral margin (Figure 19E, F).

The splenial is a small and thin unpaired bone, with a short exposure on the lateral side of the jaw (Figures 7, 19). In lateral and anterior view, the splenial is overlapped by the dentary dorsally (Figure 19A, B, E, G, H) and in posterior view the splenial is broad on the medial side of the symphysis and thins posteriorly on each jaw ramus (Figure 19D, E, G). The splenial contacts the prearticular ventral to the lateral dentary shelf (Figure 7B–D, G) and meets the angular posteromedially (Figure 19D).

The angular forms the posteroventral margin of the lower jaw (Figures 7, 19) and in lateral view it makes up the ventral margin of the mandibular fenestra (Figure 19A, B). It is overlapped by the dentary anteriorly, contacts the surangular dorsally and the articular posteriorly (Figure 19A, B). In ventral view, the angular has a long contact with the prearticular on the medial side (Figure 19D). The right reflected lamina has been shattered but the left one is intact and is broad and thin (Figure 19). In lateral view, the reflected lamina extends posteriorly as three processes (Figure 19A). It contains three distinct fossae: the anteroventral, anterodorsal and posteroventral fossae (Olroyd and Sidor, 2022). The dorsal notch of the reflected lamina is V-shaped and placed at the level of the mandibular fenestra (Figure 19A and Olroyd and Sidor, 2022).

The surangular is the dorsal-most bone of the lower jaw (Figures 7, 19) and comprises a flat horizontal dorsal process and a slender ventral keel (Figure 19B, G, H). In lateral view, the anterior margin of the keel forms the posterior border of the mandibular fenestra (Figure 19B) and the dorsal process of the surangular meets up with the dentary shelf of the dentary anteriorly (Figure 19B). This dorsal process forms the dorsal margin of the mandibular fenestra. The ventral keel of the surangular contacts the angular ventrally, and posteriorly the surangular contacts the articular with an oblique suture which is visible in dorsal view (Figure 19C). On the medial side of the lower jaw, the ventral keel of the surangular contacts the prearticular posteroventrally (Figure 19G).

In BP/1/6230, the prearticular and the articular are co-ossified (Figure 19). A similar condition is found in *Niassodon* (Castanhinha et al., 2013). Posteriorly, the articular surface comprises two articular condyles, lateral and medial (Figure 19F, G). In lateral view, the articular contacts the surangular anterodorsally and the angular anteroventrally (Figure 19B). On the medial side, the prearticular is a thin and elongated rod-like process which extends along the surangular and the angular to contact the splenial anteriorly (Figure 19–D, E, G).

Specimen NMQR 2978 bears a single well-formed closed-rooted tusk on either side of the maxilla (Figure 8 and see Supplementary Material). An additional small oval postcanine is placed posteriorly to the left tusk.

Specimen BP/1/6230 manifests the usual dicynodont tusk on either side of the maxilla, and an additional tusk is present posterior to the large tusk on the left side of the maxilla (Figure 7 and see Supplementary Material). One postcanine tooth is present on the maxilla (Figures 7, 19 and see Supplementary Material). The lower jaw has five small conical teeth on the dentary.

3.1.3 NMQR 2913, holotype of *Eodicynodon oelofseni*

SYSTEMATIC PALEONTOLOGY
THERAPSIDA Broom, 1905
ANOMODONTIA Owen, 1859
DICYNODONTIA Owen, 1859
Eodicynodon Barry, 1974
Eodicynodon oelofseni Rubidge, 1990a

Material—Skull, lower jaw and indeterminate postcranial elements.

Type locality—Botterkraal farm, Abrahamskraal Formation, *Eodicynodon* Assemblage Zone, Karoo Beaufort Group, South Africa.

List of figures—Figures 20–22.

Diagnosis—after Rubidge (1990a), canine tusk-like teeth absent; laterally situated maxillary teeth which point in an anterior direction; no coronoid eminence on the posterodorsal surface of the dentary.

Description—Specimen NMQR 2913 comprises a reasonably well-preserved skull and lower jaw, and a few postcranial elements. The cranial material was published by Rubidge (1990a) as a new taxon, *Eodicynodon oelofseni*. Here NMQR 2913 is redescribed in the light of new anatomical data which has been revealed through CT scanning and has taxonomic implications. The scan of NMQR 2913 was made after the specimen had been accidentally broken into three pieces through the years of research at the National Museum and was subsequently reassembled: snout with the anterior portion of the palate and attached; occiput with the posterior part of the palate; and the lower jaw (Figures 20–22). The specimen has been deformed through postmortem damage (Rubidge, 1990a). The posterior section of the palate is crushed and twisted though 45° and the occiput has been displaced (Figure 21).

Because of poor preservation parts of the skull were inaccessible and could not be fully described in the first publication of Rubidge (1990a), but scanning has enhanced possibilities for description. The paired premaxilla forms the anterior and anteroventral margin of the naris and the tapering dorsal extension has a wedged contact with the nasal, extending to a point behind the posterior margin of the external naris (Figure 20–A,B). Ventrally, the premaxilla has a palatal extension (Figure 20). In ventral view, the short

FIGURE 20
Snout and skull roof fragment of *Eodicynodon oelofseni*, NMQR 2913, farm Botterkraal, Prince Albert district, Western Cape, South Africa; *Eodicynodon* AZ, Guadalupian, Beaufort Group, Karoo Supergroup. 3D rendering in **(A)**, right lateral view; **(B)**, left lateral view; **(C)**, dorsal view; **(D)**, ventral view; **(E)**, posterior view; **(F)**, anterior view; **(G)**, left ventrolateral view and **(H)**, right posterolateral view. Abbreviations: app, anterior process of the parietal; ect, ectopterygoid; eo, exoccipital; f, frontal; j, jugal; l, lacrimal; m, maxilla; n, nasal; npm, nasal process of the premaxilla; p, parietal; pal, palatine; pc, postcanine; pf, postfrontal; pm, premaxilla; po, postorbital; pob, postorbital bar; pp, postparietal; ppf, posterior process of the frontal; ppm, palatal process of the premaxilla; prf, prefrontal; prp, preparietal; smx, septomaxilla; sq, squamosal; srspo, skull roof section of the postorbital; v, vomer. Scale bar = 1 cm.

FIGURE 21
Occipital piece of *Eodicynodon oelofseni*, NMQR 2913, farm Botterkraal, Prince Albert district, Western Cape, South Africa; *Eodicynodon* AZ, Guadalupian, Beaufort Group, Karoo Supergroup. 3D rendering in **(A)**, right lateral view; **(B)**, left lateral view; **(C)**, dorsal view; **(D)**, ventral view; **(E)**, posterior view and **(F)**, anterior view. Abbreviations: apt, anterior process of the pterygoid; bo, basioccipital; bptp, basipterygoid process; cf, carotid foramen; dsq, dorsal process of the squamosal; iptv, interpterygoid vacuity; op, opisthotic; pbs, parabasisphenoid; pcult, processus cultriformis; pro, prootic; pt, pterygoid; ptf, postemporal fenestra; q, quadrate; qj, quadratojugal; qpt, quadrate process of the pterygoid; so, supraoccipital; sq, squamosal; st, stapes; t, tabular; tpt, transverse process of the pterygoid; v, vomer; vas, vomer anterior septum; vest, vestibule; vsq, ventral process of the squamosal. Scale bar = 1 cm.
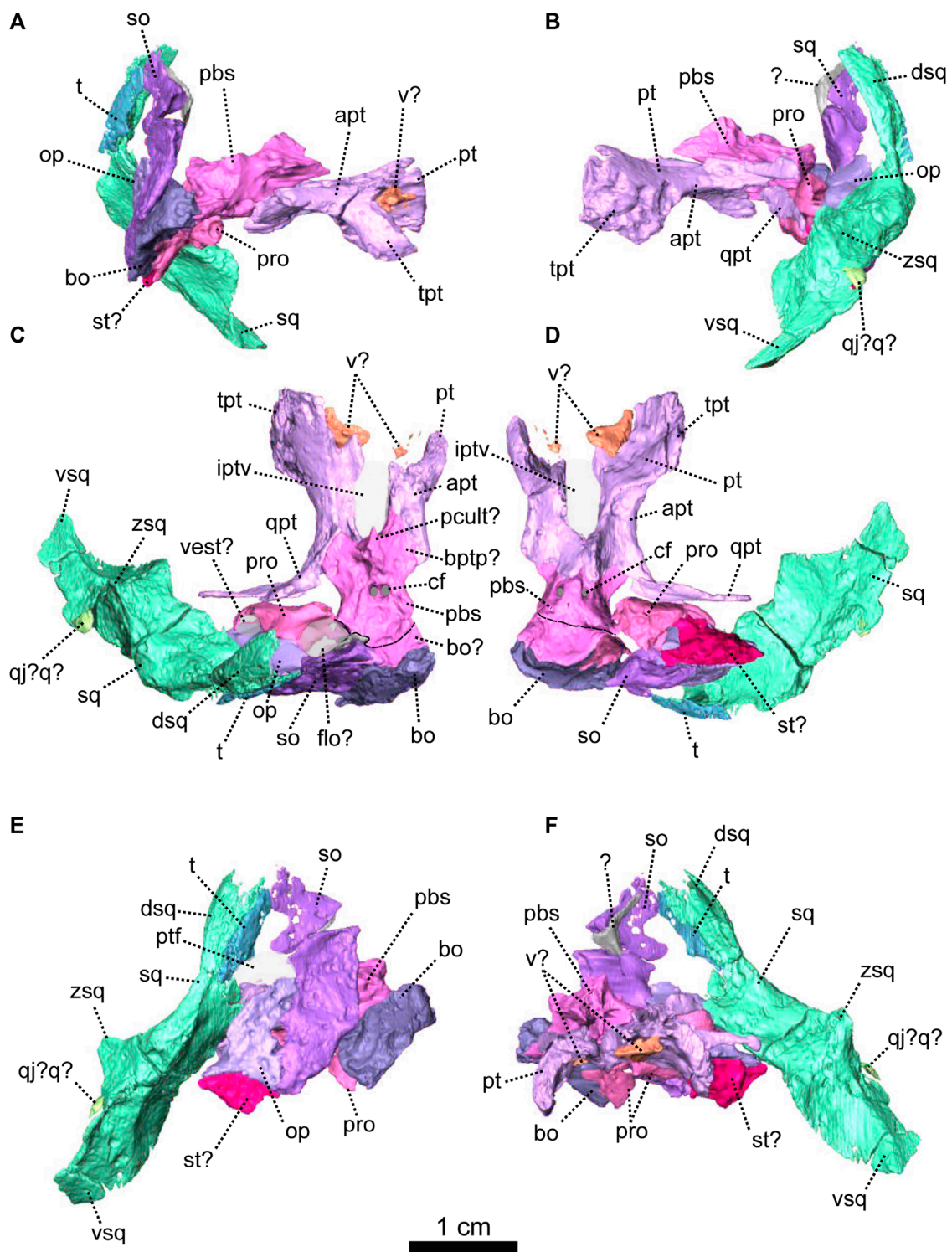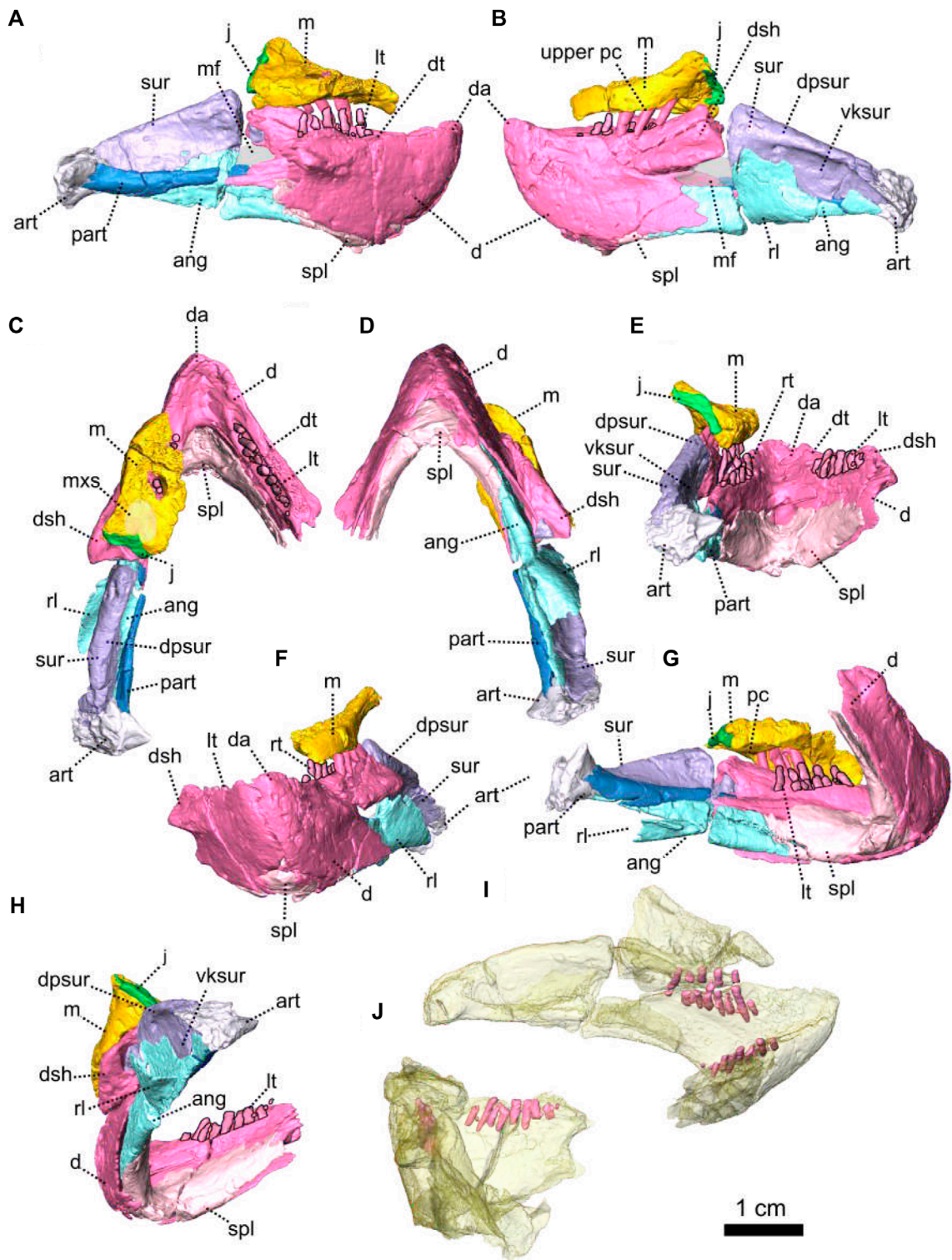
FIGURE 22
Lower jaw piece of *Eodicynodon oelofseni*, NMQR 2913, farm Botterkraal, Prince Albert district, Western Cape, South Africa; *Eodicynodon* AZ, Guadalupian, Beaufort Group, Karoo Supergroup. 3D rendering in **(A)**, right lateral view; **(B)**, left lateral view; **(C)**, dorsal view; **(D)**, ventral view; **(E)**, posterior view; **(F)**, anterior view; **(G)**, left posterolateral view and **(H)**, right lateroventral view. 3D rendering of the lower jaw teeth in **(I)**, left posteromedial view and **(J)**, right posteromedial view. Scale bar = 1 cm. Abbreviations: ang, angular; art, articular; d, dentary; da, dentary apex; dpsur, dorsal process of the surangular; dsh, dentary shelf; dt, dentary table; j, jugal; lt, lower jaw teeth; m, maxilla; mf, mandibular fenestra; mxs, maxillary sinus; part, pre-articular; pc, postcanine; rl, reflected lamina; spl, splenial; sur, surangular; vksur, ventral keel of the surangular. Scale bar = 1 cm.

premaxillary palatal extension is roughly rounded as a result of postmortem deformation (Figure 20D) and possibly has a midline suture (Rubidge, 1990a). It contacts the maxilla laterally with an oblique suture and has a short oblique contact with the septomaxilla posterolaterally (Figure 20D). Posteriorly the palatal extension of the premaxilla contacts the vomers (Figure 20D). This contact is oblique in ventrolateral view (Figure 20G).

Amongst the four basal anomodont specimens described in this paper, NMQR 2913 is the only specimen with a complete nasal process of the premaxilla which thins posteriorly on the skull roof as it wedges along the midline between the nasals. The nasal process of NMQR 2913 is visible on both the external and internal surface of the snout whereas in *Patranomodon* it intrudes the nasal and is visible only on the dorsal side (Figures 1G, 20C, H). The nasal process of NMQR 2913 is also relatively longer than those of NMQR 3000, BP/1/6230 and NMQR 2978 (Figures 1, 7, 8, 20).

Specimen NMQR 2913 is the only specimen of our sample that has the septomaxilla preserved (Figure 20). This bone, as evident from the right side of the skull, comprises two processes: an intranarial section and a lateral facial extension (Figure 20A, D). In lateral view, the lateral facial extension is triangular with the base forming the round posterodorsal margin of the naris and tapers posteriorly toward the lacrimal (Figure 20A). It has a long curved dorsal sutural contact with the nasal as evident in lateral view (Figure 20A). The septomaxilla is overlapped by the lacrimal posteroventrally and by the maxilla ventrally (Figure 20A, F). In ventral view, the intranarial section is triangular and reaches the premaxilla anteriorly with a curved contact (Figure 20D). On the left side of the skull, the lateral facial extension of the septomaxilla is not evident in the reconstruction (Figure 20B), but as the sutures are not clear on this part of the skull, it is likely to be present but was not recognised.

The maxilla forms the posteroventral border of the snout and is best preserved on the left (Figure 20). Here the maxilla is preserved in two parts: a dorsal section which is present on the snout fragment and a ventral fragment which is attached to the lower jaw fragment (Figures 20, 22). In lateral view, the maxilla is broadly triangular with the apex extending dorsally to meet the lacrimal with a rounded contact (Figure 20A, B). It has a short contact with the jugal posteriorly (Figure 22B), and an oblique suture with the nasal anterodorsally (Figure 20B). The dorsal contact with the lacrimal is shorter on the left side of the snout (Figure 20A, B). The maxilla meets the septomaxilla dorsally with a curved contact (Figure 20A). In ventral view, the left maxilla is triangular and a large maxillary sinus is present at the posterior end (Figure 20D) and is also evident in posterior view (Figure 20H). The left maxilla has three teeth while the right bears six (Figures 20, 22).

The paired nasal forms a large part of the anterior section of the snout (Figure 20) and is triangular in dorsal view with the apex pointing anteriorly (Figure 20C). In lateral view, the nasal forms the posterodorsal margin of the naris (Figure 20A, B). In dorsal view, the nasal has a straight transverse sutural contact with the frontal, but this shape is likely due to preservation (Figure 20C). Anterodorsally the nasal has a long contact with the nasal process of the premaxilla (Figure 20C). The contact is oblique in both lateral and dorsal views (Figure 20B, C). In lateral view, the nasal contacts the lacrimal posteroventrally (Figure 20A, B) but the nature of the contact is uncertain because of poor lacrimal preservation. Ventrally,

the nasal is overlapped by the maxilla (Figure 20F). This contact is oblique in lateral view and horizontal on the medial side of the skull (Figure 20H).

On both sides of the skull the lacrimal is poorly preserved (Figure 20) and typically makes up the anterodorsal border of the orbit (Figure 20A, B). In lateral view, it has a short posterodorsal contact with the prefrontal, an oblique suture with the nasal anterodorsally, touches the septomaxilla anteriorly, and contacts the maxilla anteroventrally (Figure 20A). The lacrimal foramen could not be determined because of poor preservation.

Most of the jugal is missing and this bone is present only as a thin slither, mostly on the lower jaw fragment (Figures 20, 22). It is rectangular in posterior view (Figure 20E). In lateral view, the jugal contacts the maxilla anteriorly as the maxilla surrounds the edges of the jugal (Figure 22A). In posterior view, the jugal possibly contacts the ectopterygoid ventrally (Figure 20E).

The postorbital, as preserved on the left side of the skull, is relatively small (Figure 20) and forms a small section of the skull roof on the anterodorsal margin of the temporal fenestra and the entire postorbital bar (Figure 20B). The postorbital bar is missing on the right side of the skull (Figure 20A). In lateral view, the postorbital overlaps the postfrontal anteriorly, and the parietal posteromedially (Figure 20B). In dorsal view, the contact of the postorbital with the postfrontal is curved, and oblique with the parietal (Figure 20C). The postorbital has a short contact with the squamosal posteriorly, which is evident in dorsal view (Figure 20C). In ventral view, unlike *E. oosthuizeni* specimens BP/1/6230 and NMQR 2978, the surface of the postorbital is smooth and does not show any ornamentation (Figures 13, 14, 20D). In lateral view, the postorbital bar forms the posterior margin of the orbit, and the anterior margin of the temporal fenestra (Figure 20B). It is thin and originates dorsally at the contact between the postorbital and the postfrontal.

The squamosal of NMQR 2913 is preserved as two separate pieces (Figures 20, 21). The small anterior fragment contacts the postorbital anterodorsally on the margin of the temporal fenestra (Figure 20). The posterior fragment forms the posterior and posteroventral margins of the temporal fenestra, and curves anteroventrally. On the posterior fragment, in lateral view, the squamosal is bent anteroventrally (Figure 21B). It does not fold backwards as in other dicynodonts and is rather straight, similar to the situation in *Patranomodon* (Figure 1). The zygomatic process of the squamosal is missing, and only the ventral and the dorsal processes are preserved (Figure 21). In posterior view, the ventral process is thin and rounded ventrally and bears a vertical ridge (Figure 21E). The dorsal process is broken dorsally. It is overlapped by the tabular dorsally and contacts the supraoccipital dorsomedially. In anterior view, the dorsal process has a lateral ridge (Figure 21F), and a curved ridge originates medially at the base of the dorsal process and terminates laterally at the base of the broken zygomatic process.

The orbital region of NMQR 2913 is poorly preserved and the zygomatic arches are missing (Figure 20). The jugal is damaged on both sides, the left prefrontal is missing, and the zygomatic process of the squamosal is not preserved. The postorbital bar is preserved only on the left side of the skull.

The prefrontal, preserved only on the right side (Figure 20), forms the anterodorsal margin of the orbit in lateral view (Figure 20A). It contacts the lacrimal anteroventrally. In dorsal view,

the prefrontal reaches the nasal anteromedially with a V-shaped suture, and has an oblique posteromedial sutural contact with the frontal (Figure 20C).

The frontal is a paired bone (Figure 20) with a straight midline suture which is visible only on the posterior part of the skull roof (Figure 20C). In dorsal view, the frontal covers the skull roof from the nasal to the level of the centre of the temporal fenestra (Figure 20C) and makes up the dorsal margin of the orbit between the prefrontal and the postfrontal (Figure 20A, B). It has a straight transverse contact with the nasal anteriorly, in both dorsal and ventral view (Figure 20C, D). In dorsal view, the frontal meets the prefrontal anterolaterally with an oblique contact and posteromedially the frontal overlaps the preparietal (Figure 20C, D). The posterior process of the frontal is triangular in dorsal view (Figure 20C) and extends posterolaterally as a wedge between the parietal and the postorbital in both dorsal and ventral views (Figure 20C, D). Posterolaterally, the frontal contacts the postfrontal (Figure 20) with a straight and longitudinal contact evident from the dorsal view (Figure 20C). In ventral view, the frontal bears a longitudinal ridge that reaches the parietal posteriorly (Figure 20D). In the same view, the postfrontal overlaps the frontal ridge.

In lateral view, the postfrontal forms the posterodorsal margin of the orbit (Figure 20B). It is triangular in dorsal view and is present as a wedge between the postorbital laterally, the frontal medially and its apex touches the parietal posteriorly (Figure 20C). In ventral view, the postfrontal slightly overlaps the frontal anteromedially (Figure 20D). In dorsal view, the postfrontal contacts the postorbital posterolaterally. The contact is curved in both dorsal and ventral views (Figure 20C, D).

The preparietal of NMQR 2913 is unpaired ovoid bone positioned between the parietals and the frontals (Figure 20) but does not border on the pineal foramen unlike the situation in *Patranomodon* and specimen BP/1/6230 (Figures 3C, 14C, 20C). The preparietal contacts the frontals anteriorly with a semilunate suture (Figure 20C). In ventral view, the preparietal is also ovoid, overlapping the frontals anteriorly and the parietals laterally (Figure 20D).

The parietal is a paired bone present on the skull roof and on the dorsal section of the occiput (Figure 20). In dorsal view, the parietal surrounds the pineal foramen and the medial anterior process tapers between the frontal laterally and the preparietal medially (Figure 20C). A smaller lateral anterior process is present between the frontal and the postfrontal. In dorsal view, the parietal has a long lateral contact with the postorbital (Figure 20C). In dorsal, ventral and posterior views, this contact is curved (Figure 20C, D, E). In dorsal and posterior views, the parietal sutures with the squamosal posterolaterally (Figure 20C, E) and extends onto the occiput where it is overlapped by the postparietal (Figure 20E).

The occiput of NMQR 2913 is poorly preserved and has been displaced dorsolaterally (Figure 21). Both exoccipitals are missing as well as all the occipital bones on the right side of the skull. Preserved bones on the left are incomplete and greatly deformed (Figures 20, 21). The identification of the supraoccipital and the opisthotic is uncertain.

The postparietal of NMQR 2913 is unpaired and diamond-shaped, similar to that in *Patranomodon* (Figures 4, 20). In posterior view, it is displaced dorsolaterally and as a result, overlaps the

occipital section of the parietal (Figure 20E). It does not show any sutural contacts.

A small part of the tabular is preserved on the left side of the occiput (Figure 21B, E). In posterior view, the tabular is a thin and oval bone that overlaps the dorsal process of the squamosal (Figure 21E).

The supraocipital and the opisthotic of NMQR 2913 are very badly preserved and are probably fused, as the sutures are extremely difficult to distinguish on the specimen and CT images (Figure 21). The supraoccipital of NMQR 2913 is partially preserved on the left in two pieces around the postemporal fenestra (Figure 21). In posterior view, the dorsal-most part of the supraoccipital is flat and it has a S-shaped ventrolateral margin (Figure 21E). It forms the dorsal margin of the postemporal fenestra and contacts the tabular laterally. A second piece of supraoccipital forms the medial margin of the temporal fenestra in posterior view (Figure 21E). Its dorsal and lateral borders are straight and the ventral margin is curved (Figure 21E). The supraoccipital has a short contact with the basioccipital medially and, in posterior view, contacts the opisthotic laterally. No distinct sulci for the semicircular canals are evident.

Part of the left prootic is preserved on the left side of the occiput and reaches the opisthotic posteriorly (Figure 21). In ventral view, the prootic is roughly triangular. It has a short contact with the parabasisphenoid medially. The prootic contacts the basioccipital posteromedially with a horizontal suture, and the stapes laterally (Figure 21D). In dorsal view, the prootic contacts the opisthotic posteriorly (Figure 21C). In the same view, the prootic extends into a small curved process laterally (Figure 21C). This would have possibly accommodated the vestibule, and symmetrically on the medial side, the floccular fossa.

The opisthotic is rectangular in posterior view and forms the lateral border of the postemporal fenestra (Figure 21C). It contacts the stapes ventrally. In dorsal view, it has a short contact with the opisthotic anteriorly (Figure 21C). No sulci for the semicircular canals are preserved.

The basioccipital is only partially preserved on specimen NMQR 2913, without its tubera (Figure 21). In posterior view, the basioccipital is rectangular, displaced dorsolaterally and the surface is smooth (Figure 21E). It contacts the supraoccipital ventromedially. In both ventral and dorsal views, the basioccipital outline is semicircular (Figure 21C, D). In ventral view, it meets with the prootic laterally (Figure 21D) and contacts the parabasisphenoid anteriorly with a curved contact. By comparing NMQR 2913 with *Patranomodon* and *E. oosthuizeni*, the placement of the basioccipital-parabasisphenoid suture might have been mistakenly placed on the CT reconstruction of NMQR 2913 and could be actually located more anteriorly, as indicated by the dotted lines on Figure 21.

A possible remnant of the stapes is preserved on NMQR 2913 (Figure 21). The identification is however uncertain, due to the poor preservation of the occiput. In posterior view, the stapes contacts the opisthotic dorsally (Figure 21E). In ventral view, the stapes is triangular (Figure 21D) and tapers laterally towards the squamosal. In the same view, it contacts the prootic anteromedially. In anterior view, the stapes bears a lateral vertical ridge (Figure 21F).

The palate of NMQR 2913 is preserved in two pieces (Figures 20, 21). The vomers, part of the palatine and possibly the ectopterygoid are preserved on the anterior piece (Figure 20). The pterygoid

and the parabasisphenoid are preserved on the posterior fragment (Figure 21).

The vomer of NMQR 2913 is a paired bone mainly preserved on the anterior fragment (Figure 20) with possible small pieces of the posterior part of the vomers present on the other fragment (Figure 21). In posterior view, the vomer extends dorsally as a thin septum (Figure 20E) and in ventral view, it is slender and broadly rectangular It contacts the palatine extension of the premaxilla anteriorly and the palatine posteriorly (Figure 20D). In lateroventral view, this contact is oblique and the vomer overlaps the premaxilla anteriorly. In ventral view, the left vomer has a short anterolateral contact with the septomaxilla (Figure 20D).

The palatine is incomplete (Figure 20). The anterior-most portion is preserved on the anterior fragment and a small portion is likely preserved on the posterior fragment (Figures 20, 21). In ventral view, the preserved section of the palatine is a small rectangular bone which has a short contact with the vomer medially (Figure 20D). In posterior view, it possibly reaches the ectopterygoid laterally (Figure 20E).

The pterygoid is a paired bone (Figure 21). As in *Patranomodon* and *E. oosthuizeni* it comprises a transverse process, an anterior ramus, and a quadrate ramus (Figure 21D). The left pterygoid is complete, but the right pterygoid is missing its quadrate ramus. In lateral view, the ventral keel of the palate bears a large transverse ramus (Figure 21A,B) which makes an angle of 20° with the frontal plane (Figure 21F). The anterior process bears a small posteroventral keel (Figure 21A, B). In ventral view, the anterior ramus encloses the oval interpterygoid vacuity and a curved ridge links the two ventral keels (Figure 21D). In lateral view, the posterior portion of the anterior ramus is overlapped by the parabasisphenoid and the quadrate ramus extends posterolaterally. This ramus makes an angle of 85° with the sagittal plane (Figure 21A, B).

The parabasisphenoid of NMQR 2913 is a co-ossification of the parasphenoid and the basisphenoid (Figure 21) and has two well-defined carotid foramina which are visible in both ventral and dorsal views (Figure 21C, D). Anteriorly, the parabasisphenoid forms two lateral flat extensions that overlap the pterygoids (Figure 21A–C). These extensions are similar to the basisphenoid wings observed in *Patranomodon*. In lateral view, above the posteroventral keel of the pterygoid, the parabasisphenoid forms a conical dorsal process (Figure 21A, B). Posteriorly, in ventral and dorsal views, the parabasisphenoid broadens and contacts the basioccipital posteromedially and the prootic posterolaterally (Figure 21C, D).

As reported in Rubidge (1990a), the lower jaw of NMQR 2913 is incomplete as the posterior section of the right ramus is not preserved (Figure 22G, H). The left ramus has a crack at the level of the prominent mandibular fenestra, which is surrounded by the dentary, surangular, angular and prearticular bones (Figure 22A, B). Rubidge (1990a) could not determine the presence of a symphysial suture and our reconstruction confirms that the symphysis is fused. The left dentary shows a posterodorsal lateral dentary shelf similar to that of BP/1/6230 (Figures 19, 22), but this section is not preserved on the right dentary.

The dentary covers about 50% of the lower jaw ramus and, in lateral view, forms its anterior-most portion (Figure 22). As in BP/1/6230, the dentary of NMQR 2913 comprises a dentary table, dentary shelf, and a thin posteroventral process (Figures 19, 22G, H). The dorsal edge of the dentary is curved, with the anterior tip and the shelf being higher than the median part of the dentary. In lateral view, the dentary shelf forms the dorsal margin of the mandibular fenestra (Figure 22B). A dorsal fossa of the dentary accommodates the surangular posteriorly. The dentary extends posteroventrally into a thin triangular process below the mandibular fenestra. In ventral view, this process contacts the angular posteromedially (Figure 22D) and the dentary contacts the splenial anteromedially. The left dentary accommodates six teeth with alternating replacement teeth (Figure 22A) and the right dentary bears eight teeth, with four small replacement teeth (Figure 22C, E). The replacement teeth are placed lingually to the main tooth row.

The splenial is an unpaired bone which forms the anteroventral margin of the lower jaw (Figure 22). Morphologically it is similar to that of BP/1/6230: a thin bone with small anterior and lateral exposure (Figure 22A, B, F). In ventral view, the splenial contacts the dentary laterally and it has a short contact with the angular on the posterior end (Figure 22D). In posterior view, the splenial is roughly triangular and the anterodorsal margin of the splenial is hooked (Figure 22E), similar to that of BP/1/6230 (Figure 19E).

In lateral view, the angular forms the ventral and the posteroventral margin of the mandibular fenestra and of the lower jaw (Figure 22B). Posterior to the mandibular fenestra, the angular extends into a dorsomedial process and the reflected lamina (Figure 22B, G, H). The dorsomedial process overlaps the surangular up to the level of the dorsal margin of the mandibular fenestra (Figure 22B). The reflected lamina is a thin sheet of bone which is broadly triangular in lateral view (Figure 22B, G). In posterior view, the reflected lamina curves ventromedially to join the angular (Figure 22E, G). In lateral view, the angular extends posteriorly into a thin rectangular process, has a long dorsal contact with the surangular and touches the articular posteriorly (Figure 22B). In ventral view, the angular tapers in between the dentary laterally and the splenial medially (Figure 22D). In medial view, the angular has a flat long contact with the prearticular (Figure 22A, C, D, G).

The surangular forms the dorsal-most section of the lower jaw (Figure 22) and makes up the posterolateral and dorsomedial margin of the mandibular fenestra (Figure 22A, B). As in BP/1/6230, the surangular of NMQR 2913 comprises a thick dorsal section and a thin ventral keel (Figures 19, 22), but the keel of NMQR 2913 is less pronounced than that of *E. oosthuizeni* (BP/1/6230). In lateral view, the dorsal section bears a thick horizontal ridge dorsally (Figure 22B), also visible in posterolateral view (Figure 22G). In medial and lateral views, the dorsal section of the surangular extends anteriorly to the dentary shelf (Figure 22A, B) and the ventral keel is overlain by the angular laterally (Figure 22A, B, H). In lateral view, the surangular has a short contact with the articular posteroventrally (Figure 19B) and in medial view, the ventral keel of the surangular contacts the prearticular ventrally (Figure 22A, H).

The prearticular and the articular of NMQR 2913 are not fused, unlike the situation in BP/1/6230 (Figure 22). The prearticular is a long horizontal strip of bone, visible on the medial side of the lower jaw ramus (Figure 22A, H). It extends from the articular to the level of the mandibular fenestra (Figure 22A, C, D, H) and forms medially the posteroventral corner of the mandibular fenestra while reaching the articular posteriorly (Figure 22A). In medial and ventral views, the contact between the prearticular and the articular is oblique (Figure 22A, D). In medial view only, the

prearticular contacts the angular ventrally and the surangular dorsally (Figure 22A, H).

The articular forms the posterior part of the lower jaw and would have accommodated the quadrate to form the mandibular articulation (Figure 22). In posterior view, the articular extends medially in a triangular process (Figure 22E). In lateral view, the articulation surface is oblique and the articular bears an oblique ridge that extends from the surangular anteriorly to the posterior tip of the lower jaw (Figure 22B). In lateral and ventral views, the articular has a short anterior contact with the angular (Figure 22B, D). In medial and ventral views, the articular has an oblique contact with the prearticular anteromedially (Figure 22A, D, H).

Unlike *E. oosthuizeni* specimens, NMQR 2913, the holotype of *Eodicynodon oelofseni*, does not have a tusk-like caniniform (Figure 20). Its upper dentition comprises homodont cylindrical teeth located only on the maxilla. In contrast, *Patranomodon* has its anterior-most tooth positioned at the suture between the maxilla and the premaxilla. The right maxilla of NMQR 2913 bears six teeth, two of which are located posteromedially and may be replacement teeth (Figure 20D). The left maxilla bears only three teeth (Figure 22B). On the lower jaw, NMQR 2913 has eight cylindrical teeth (Figure 22I, J). The left dentary shows a pattern of continuous replacement similar to that described by Olroyd et al. (2021). The right dentary has smaller teeth alongside the main eight teeth, which might be remnants of an earlier stage of replacement teeth (Figure 22C, J).

3.2 Phylogenetic results

3.2.1 Cladistics: Heuristic analysis using TNT

The Cladistic analysis was run with TNT version 1.5 (Goloboff and Catalano, 2016). It retained 58 trees and 147 223 106 672 rearrangements were examined for the Sectorial Search, Ratchet and Tree Fusing algorithm. The minimum length is 167 steps, the maximum length is 877 steps and the length of the consensus tree is 383 steps. Then $RI = 0,70$ $CI = 0,44$ and $HI = 0.56$. The strict consensus tree is relatively well-resolved except for early-diverging anomodonts (Figure 23). Specimen NMQR 2913 is retrieved as the basal-most dicynodont and the clade is supported by the following synapomorphies:

- The premaxilla does not have teeth (character 8)
- The septomaxilla posterodorsal extension is long and separates the maxilla and nasal (character 19)
- The contact between the premaxilla and maxilla is absent (character 32)
- The preparietal is present (character 50)
- The contribution of the parietal to the skull table is transversely as broad as long (character 53)
- The squamosal bears a lateral fossa above the quadrate-quadratojugal complex (character 63)
- The squamosal has a dorsolateral notch below the zygomatic arch (character 65)
- The posteroventral process of the squamosal is short, such that there is a relative extensive exposure of the quadrate and quadratojugal in posterior view (character 66)

- The zygomatic process of the squamosal is transversely expanded (character 68)
- The pterygoids are separated by the vomers anteriorly, so that the vomers contribute to the interpterygoid vacuity (character 90)
- The tranverse flange of the pterygoid does not project laterally (character 91)
- The pterygoid keels are present (character 92)
- The dentary table is present (character 126)
- The coronoid is absent (character 136)
- The angular has an anterolateral trough for the posterior process of the dentary (character 137)

The analysis gave the following autapomorphies for specimen NMQR 2913:

- The lacrimal contacts the septomaxilla (character 43)
- The zygomatic process of the squamosal is narrowly based and in line with the occipital condyle (character 69)
- The exposure of the internal carotid is directed medially (character 104)
- The height of the dorsum sellae is moderate, clearly distinct but does not reach the height of the pila antotica

Other dicynodonts (node A, see Figure 23) are supported by the following synapomorphies:

- The posterior median ridge on the palatal surface of the premaxilla is present (character 5)
- The posterodorsal spur of the septomaxilla is absent (character 18)
- The caniniform tooth is present on the maxilla (tusk, character 25)
- The caniniform process of the maxilla is present (character 33)
- The parasphenoid is excluded from the interpterygoid vacuity (character 101)
- The exit of the carotid canals on the sella turcica is a single foramen (character 145)

3.2.2 Bayesian analysis using MrBayes

In the Bayesian Inference analysis utilising MrBayes, a total of 4,506 trees were sampled and examined, with 8 chains, 6 runs and 4 swaps, and the relburnin option was set to 0.25. The gamma model was used for the substitution rate among characters that follows an exponential distribution. The branch length also follows an exponential distribution. The statistical results for the parameters are presented in Supplementary Material.

The Bayesian analysis using MrBayes provided good values for the clade credibility (ie. the Bayesian support and posterior probability value for the node), and extra phylogenetic resolution compared to the cladistic analysis (Figures 23, 24). The Dicynodontia node has a posterior probability support of 1, with NMQR 2913 as the basal-most taxon (Figure 24). Specimens BP/1/6230, NMQR 2978 and ROZ 1 are placed in a polytomy at the base of the dicynodont clade. Specimens BP/1/6230 and ROZ 1 are branching together with a low probability of 0.60. Posterior probability values for other nodes are figured in Figure 24.

FIGURE 23
Cladistic analysis of the Anomodontia. Strict consensus of 58 trees obtained with a Heuristic Search. The numbers at the nodes are Bremer indices.

3.2.3 Bayesian analysis using RevBayes

The analysis from RevBayes provided a complete resolution of the phylogenetic analysis (Figure 25). *Patranomodon* is placed as the sister taxon to the "Dromasauria" with a good posterior probability of 0.8. Specimen NMQR 2913 also places as the earliest diverging dicynodont, with an excellent posterior probability of 1. The phylogenetic result from RevBayes also supports specimens BP/1/6230 and ROZ 1 being sister taxa with 0.78 posterior probability. NMQR 2978 is within Dicynodontia with a low posterior probability of 0.29. When a more complex model (SHDM) is used, BP/1/6230 and ROZ 1 are supported as sisters with posterior support of 0.983, and NMQR 2978 is within Dicynodontia with posterior probability of 0.653.

3.2.4 Description of the phylogenetic results

The cladistic analysis provided a well-resolved tree, apart from the relationship between the basal anomodonts, including *Patranomodon* (Figure 23). Derived dicynodonts are well-resolved, and similar topology to that of previous work was obtained (Fröbisch and Reisz, 2008; Kammerer et al., 2011; Castanhinha et al., 2013; Boos et al., 2016; Kammerer and Smith, 2017; Angielczyk et al., 2021; Macungo et al., 2022), with the cistecephalids *Niassodon*, *Kawingasaurus* and *Endothiodon* branching together; as well as *Robertia*, *Diictodon* and *Eosimops* (Pylaecephalidea) being closely related.

The Bayesian Inference analysis using MrBayes provided a relatively well-resolved tree, and partially elucidated the relationship amongst basal anomodonts whereas the Cladistics shows an irresolution (Figures 23, 24). The relationship of early-diverging anomodonts is fully resolved in the RevBayes analysis (Figure 25).

MrBayes and RevBayes returned trees with similar phylogenetic topologies and support values. The main phylogenetic result was extremely robust to both the software and the model choice. When a different model of character evolution was used with RevBayes (SHDM), some aspects of the crown topology changed, but the placement of the BP/1/6230, ROZ 1, and NMQR 2978 specimens remained the same with similar support. The preferred model found three unique SHDM rate categories, with the majority of characters showing a preference for a Mk-like q-matrix, in which the forward rates (0 -> 1) are roughly equivalent to the backward rates (1 -> 0). The other two SHDM categories suggest that a smaller proportion of characters are presented that more frequently transition forward (4:1), and an even smaller proportion that favors almost exclusively forward transitions. This means that characters that are poorly-described by the Mk model will be biased towards gains rather than losses.

The clade Anomodontia is supported by a Bremer index of 3 and an excellent posterior probability of 0.97 in both Bayesian analyses (Figures 23–25). The following synapomorphies support the clade:

- On the palate, the posterior exposure of the premaxilla is present (character 10)
- The palatine has a shelf ventral to the naris (character 12)
- The maxilla has a caniniform tooth (character 25)
- The posterolateral process of the parietal is short (character 54)
- The zygomatic process of the squamosal is widely based and flares posteriorly beyond the occipital condyle (character 68)
- The level of the palatine flush with surrounding bones and does not have any elevated portions (character 79)
- The pterygoid does not have teeth (character 96)

FIGURE 24
Bayesian phylogenetic analysis of the Anomodontia with MrBayes. Values at nodes indicate the posterior probability of the node.

- The tabular is separated from the opisthotic by the squamosal (character 110)
- The lower jaw has a mandibular fenestra (character 116)
- The dentary does not have an enlarged canine (character 141)

In both the cladistic and Bayesian analyses, *Biseridens* is placed as the most basal anomodont (Figures 23–25), as previously argued by Liu et al. (2010) and supported by Cisneros et al. (2011), Kammerer et al. (2011) and Angielczyk et al. (2021). As already proposed by Cisneros et al. (2011), the Anomocephaloidea *Tiarajudens* and *Anomocephalus* form a clade that is the sister group to other anomodonts in both Bayesian analyses with a posterior probability of 0.89 in MrBayes and 0.92 in RevBayes (Figures 24, 25). Before the relatively recent description of *Tiarajudens* in 2011, *Anomocephalus* was considered as the second most basal anomodont (Modesto et al., 1999; Fröbisch and Reisz, 2008; Liu et al., 2010; Kammerer et al., 2011). Angielczyk and Kammerer (2017) and Angielczyk et al. (2021) however suggested a more derived position for the Anomocephaloidea, more derived than *Galepus* but more basal than *Patranomodon*.

The Russian venyukovioids *Otsheria*, *Ulemica* and *Suminia* are left unresolved in both the cladistic and the MrBayes analyses (Figures 23, 24). The MrBayes analysis suggests that *Ulemica* and *Suminia* branch with a moderate posterior probability of 0.66 (Figure 24). The RevBayes analysis supports the monophyly of the venyukovioids with a strong posterior probability of 0.96, supporting previous phylogenetic works (Liu et al., 2010; Kammerer et al., 2011; Boos et al., 2016; Angielczyk et al., 2021).

Similarly to the MrBayes analysis, *Suminia* and *Ulemica* form a clade with a strong posterior probability of 0.99 (Figure 25).

In both the cladistic and MrBayes analyses, the phylogenetic relationship of *Patranomodon* with the dromasaurs (non monophyletic group including *Galeops*, *Galechirus* and *Galepus*) is left unresolved (Figures 23, 24 and see Kammerer and Angielczyk, 2009). The RevBayes analysis retrieves the dromasaurs as a clade, with a moderate support of 0.69 (Figure 25). *Patranomodon* places as the sister taxon and the node is supported by a good posterior probability of 0.8. This phylogenetic position is not supported by recent phylogenetic work, that retrieved the dromasaurs as non-monophyletic (Boos et al., 2016; Angielczyk and Kammerer, 2017; Angielczyk et al., 2021).

In Angielczyk and Kammerer (2017) and Angielczyk et al. (2021), *Patranomodon* is in a more basal postion than *Galechirus* and *Galeops*, but more derived than *Galepus* and the Anomocephaloidea. In Boos et al. (2016) and Kammerer and Smith (2017), *Patranomodon* holds a very basal position, between the Anomocephaloidea and the Venyukovioidea, *Galepus* and *Galechirus* branch together but are more basal than *Galeops*. Most previous phylogenetic works place *Galeops* as the sister group to the Dicynodontia (Cisneros et al., 2011; Kammerer et al., 2011; Boos et al., 2016) whereas Fröbisch and Reisz (2008) suggested the placement of *Galeops* as the sister taxon to the Venyukovioidea.

In both the cladistic and Bayesian analyses, NMQR 2913 is placed as the basal-most dicynodont, following the definition of Kammerer and Angielczyk (2009) (Figures 23–25). This was

FIGURE 25
Bayesian phylogenetic analysis of the Anomodontia with RevBayes. Values at nodes indicate the posterior probability of the node.
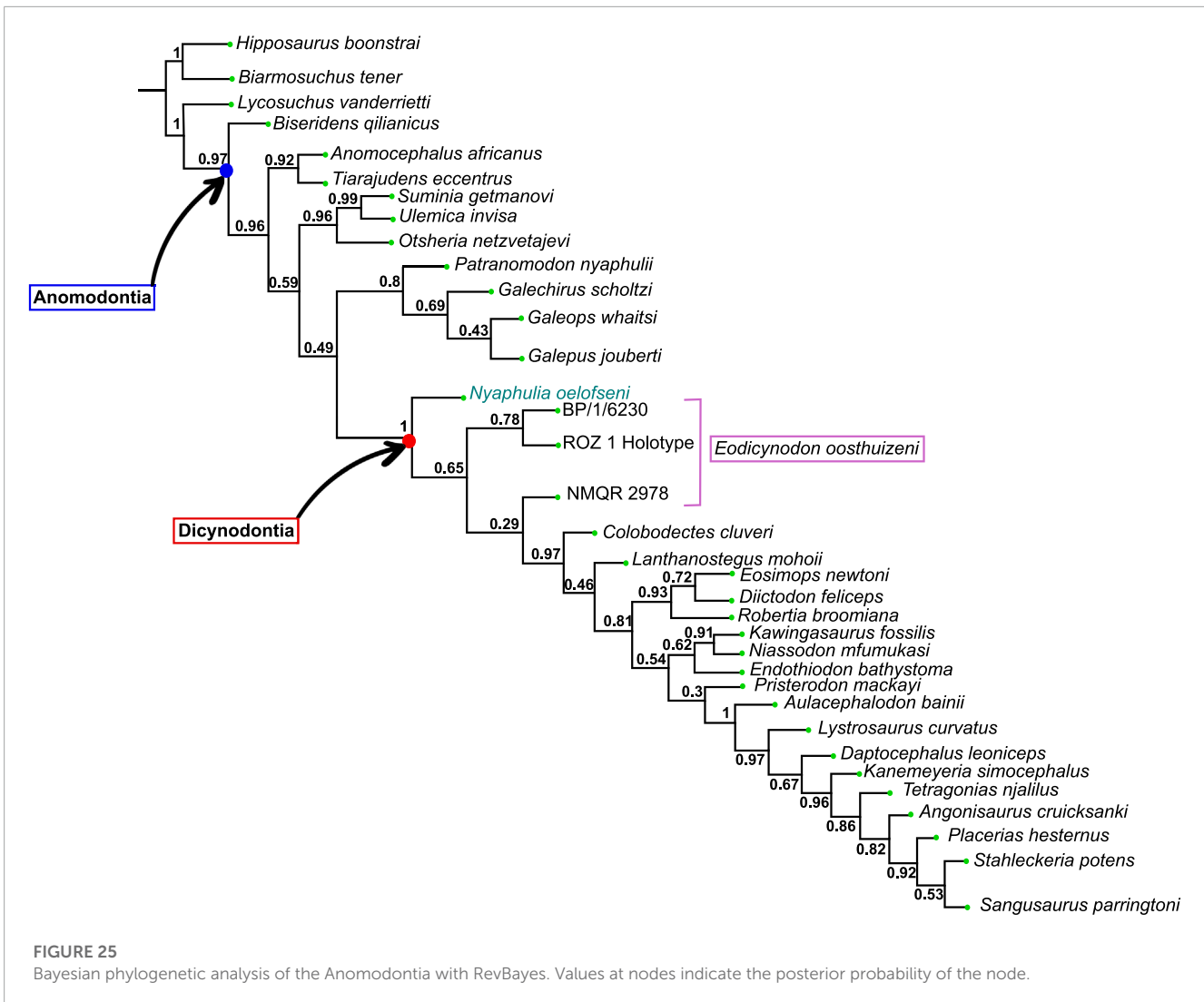
previously suggested by several authors and it is discussed below. The clade Dicynodontia is supported by a low Bremer index of 1, but a strong posterior probability of 1 with both Bayesian softwares (Figures 23–25).

The phylogenetic position of *Lanthanostegus* and *Colobodectes* is left unresolved at the base of the dicynodont clade in both cladistic and MrBayes analyses (Figures 23, 24). The RevBayes analysis elucidates their position and places *Colobodectes* as early diverging (Figure 25).

The pylaecephalids *Eosimops*, *Diictodon* and *Robertia* are retrieved as a clade in the three analyses, with a low Bremer index of 1 but good posterior probabilities of 0.9 and 0.93 (Figures 23–25).

Endothiodon and the emydopoids *Niassodon* and *Kawingasaurus* form a clade in the three analyses, with a Bremer index of 2 and posterior probabilities of 0.86 and 0.62 (Figures 23, 24). The position of that clade in relation to *Pristerodon* and later diverging dicynodonts is left unresolved in the cladistic and MrBayes analysis (Figures 23, 24). The RevBayes analysis gives a full resolution, with *Pristerodon* placed in a more derived position, but the posterior probabilities are low (Figure 25). *Pristerodon* is retrieved

one step after the pylaecephalids in Kammerer and Angielczyk (2009).

The Dicynodontoidea are undersampled in the analyses but place as a terminal clade in both the Bayesian and the cladistic analyses with a similar topology, with a Bremer index of 1 and a Bayesian posterior probabilities of 0.99 and 1 (Figures 23–25). Among them, the relation between *Lystrosaurus* and *Daptocephalus* is unresolved in the MrBayes analysis, whereas they branch together in the cladistic analysis (Figures 23, 24). The RevBayes analysis gives a third topology, with *Lystrosaurus* forming the sister taxon to all other dicynodontoids (Figure 25).

4 Discussion

Described and named by Rubidge (1990a), NMQR 2913 was previously assigned to a new species of the genus *Eodicynodon*, *Eodicynodon oelofseni*. It was later scored in a phylogenetic analysis as *Eodicynodon* along with the type of *E. oosthuizeni* (Fröbisch and Reisz, 2008). Later, It was suggested that NMQR 2913, the holotype of *Eodicynodon oelofseni*, does not form a

clade with *E. oosthuizeni* and therefore, should be assigned to a different genus (Modesto et al., 2003; Abdala et al., 2008). This hypothesis was supported by recent studies in which NMQR 2913 and *E. oosthuizeni* were scored separately in phylogenetic analyses (Boos et al., 2016; Angielczyk and Kammerer, 2017; Kammerer and Smith, 2017; Angielczyk et al., 2021). They consistently resulted in the placement of NMQR 2913 in a more basal position than *E. oosthuizeni* (Modesto et al., 2003; Abdala et al., 2008; Kammerer et al., 2011; Angielczyk et al., 2021). The current work addresses these phylogenetic hypotheses.

4.1 Identity of NMQR 2913: anatomical comparisons and phylogeny

As in *Patranomodon*, NMQR 2913 does not bear tusks, and has homodont conical maxillary and dentary teeth. A similar condition is present in most other non-dicynodont anomodonts, with the exception of *Tiarajudens* and *Biseridens* which both have a well-formed caniniform (Liu et al., 2010; Cisneros et al., 2011). *Suminia* has homodont teeth but, in contrast to those of NMQR 2913, they are massive and have a talon-and-heel morphology, similar to tapinocephalid dinocephalians (Rybczynski, 2000; Ivakhnenko, 2003).

All basal dicynodonts, including *E. oosthuizeni*, have a well-formed tusk-like caniniform while NMQR 2913 does not (Figures 7, 8, 20, and Kammerer et al., 2011). The presence of a well-formed caniniform tusk is a synapomorphy to all the dicynodonts more derived than NMQR 2913 (Rubidge and Sidor, 2001).

Specimen NMQR 2913 and *E. oosthuizeni* do not possess premaxillary teeth, *Patranomodon*, specimen NMQR 3000 has a tooth at the suture between the maxilla and premaxilla (Figures 1D, 8D, 20D and Modesto et al., 1999; Liu et al., 2010), which supports that it had premaxillary teeth, as in most non-dicynodont anomodonts. A newly discovered, but yet unprepared, specimen with a complete snout supports the idea that *Patranomodon* has premaxillary teeth (pers. obv.). Early-diverging anomodonts including *Tiarajudens* and *Anomocephalus* (Anomocephaloidea), the Venyukovioidea (*Otsheria*, *Suminia* and *Ulemica*) and "Dromasauria" (*Galeops* (?), *Galepus* and *Galechirus*) all have incisiform teeth on the premaxilla (Olson, 1962; Brinkman, 1981; Modesto et al., 1999; Rybczynski, 2000; Ivakhnenko, 2003; Cisneros et al., 2011). The Anomocephaloidea bear premaxillary teeth with a unique spade-like morphology, which is not found in any other anomodont (Cisneros et al., 2015). The relatively slender maxillary and dentary teeth of NMQR 2913 more closely resemble those of *Galeops* and *Eodicynodon* than those of *Biseridens*, *Suminia*, *Ulemica*, *Tiarajudens* and *Anomocephalus* that are mediolaterally broad (Brinkman, 1981; Modesto et al., 1999; Ivakhnenko, 2003; Liu et al., 2010; Cisneros et al., 2011).

The general shape and morphology of the skull in NMQR 2913 more closely resemble that of *Patranomodon* and *Galeops* rather than *Eodicynodon* (Figures 1, 8, 20). The snout in NMQR 2913, does not slope anteriorly gently as in dicynodonts or *Suminia*, but slopes more abruptly, as in *Patranomodon* or *Ulemica*. The snout in *Tiarajudens*, *Anomocephalus* and *Otsheria* steeply slopes upwards whereas that of NMQR 2913 slopes more gently

(Modesto et al., 1999; Cisneros et al., 2011; 2015). The snout of NMQR 2913 resembles that of *Patranomodon*, but the nasal process of the premaxilla in *Patranomodon* intrudes into the nasal (Figure 1G) whereas it does not in NMQR 2913 (Figure 20C, D). The squamosal is unfolded and slender as in most other non-dicynodont anomodonts (with the exception of *Ulemica* and *Galeops*, see Ivakhnenko (2003); Brinkman (1981)). In contrast *Eodicynodon* has a robust and folded squamosal, like that of all dicynodonts (Figures 7, 8).

Otsheria and *Biseridens* have a pachyostotic skull whereas that of NMQR 2913 and other anomodonts is gracile (Brinkman, 1981; Rubidge and Hopson, 1996; Ivakhnenko, 2003; Liu et al., 2010; Cisneros et al., 2015). The general shape of the lower jaw of NMQR 2913 is close to that of *Galeops* and *Eodicynodon*. It differs from *Ulemica* in the absence of an anteroventral notch on the dentary (Ivakhnenko, 2003), and is more gracile than the lower jaw of *Biseridens* (Liu et al., 2010).

The anterior margin of the orbit in NMQR 2913 and *Patranomodon* is relatively vertical, whereas it is rounded in the *E. oosthuizeni* specimens NMQR 2978 and BP/1/6230 (Figures 7B, 8B and 20B). In lateral view, NMQR 2913 has an exposed septomaxilla. This bone is absent in *Patranomodon* and *Eodicynodon*. The septomaxilla is not exposed laterally in most dicynodonts (with the exception of some derived taxa such as *Sangusaurus*, see Angielczyk et al., 2017). On the other hand, the septomaxilla is present and laterally exposed in most basal therapsids and in all basal anomodonts (Brinkman, 1981; Ivakhnenko, 2003; Liu et al., 2009; Liu et al., 2010; Day et al., 2018). It borders the posteroventral margin of the naris and is relatively reduced in *Otsheria*, *Ulemica*, *Tiarajudens*, *Biseridens* and *Galeops* (Olson, 1962; Ivakhnenko, 2003; Liu et al., 2010; Cisneros et al., 2011). In *Suminia*, it extends posteriorly (Rybczynski, 2000; Ivakhnenko, 2003) and resembles that of NMQR 2913 but is likely incomplete (Figure 20A).

Patranomodon does not have a secondary palate (Figure 1D). A similar condition is found in NMQR 2913, *Ulemica*, *Otsheria* and *Biseridens* where the choanae open directly at the level of the first maxillary teeth (Figure 20D). In contrast, *E. oosthuizeni* and other dicynodonts have a secondary palate comprising mainly the premaxilla and choanae opening behind the level of the tusk (Figures 8D, 1G; see Modesto et al., 2003; Fröbisch and Reisz, 2008; Kammerer et al., 2011).

On the palate, the posterior section of the parabasisphenoid in NMQR 2913 has a similar morphology to the parabasisphenoid wings in *Patranomodon* (Figures 6, 21). However, the general morphology of the pterygoids in NMQR 2913 resembles that of *Eodicynodon*, with pronounced posterior and anterior ventral keels (=transverse flange of the pterygoid). The interpterygoid vacuity is wider in NMQR 2913 and *Eodicynodon* than in *Patranomodon*, which has a very narrow interpterygoid vacuity (Figures 6, 18, 21).

The parasphenoid reaches the interpterygoid vacuity in *Suminia*, *Ulemica* and NMQR 2913, while it is excluded from it in *Patranomodon* and all dicynodonts; including *Eodicynodon* (Figures 6, 17, 21). On the dorsal side of the parasphenoid of *Patranomodon*, the two carotid foramina are widely separated; while they are close to each other in NMQR 2913.

Co-ossification of cranial and jaw bones can occur in Anomodontia and is documented in different taxa. On the lower jaw, the articular and prearticular are sometimes fused, as in *E. oosthuizeni* or *Niassodon* (see Figure 19 and Castanhinha et al., 2013). In NMQR 2913, on the medial side of the lower jaw, there is a clear suture between the articular and prearticular (Figure 22). A similar condition is found in the lower jaw of *Patranomodon* and likely in *Galeops* (Brinkman, 1981; Rubidge and Hopson, 1996). On the occiput, some co-ossification can occur, especially in the bones of the periotic region (Castanhinha et al., 2013; Pusch et al., 2019; Macungo et al., 2022). In some cases, the fusion of the opisthotic and prootic forms a periotic bone in therapsids. In *Eodicynodon*, the periotic region is partly co-ossified, as some sutures between the supraoccipital, opisthotic and prootic are unclear (Figures 11, 12). In *Patranomodon*, all sutures of the periotic region are clearly defined, indicating that the bones in this area are not fused (Figures 4, 5). Lastly, at the base of the hindbrain, the parabasisphenoid results from the co-ossification of the parasphenoid and basisphenoid in most basal anomodonts (*Suminia*, *Ulemica*, *Otsheria*…), in NMQR 2913, in therapsids as a whole and in "pelycosaurs" (Romer and Price, 1940; Cluver, 1971; Rubidge, 1990a; Modesto et al., 2003; Sidor and Rubidge, 2006; Day et al., 2018; Pusch et al., 2019). However, in *Patranomodon*, NMQR 2978 and BP/1/6230, the parabasisphenoid is divided between the parasphenoid and basisphenoid (Figures 1, 7, 8). This has been observed in *Niassodon*, some cistecephalids and *Pristerodon* (Castanhinha et al., 2013; Macungo et al., 2022).

To sum up, in addition to the autapomorphic characters presented in the phylogenetic results section, specimen NMQR 2913 possesses a combination of anatomical features and is different from other early-diverging anomodonts. It is closer to *Patranomodon* or *Galeops* (and other dromasaurians) in overall morphology, by being gracile and not heavily pachyostotic like *Otsheria* or *Suminia*. Specimen NMQR 2913 has non-gomphodont, peg-like, maxillary and dentary teeth, unlike *Anomocephalus*, *Tiarajudens* and *Suminia*. It does not have a tusk-like caniniform tooth, unlike *Tiarajudens* and *Eodicynodon* and most other dicynodonts. Its lower jaw is slender as in *Patranomodon* and *Eodicynodon*, while the lower jaw of *Ulemica* is robust with an anteroventral notch on the dentary. This suggests that NMQR 2913 differs from every other basal anomodont, including *Eodicynodon*, and as suggested by previous authors (Modesto et al., 2003; Abdala et al., 2008; Angielczyk et al., 2021), should be distinguished at generic level.

In their latest review, Kammerer and Angielczyk (2009) (page 5) stated that dicynodonts are "all taxa more closely related to *Dicynodon lacerticeps* than *G. whaitsi*". From a taxonomic point of view, in both Bayesian and cladistic analyses (Figures 23, 24), NMQR 2913 is thus a dicynodont. If NMQR 2913 is considered as a Dicynodontia, the presence of tusks and secondary palate can no longer be considered synapomorphies of the Dicynodontia clade. This taxon thus represents an important transitional stage in the development of dicynodont synapomorphies.

Modesto et al. (2003) (page 211) were the first to question the taxonomic affiliation of NMQR 2913 to the genus *Eodicynodon* and stated that there is "little basis for recognizing *Eodicynodon oelofseni* as the closest relative of *E. oosthuizeni*". Their analysis placed NMQR 2913 as the sister taxon to Dicynodontia. Later, the analysis

of Kammerer et al. (2011) retrieved this phylogenetic topology with strong cladistic support. Some phylogenies have retrieved NMQR 2913 as the earliest diverging member of Dicynodontia (Abdala et al., 2008; Angielczyk et al., 2017; Angielczyk et al., 2021; Macungo et al., 2022). Others did not score NMQR 2913 separately from *E. oosthuizeni* (Angielczyk, 2007; Fröbisch and Reisz, 2008; Cisneros et al., 2011). Boos et al. (2016) retrieved NMQR 2913 as a non-dicynodont anomodont. In the cladistic analysis proposed here (Figure 23), the strict consensus suggests that NMQR 2913 does not form a clade with *E. oosthuizeni* and is the sister taxon to the clade gathering *E. oosthuizeni* and all other dicynodonts. All specimens attributed to *E. oosthuizeni* form a clade sister to all other derived dicynodonts in the cladistic analysis but not in the Bayesian analyses. The latter supports the exclusion of NMQR 2913 from the genus *Eodicynodon* and gives a posterior probability support of 1 for the clade Dicynodontia with NMQR 2913 as the basal-most taxon (Figure 24).

4.2 Taxonomy and updated systematic paleontology of NMQR 2913

Following the results obtained from the parsimony analysis with TNT presented above, NMQR 2913 can be distinguished from the genus *Eodicynodon* by the following features:

- The absence of canine-like tusks
- The absence of contact between the prefrontal and maxilla
- The base of the zygomatic process of the squamosal is narrow
- The internal carotid foramen (dorsal surface of the parasphenoid) is directed medially
- The height of the dorsum sellae is moderate, as clearly distinct but does not reach the height of the pila antotica

Specimen NMQR 2913 differs from early-diverging anomodonts in the absence of premaxillary teeth (Character 8, state 1), presence of a transverse process of the pterygoid that does not project laterally (Character 91, state 2), the presence of a pterygoid keel (Character 92, state 1), a well-developed dentary shelf (Character 129, state 1), and a surangular without a vertical lamina (Character 139, state 1). It differs from other dicynodonts in the presence of a lateral exposure of the septomaxilla (Character 18, state 0), the absence of a secondary palate, the absence of a canine-like tusk (Character 25 and 26, state 1 and "-" respectively), a parasphenoid that reaches the interpterygoid vacuity (Character 101, state 1; present in all basal anomodonts except *Patranomodon*).

Based on the updated descriptions and comparisons presented above, the phylogenetic analyses produced and literature (Modesto et al., 2003; Abdala et al., 2008; Fröbisch and Reisz, 2008; Kammerer et al., 2011; Boos et al., 2016; Angielczyk et al., 2021), all evidence indicates that NMQR 2913 is a distinct genus from *Eodicynodon* and is the most basal dicynodont. A new taxonomic unit, *Nyaphulia olofseni*, is introduced and refers specimen NMQR 2913 as the holotype.

Systematic Paleontology
Therapsida Broom, 1905

ANOMODONTIA Owen, 1859

DICYNODONTIA Owen, 1859

Nyaphulia gen. nov.

urn:lsid:zoobank.org:act:A1873A91-F8FE-4A35-9FB4-4A13BF35066B

Type species—*oelofseni*.

Diagnosis—As for the species.

Etymology—The name refers to John Nyaphuli, a former employee of the National Museum of Bloemfontein, that extensively contributed to South African paleontology with his numerous fossil finds, particularly of the most basal therapsids from South Africa. He additionally discovered specimen NMQR 2913 in 1982.

Nyaphulia oelofseni gen. nov.

Holotype—NMQR 2913.

Material—Skull, lower jaw and postcranial elements.

Type locality—Botterkraal farm, Abrahamskraal Formation, *Eodicynodon* Assemblage Zone, Beaufort Group, Karoo Supergroup, South Africa.

Diagnosis—Anomodont that uniquely combines the absence of a tusk-like caniniform tooth and secondary palate, with the absence of premaxillary and anterior dentary teeth (osseous beak present). Also comprises the following unique combination of characters: laterally situated maxillary teeth that point in an anterior direction; absence of contact between the maxilla and the prefrontal; septomaxilla with a lateral projection present; a narrowly based zygomatic process of the squamosal; internal carotid foramina directed medially on the dorsal surface of the parabasisphenoid; a moderate height of the dorsum sellae that does not reach the level of the pila antotica and no coronoid eminence on posterodorsal surface of the dentary.

Description—See the Description above.

5 Conclusion

We describe in detail four early-diverging anomodont specimens from the *Eodicynodon* Assemblage Zone of the Karoo Supergroup, to feed an updated revision of basal anomodont phylogenetic relationships. The ultimate goal is to address the taxonomic attribution of NMQR 2913 to the genus *Eodicynodon*.

The detailed redescription of *Patranomodon nyaphuli*, two specimens of *E. oosthuizeni* and NMQR 2913 using CT-data provides crucial data on the external and endocranial anatomy of basal anomodonts. This supports that NMQR 2913 differs at the generic level from *E. oosthuizeni* in the structure of its braincase floor (parasphenoid, basisphenoid), anatomy of the interpterygoid vacuity, sutural contacts of the snout bones, presence of a septomaxilla, absence of a tusk and secondary palate, and morphology of the dentition and general shape of the skull and skull roof. Overall, NMQR 2913 appears anatomically dissimilar to *E. oosthuizeni*. Fully resolved phylogenetic analyses with TNT, MrBayes and RevBayes indicate that NMQR 2913 is better interpreted as a new genus, here named *Nyaphulia oelofseni*, and supports that it is the earliest diverging dicynodont.

Data availability statement

The original contributions presented in the study are included in the article/Supplementary Material, further inquiries can be directed to the corresponding author.

Author contributions

AD conceived the study, produced the 3D models, created the figures and wrote the manuscript. JB and BR supervised the study, provided input on the cranial morphology of basal anomodonts and undertook extensive reviews of the manuscript. BW and AW reviewed the Bayesian Inference method, produced the RevBayes analysis and made extensive comments and reviews on the manuscript. All authors contributed to the article and approved the submitted version.

Conflict of interest

The authors declare that the research was conducted in the absence of any commercial or financial relationships that could be construed as a potential conflict of interest.

Publisher's note

All claims expressed in this article are solely those of the authors and do not necessarily represent those of

their affiliated organizations, or those of the publisher, the editors and the reviewers. Any product that may be evaluated in this article, or claim that may be made by its manufacturer, is not guaranteed or endorsed by the publisher.

Supplementary material

The Supplementary Material for this article can be found online at: https://www.frontiersin.org/articles/10.3389/feart.2023. 1220341/full#supplementary-material

References

Abdala, F., Rubidge, B. S., and van den Heever, J. (2008). The oldest therocephalians (Therapsida, Eutheriodontia) and the early diversification of Therapsida. *Palaeontology* 51, 1011–1024. doi:10.1111/j.1475-4983.2008. 00784.x

Angielczyk, K., Benoit, J., and Rubidge, B. S. (2019). A new tusked cistecephalid dicynodont (Therapsida, Anomodontia) from the upper Permian upper Madumabisa Mudstone formation, Luangwa Basin, Zambia. *Pap. Palaeontol.* 7, 405–446. doi:10. 1002/spp2.1285

Angielczyk, K., and Kammerer, C. (2018). *Non-mammalian synapsids: the deep roots of the mammalian family tree.* Berlin: De Gruyter, 117–198.

Angielczyk, K. D. (2007). New specimens of the Tanzanian dicynodont *Cryptocynodon parringtoni* von Huene, 1942 (Therapsida, Anomodontia), with an expanded analysis of Permian dicynodont phylogeny. *J. Vertebrate Paleontology* 27, 116–131. doi:10.1671/0272-4634(2007)27[116:nsottd]2. 0.co;2

Angielczyk, K. D., Hancox, P., and Nabavizadeh, A. (2017). A redescription of the Triassic kannemeyeriiform dicynodont *Sangusaurus* (Therapsida, Anomodontia), with an analysis of its feeding system. *J. Vertebrate Paleontology* 37, 189–227. doi:10. 1080/02724634.2017.1395885

Angielczyk, K. D., and Kammerer, C. F. (2017). The cranial morphology, phylogenetic position and biogeography of the upper Permian dicynodont *Compsodon helmoedi* van Hoepen (Therapsida, Anomodontia). *Pap. Palaeontol.* 3, 513–545. doi:10.1002/spp2. 1087

Angielczyk, K. D., Liu, J., and Yang, W. (2021). A redescription of *Kunpania scopulusa*, a bidentalian dicynodont (Therapsida, Anomodontia) from the Guadalupian of Northwestern China. *J. Vertebrate Paleontology* 41, e1922428. doi:10.1080/02724634. 2021.1922428

Angielczyk, K. D., and Rubidge, B. S. (2010). A new pylaecephalid dicynodont (Therapsida, Anomodontia) from the *Tapinocephalus* Assemblage Zone, Karoo basin, Middle Permian of South Africa. *J. Vertebrate Paleontology* 30, 1396–1409. doi:10. 1080/02724634.2010.501447

Araújo, R. M. N., Fernandez, V., Polcyn, M. J., Fröbisch, J., and Martins, R. M. S. (2017). Aspects of gorgonopsian paleobiology and evolution: insights from the basicranium, occiput, osseous labyrinth, vasculature, and neuroanatomy. *PeerJ* 5, e3119. doi:10.7717/peerj.3119

Barry, T. (1974). A new dicynodont ancestor from the Upper Ecca (lower middle Permian) of South Africa. *Ann. South Afr. Mus.* 64, 117–136.

Benoit, J., Angielczyk, K. D., Miyamae, J. A., Manger, P., Fernandez, V., and Rubidge, B. (2018). Evolution of facial innervation in anomodont therapsids (Synapsida): insights from X-ray computerized microtomography. *J. Morphol.* 279, 673–701. doi:10. 1002/jmor.20804

Benoit, J., Jasinoski, S. C., Fernandez, V., and Abdala, F. (2017). The mystery of a missing bone: revealing the orbitosphenoid in basal Epicynodontia (Cynodontia, Therapsida) through computed tomography. *Sci. Nat.* 104, 66–10. doi:10.1007/s00114-017-1487-z

Benton, M. (2015). *Vertebrate palaeontology.* John Wiley & Sons.

Boos, A. D. S., Kammerer, C. F., Schultz, C. L., Soares, M. B., and Iiha, A. L. R. (2016). A new dicynodont (Therapsida: Anomodontia) from the Permian of Southern Brazil and its implications for bidentalian origins. *PLoS ONE* 11, e0155000. doi:10. 1371/journal.pone.0155000

Botha-Brink, J., and Angielczyk, K. D. (2010). Do extraordinarily high growth rates in Permo-Triassic dicynodonts (Therapsida, Anomodontia) explain their success before and after the end-Permian extinction? *Zoological J. Linn. Soc.* 160, 341–365. doi:10. 1111/j.1096-3642.2009.00601.x

Brinkman, D. (1981). The structure and relationships of the dromasaurs (Cambridge: Therapsida). *Breviora* 465, 1–34.

Broom, R. (1905). On the use of the term Anomodontia. *Rec. Albany Mus.* 1, 266–269.

Brown, J. M., and Lemmon, A. R. (2007). The importance of data partitioning and the utility of Bayes factors in Bayesian phylogenetics. *Syst. Biol.* 56, 643–655. doi:10. 1080/10635150701546249

Castanhinha, R., Araújo, R. M. N., Júnior, L. C., Angielczyk, K. D., Martins, G. G., Martins, R. M. S., et al. (2013). Bringing dicynodonts back to life: paleobiology and anatomy of a new emydopoid genus from the Upper Permian of Mozambique. *PLoS ONE* 8, e80974. doi:10.1371/journal.pone. 0080974

Chinsamy-Turan, A. (2011). *Forerunners of mammals: radiation, histology, biology.* Indiana University Press.

Cifelli, R., Luo, Z.-X., and Kielan-Jaworowska, Z. (2004). *Mammals from the age of dinosaurs: origins, evolution, and structure.* Columbia University Press.

Cisneros, J. C., Abdala, F., Jashashvili, T., de Oliveira Bueno, A., and Dentzien-Dias, P. (2015). *Tiarajudens eccentricus* and *Anomocephalus africanus*, two bizarre anomodonts (Synapsida, Therapsida) with dental occlusion from the Permian of Gondwana. *Open Sci.* 2, 150090. doi:10.1098/rsos. 150090

Cisneros, J. C., Abdala, F., Rubidge, B. S., Dentzien-Dias, P. C., and de Oliveira Bueno, A. (2011). Dental occlusion in a 260-million-year-old therapsid with saber canines from the Permian of Brazil. *Science* 331, 1603–1605. doi:10.1126/science. 1200305

Cluver, M. A. (1971). The cranial morphology of the dicynodont genus *Lystrosaurus*. Ph.D. thesis. Stellenbosch: Stellenbosch University.

Cox, C. B., and Broom, R. (1962). A natural cast of the inner ear of a dicynodont. *Am. Mus. novitates* 2116, 1–6.

Crompton, A., Musinsky, C., Rougier, G., Bhullar, B.-A., and Miyamae, J. (2018). Origin of the lateral wall of the mammalian skull: fossils, monotremes and therians revisited. *J. Mammalian Evol.* 25, 301–313. doi:10.1007/s10914-017-9388-7

Damiani, R., Vasconcelos, C., Renaut, A., Hancox, J., and Yates, A. (2007). *Dolichuranus primaevus* (Therapsida: Anomodontia) from the Middle Triassic of Namibia and its phylogenetic relationships. *Palaeontology* 50, 1531–1546. doi:10.1111/j. 1475-4983.2007.00727.x

Day, M. O., and Rubidge, B. S. (2014). A brief lithostratigraphic review of the Abrahamskraal and Koonap Formations of the Beaufort Group, South Africa: towards a basin-wide stratigraphic scheme for the middle Permian Karoo. *J. Afr. Earth Sci.* 100, 227–242. doi:10.1016/j.jafrearsci.2014. 07.001

Day, M. O., Smith, R. M. H., Benoit, J., Fernandez, V., and Rubidge, B. S. (2018). A new species of burnetiid (Therapsida, Burnetiamorpha) from the early Wuchiapingian of South Africa and implications for the evolutionary ecology of the family Burnetiidae. *Pap. Palaeontol.* 4, 453–475. doi:10.1002/spp2. 1114

de Simão-Oliveira, D., Kerber, L., and L Pinheiro, F. (2019). Endocranial morphology of the Brazilian Permian dicynodont *Rastodon procurvidens* (Therapsida: Anomodontia). *J. Anat.* 236, 384–397. doi:10.1111/joa.13107

Duhamel, A., Benoit, J., Day, M. O., Rubidge, B. S., and Fernandez, V. (2021). Computed tomography elucidates ontogeny within the basal therapsid clade Biarmosuchia. *PeerJ* 9, e11866. doi:10.7717/peerj.11866

Dzik, J., Sulej, T., and Niedźwiedzki, G. (2008). A dicynodont-theropod association in the latest Triassic of Poland. *Acta Palaeontol. Pol.* 53, 733–738. doi:10.4202/app.2008. 0415

Fourie, S. (1974). The cranial morphology of *Thrinaxodon liorhinus* Seeley. *Ann. South Afr. Mus.* 65, 337–400.

Fröbisch, J. (2009). Composition and similarity of global anomodont-bearing tetrapod faunas. *Earth-Science Rev.* 95, 119–157. doi:10.1016/j.earscirev.2009.04.001

Fröbisch, J., and Reisz, R. R. (2008). A new species of *Emydops* (Synapsida, Anomodontia) and a discussion of dental variability and pathology in dicynodonts. *J. Vertebrate Paleontology* 28, 770–787. doi:10.1671/0272-4634(2008)28[770:ansoes]2. 0.co;2

Fröbisch, J., and Reisz, R. R. (2009). The late Permian herbivore *Suminia* and the early evolution of arboreality in terrestrial vertebrate ecosystems. *Proc. R. Soc. B Biol. Sci.* 276, 3611–3618. doi:10.1098/rspb.2009.0911

Geyer, C. J. (1991). "Markov chain Monte Carlo maximum likelihood," in Proceedings of the 23rd Symposium on the Interface (Interface Foundation of North America), 156–163.

Goloboff, P. A., and Catalano, S. A. (2016). TNT version 1.5, including a full implementation of phylogenetic morphometrics. *Cladistics* 32, 221–238. doi:10. 1111/cla.12160

Goloboff, P. A., Farris, J. S., and Nixon, K. (2003). TNT: tree analysis using new technology. *Syst. Biol.* 54, 176–178. doi:10.1080/10635150590905830

Green, P. J. (1995). Reversible jump Markov chain Monte Carlo computation and Bayesian model determination. *Biometrika* 82, 711–732. doi:10.1093/biomet/82.4.711

Hammer, W., and Cosgriff, J. (1981). *Myosaurus gracilis*, an anomodont reptile from the Lower Triassic of Antarctica and South Africa. *J. Paleontology* 55, 410–424.

Hancox, P. J., Angielczyk, K. D., and Rubidge, B. S. (2013). *Angonisaurus* and *Shansiodon*, dicynodonts (Therapsida, Anomodontia) from Subzone C of the *Cynognathus* Assemblage Zone (Middle Triassic) of South Africa. *J. Vertebrate Paleontology* 33, 655–676. doi:10.1080/02724634.2013.723551

Hastings, W. K. (1970). Monte Carlo sampling methods using Markov chains and their applications. *Biometrika* 57, 97–109. doi:10.1093/biomet/57.1.97

Höhna, S., Landis, M. J., Heath, T. A., Boussau, B., Lartillot, N., Moore, B. R., et al. (2016). RevBayes: Bayesian phylogenetic inference using graphical models and an interactive model-specification language. *Syst. Biol.* 65, 726–736. doi:10.1093/sysbio/syw021

Huelsenbeck, J. P., and Ronquist, F. (2001). MRBAYES: Bayesian inference of phylogenetic trees. *Bioinformatics* 17, 754–755. doi:10.1093/bioinformatics/17.8.754

Ivakhnenko, M. F. (2003). Eotherapsids from the east European placket (late Permian). *Paleontological J.* 37, 339–465.

Ivakhnenko, M. F. (2008). Cranial morphology and evolution of Permian dinomorpha (Eotherapsida) of Eastern Europe. *Paleontological J.* 42, 859–995. doi:10.1134/s0031030108090013

Jinnah, Z. A., and Rubidge, B. (2007). A double-tusked dicynodont and its biostratigraphic significance. *South Afr. J. Sci.* 103, 51–53.

Kammerer, C. F. (2016a). Systematics of the Rubidgeinae (Therapsida: Gorgonopsia). *PeerJ* 4, e1608. doi:10.7717/peerj.1608

Kammerer, C. F. (2016b). Two unrecognised burnetiamorph specimens from historic Karoo collections. *Palaeontol. Afr.* 50, 64–75.

Kammerer, C. F., Angielczyk, K., and Fröbisch, J. (2014). *Early evolutionary history of the Synapsida*. Netherlands: Springer.

Kammerer, C. F., and Angielczyk, K. D. (2009). A proposed higher taxonomy of anomodont therapsids. *Zootaxa* 2018, 1–24. doi:10.11646/zootaxa.2018.1.1

Kammerer, C. F., Angielczyk, K. D., and Fröbisch, J. (2011). A comprehensive taxonomic revision of *Dicynodon* (Therapsida, Anomodontia) and its implications for dicynodont phylogeny, biogeography, and biostratigraphy. *J. Vertebrate Paleontology* 31, 1–158. doi:10.1080/02724634.2011.627074

Kammerer, C. F., and Smith, R. M. H. (2017). An early geikiid dicynodont from the *Tropidostoma* Assemblage Zone (late Permian) of South Africa. *PeerJ* 5, e2913. doi:10.7717/peerj.2913

Kemp, T. S. (2005). *The origin and evolution of mammals*. Oxford: Oxford University.

Kruger, A., Rubidge, B. S., and Abdala, F. (2018). A juvenile specimen of *Anteosaurus magnificus* Watson, 1921 (Therapsida: Dinocephalia) from the South African Karoo, and its implications for understanding dinocephalian ontogeny. *J. Syst. Palaeontol.* 16, 139–158. doi:10.1080/14772019.2016.1276106

Laaß, M. (2015a). Bone-conduction hearing and seismic sensitivity of the Late Permian anomodont *Kawingasaurus fossilis*. *J. Morphol.* 276, 121–143. doi:10.1002/jmor.20325

Laaß, M. (2015b). Virtual reconstruction and description of the cranial endocast of *Pristerodon mackayi* (Therapsida, Anomodontia). *J. Morphol.* 276, 1089–1099. doi:10.1002/jmor.20397

Laaß, M., and Schillinger, B. (2015). Reconstructing the auditory apparatus of therapsids by means of neutron tomography. *Phys. Procedia* 69, 628–635. doi:10.1016/j.phpro.2015.07.089

Laaß, M., Schillinger, B., and Kaestner, A. (2017). What did the "Unossified zone" of the non-mammalian therapsid braincase house? *J. Morphol.* 278, 1020–1032. doi:10.1002/jmor.20583

Larget, B., and Simon, D. L. (1999). Markov chain Monte Carlo algorithms for the Bayesian analysis of phylogenetic trees. *Mol. Biol. Evol.* 16, 750–759. doi:10.1093/oxfordjournals.molbev.a026160

Lewis, P. O. (2001). A likelihood approach to estimating phylogeny from discrete morphological character data. *Syst. Biol.* 50, 913–925. doi:10.1080/106351501753462876

Liu, J., Rubidge, B., and Li, J. (2009). New basal synapsid supports Laurasian origin for therapsids. *Acta Palaeontol. Pol.* 54, 393–400. doi:10.4202/app.2008.0071

Liu, J., Rubidge, B., and Li, J. (2010). A new specimen of *Biseridens qilianicus* indicates its phylogenetic position as the most basal anomodont. *Proc. R. Soc. Lond. B Biol. Sci.* 277, 285–292. doi:10.1098/rspb.2009.0883

Luo, Z., Crompton, A. W., and Lucas, S. G. (1995). Evolutionary origins of the mammalian promontorium and cochlea. *J. Vertebrate Paleontology* 15, 113–121. doi:10.1080/02724634.1995.10011211

Luo, Z.-X. (2001). The inner ear and its bony housing in tritylodontids and implications for evolution of the mammalian ear. *Bull. Mus. Comp. Zoology* 156, 81–97.

Luo, Z.-X., Kielan-Jaworowska, Z., and Cifelli, R. L. (2002). In quest for a phylogeny of Mesozoic mammals. *Acta Palaeontol. Pol.* 47, 113–121.

Macungo, Z., Benoit, J., Fernandez, V., and Araújo, R. M. N. (2022). X-ray microcomputed and synchrotron tomographic analysis of the basicranial axis of emydopoid dicynodonts: implications for fossoriality and phylogeny. *Zoological J. Linn. Soc.* 198, 1–46. doi:10.1093/zoolinnean/zlac033

Maddison, W. P., and Maddison, D. R. (2015). *Mesquite: a modular system for evolutionary analysis*. Version 3.04.

Marilao, L. M., Kulik, Z. T., and Sidor, C. A. (2020). Histology of the preparietal: a neomorphic cranial element in dicynodont therapsids. *J. Vertebrate Paleontology* 40, e1770775. doi:10.1080/02724634.2020.1770775

Metropolis, N., Rosenbluth, A. W., Rosenbluth, M. N., Teller, A. H., and Teller, E. (1953). Equation of state calculations by fast computing machines. *J. Chem. Phys.* 21, 1087–1092. doi:10.1063/1.1699114

Modesto, S., Rubidge, B. S., Visser, I., and Welman, J. (2003). A new basal dicynodont from the Upper Permian of South Africa. *Palaeontology* 46, 211–223. doi:10.1111/1475-4983.00295

Modesto, S., Rubidge, B. S., and Welman, J. (1999). The most basal anomodont therapsid and the primacy of Gondwana in the evolution of the anomodonts. *Proc. R. Soc. B Biol. Sci.* 266, 331–337. doi:10.1098/rspb.1999.0642

Nicolas, M., and Rubidge, B. S. (2010). Changes in Permo-Triassic terrestrial tetrapod ecological representation in the Beaufort Group (Karoo Supergroup) of South Africa. *Lethaia* 43, 45–59. doi:10.1111/j.1502-3931.2009.00171.x

Nylander, J. A., Ronquist, F., Huelsenbeck, J. P., and Nieves-Aldrey, J. (2004). Bayesian phylogenetic analysis of combined data. *Syst. Biol.* 53, 47–67. doi:10.1080/10635150490264699

Olroyd, S. L., LeBlanc, A. R., Araújo, R., Angielczyk, K. D., Duhamel, A., Benoit, J., et al. (2021). Histology and µCT reveal the unique evolution and development of multiple tooth rows in the synapsid *Endothiodon*. *Sci. Rep.* 11, 16875–16923. doi:10.1038/s41598-021-95993-6

Olroyd, S. L., and Sidor, C. A. (2022). Nomenclature, comparative anatomy, and evolution of the reflected lamina of the angular in non-mammalian synapsids. *J. Vertebrate Paleontology* 42, e2101923. doi:10.1080/02724634.2022.2101923

Olroyd, S. L., Sidor, C. A., and Angielczyk, K. D. (2018). New materials of the enigmatic dicynodont *Abajudon kaayai* (Therapsida, Anomodontia) from the lower Madumabisa Mudstone Formation, middle Permian of Zambia. *J. Vertebrate Paleontology* 37, e1403442. doi:10.1080/02724634.2017.1403442

Olson, E. C. (1944). *Origin of mammals based upon cranial morphology of the therapsid suborders*. Geological Society of America Special Papers 55, 1–137.

Olson, E. C. (1962). Late Permian terrestrial vertebrates, USA and USSR. *Trans. Am. Philosophical Soc.* 52, 1–224. doi:10.2307/1005904

Owen, R. (1859). On the orders of fossil and recent Reptilia and their distribution in time. *Rep. Br. Association Adv. Sci.* 1859, 153–166.

Pusch, L. C., Kammerer, C. F., and Fröbisch, J. (2019). Cranial anatomy of the early cynodont *Galesaurus planiceps* and the origin of mammalian endocranial characters. *J. Anat.* 234, 592–621. doi:10.1111/joa.12958

Pusch, L. C., Ponstein, J., Kammerer, C. F., and Fröbisch, J. (2020). Novel endocranial data on the early therocephalian *Lycosuchus vanderrieti* underpin high character variability in early theriodont evolution. *Front. Ecol. Evol.* 7, 464. doi:10.3389/fevo.2019.00464

Rambaut, A., Drummond, A. J., Xie, D., Baele, G., and Suchard, M. A. (2018). Posterior summarization in Bayesian phylogenetics using tracer 1.7. *Syst. Biol.* 67, 901–904. doi:10.1093/sysbio/syy032

Ray, S., Botha, J., and Chinsamy, A. (2004). Bone histology and growth patterns of some nonmammalian therapsids. *J. Vertebrate Paleontology* 24, 634–648. doi:10.1671/0272-4634(2004)024[0634:bhagpo]2.0.co;2

Reisz, R. R. (2006). Origin of dental occlusion in tetrapods: signal for terrestrial vertebrate evolution? *J. Exp. Zoology Part B Mol. Dev. Evol.* 306, 261–277. doi:10.1002/jez.b.21115

Reisz, R. R., and Sues, H.-D. (2000). Herbivory in late Paleozoic and Triassic terrestrial vertebrates. *Evol. herbivory Terr. vertebrates* 9–41, 9–41. doi:10.1017/cbo9780511549717.003

Romer, A. S., and Price, L. W. (1940). Review of the Pelycosauria. *Geol. Soc. Am. Special Pap.* 28, 1–534. doi:10.1130/spe28-p1

Rougier, G. W., Martinelli, A. G., and Forasiepi, A. M. (2021). *Mesozoic mammals from South America and their forerunners*. Springer.

Rubidge, B. S. (1990a). The cranial morphology of a new species of the genus *Eodicynodon* (Therapsida, Dicynodontia). *Navorsinge Nas. Mus.* 7, 38–39.

Rubidge, B. S. (1990b). Redescription of the cranial morphology of *Eodicynodon oosthuizeni* (Therapsida; Dicynodontia). *Navorsinge Nas. Mus.* 7.

Rubidge, B. S. (1995). Biostratigraphy of the Beaufort Group (Karoo, Supergroup). South African committee for stratigraphy. *Biostratigraphic Series No. 1, Council for Geosciences, Pretoria*, 1–7.

Rubidge, B. S., and Day, M. O. (2020). Biostratigraphy of the *Eodicynodon* Assemblage Zone (Beaufort Group, Karoo Supergroup), South Africa. *South Afr. J. Geol.* 123, 141–148. doi:10.25131/sajg.123.0010

Rubidge, B. S., and Hopson, J. A. (1990). A new anomodont therapsid from South Africa and its bearing on the ancestry of Dicynodontia. *South Afr. J. Sci.* 86, 43–45.

Rubidge, B. S., and Hopson, J. A. (1996). A primitive anomodont therapsid from the base of the Beaufort Group (Upper Permian) of South Africa. *Zoological J. Linn. Soc.* 117, 115–139. doi:10.1111/j.1096-3642.1996.tb02152.x

Rubidge, B. S., and Kitching, J. W. (2003). A new burnetiamorph (Therapsida: Biarmosuchia) from the lower Beaufort Group of South Africa. *Palaeontology* 46, 199–210. doi:10.1111/1475-4983.00294

Rubidge, B. S., and Sidor, C. A. (2001). Evolutionary patterns among Permo-Triassic therapsids. *Annu. Rev. Ecol. Syst.* 32, 449–480. doi:10.1146/annurev.ecolsys.32.081501.114113

Ruta, M., Angielczyk, K. D., Fröbisch, J., and Benton, M. J. (2013). Decoupling of morphological disparity and taxic diversity during the adaptive radiation of anomodont therapsids. *Proc. R. Soc. B Biol. Sci.* 280, 20131071. doi:10.1098/rspb.2013.1071

Rybczynski, N. (2000). Cranial anatomy and phylogenetic position of *Suminia getmanovi*, a basal anomodont (Amniota: Therapsida) from the Late Permian of Eastern Europe. *Zoological J. Linn. Soc.* 130, 329–373. doi:10.1111/j.1096-3642.2000.tb01634.x

Rybczynski, N., and Reisz, R. R. (2001). Earliest evidence for efficient oral processing in a terrestrial herbivore. *Nature* 411, 684–687. doi:10.1038/35079567

Sidor, C. A. (2001). *Evolutionary trends and relationships within the Synapsida*. Ph.D. thesis. The University of Chicago.

Sidor, C. A. (2003). The naris and palate of *Lycaenodon longiceps* (Therapsida: Biarmosuchia), with comments on their early evolution in the Therapsida. *J. Paleontology* 77, 977–984. doi:10.1666/0022-3360(2003)077<0977:tnapol>2.0.co;2

Sidor, C. A., and Rubidge, B. S. (2006). *Herpetoskylax hopsoni, a new biarmosuchian (Therapsida: Biarmosuchia) from the Beaufort Group of South Africa*. University of Chicago Press, 76–113.

Sigogneau, D. (1974). The inner ear of *Gorgonops* (Reptilia, Therapsida, Gorgonopsia). *Ann. South Afr. Mus.* 64, 53–69.

Smith, R. M. H., Rubidge, B. S., Day, M. O., and Botha, J. (2020). Introduction to the tetrapod biozonation of the Karoo Supergroup. *South Afr. J. Geol.* 123, 131–140. doi:10.25131/sajg.123.0009

Smith, R. M. H., Rubidge, B. S., and Van der Walt, M. (2012). *Therapsid biodiversity patterns and paleoenvironments of the Karoo Basin, South Africa*. Bloomington, Indiana: Indiana University Press, 30–62. chap.

Sulej, T., Bronowicz, R., Tałanda, M., and Niedźwiedzki, G. (2010). A new dicynodont–archosaur assemblage from the Late Triassic (Carnian) of Poland. *Earth Environ. Sci. Trans. R. Soc. Edinb.* 101, 261–269. doi:10.1017/s1755691011020123

Sullivan, C., and Reisz, R. R. (2005). Cranial anatomy and taxonomy of the late Permian dicynodont *Diictodon*. *Ann. Carnegie Mus.* 74, 45–75. doi:10.2992/0097-4463(2005)74[45:caatot]2.0.co;2

Surkov, M. V., and Benton, M. J. (2004). The basicranium of dicynodonts (Synapsida) and its use in phylogenetic analysis. *Palaeontology* 47, 619–638. doi:10.1111/j.0031-0239.2004.00382.x

van Heerden, J. (1972). Interspecific variation and growth changes in the cynodont reptile *Thrinaxodon liorhinus*. *Navorsinge Nas. Mus. Bloemfontein* 2, 307–347.

Wasserman, L. (2000). Bayesian model selection and model averaging. *J. Math. Psychol.* 44, 92–107. doi:10.1006/jmps.1999.1278

Wright, A. M., Lloyd, G. T., and Hillis, D. M. (2016). Modeling character change heterogeneity in phylogenetic analyses of morphology through the use of priors. *Syst. Biol.* 65, 602–611. doi:10.1093/sysbio/syv122